



<https://theses.gla.ac.uk/>

Theses Digitisation:

<https://www.gla.ac.uk/myglasgow/research/enlighten/theses/digitisation/>

This is a digitised version of the original print thesis.

Copyright and moral rights for this work are retained by the author

A copy can be downloaded for personal non-commercial research or study,
without prior permission or charge

This work cannot be reproduced or quoted extensively from without first
obtaining permission in writing from the author

The content must not be changed in any way or sold commercially in any
format or medium without the formal permission of the author

When referring to this work, full bibliographic details including the author,
title, awarding institution and date of the thesis must be given

Enlighten: Theses

<https://theses.gla.ac.uk/>
research-enlighten@glasgow.ac.uk

Techniques in laser interferometry for the detection of gravitational radiation

by

Kenneth Alexander Strain

Department of Physics and Astronomy
University of Glasgow.

Presented as a thesis for the degree of
Ph.D. in the University of Glasgow.

November 1990.

©Kenneth Alexander Strain 1990.

ProQuest Number: 11007976

All rights reserved

INFORMATION TO ALL USERS

The quality of this reproduction is dependent upon the quality of the copy submitted.

In the unlikely event that the author did not send a complete manuscript and there are missing pages, these will be noted. Also, if material had to be removed, a note will indicate the deletion.



ProQuest 11007976

Published by ProQuest LLC (2018). Copyright of the Dissertation is held by the Author.

All rights reserved.

This work is protected against unauthorized copying under Title 17, United States Code
Microform Edition © ProQuest LLC.

ProQuest LLC.
789 East Eisenhower Parkway
P.O. Box 1346
Ann Arbor, MI 48106 – 1346

Contents

1	Introduction to gravitational radiation and its detection	1
1.1	Introduction	1
1.2	Some properties of gravitational radiation	1
1.3	Sources of gravitational radiation	4
1.3.1	Production of gravitational radiation	4
1.3.2	Burst sources	5
1.3.3	Periodic sources	7
1.3.4	Stochastic sources	8
1.3.5	Summary	8
1.4	Introduction to the detection of gravitational radiation	10
1.4.1	Resonant bar detectors	10
1.4.2	Broadband detectors	11
1.5	Laser interferometric gravitational wave detectors	11
1.5.1	The signal from a Michelson interferometer	15
1.5.2	Fundamental noise sources	16
1.5.3	Technical noise sources	18
2	Advanced interferometry techniques applicable to gravitational wave detection	23
2.1	Introduction	23
2.2	Modulation schemes	24
2.2.1	Internal modulation	24
2.2.2	External modulation	28
2.2.3	Modulation and measurement noise	35

2.3	A Michelson interferometer with cavities in the arms and internal modulation	42
2.3.1	Introduction	42
2.3.2	The signal from an interferometer with cavities in its arms .	43
2.4	Recycling	49
2.4.1	Introduction to recycling	49
2.4.2	The split-cavity argument applied to power recycling	51
2.4.3	Interferometer contrast and recycling	55
2.4.4	Conclusion	59
2.5	Dual recycling	60
2.5.1	Introduction to dual recycling	60
2.5.2	A control system for dual recycling	65
2.5.3	Contrast and dual recycling	67
2.5.4	Conclusion	68
3	Experimental tests of advanced interferometry techniques	70
3.1	Introduction	70
3.2	A Michelson interferometer with internal modulation and cavities in its arms	71
3.2.1	Optics	71
3.2.2	Signals, feedback elements and control systems	74
3.2.3	Results	82
3.2.4	Conclusion	86
3.3	External modulation	86
3.3.1	Results	92
3.3.2	Conclusion	95
3.4	Power recycling	96
3.4.1	An automatic gain control for power recycling.	96
3.4.2	The power recycling mirror control system	99
3.4.3	The experimental test of power recycling	99
3.4.4	The effects of misaligning one of the arms in the power recycling interferometer	100

3.4.5	Conclusion	105
3.5	Dual recycling	105
3.5.1	The experimental test of the frequency response and signal to noise ratio of the dual recycling interferometer.	109
3.5.2	The alignment properties of the dual recycling interferometer	112
3.5.3	Conclusion	117
3.6	Internal modulation and measurement noise	119
3.7	General conclusion	124
4	Mirrors for gravitational wave detectors	125
4.1	Low loss mirrors	125
4.2	A test of the effect of mirror heating in a cavity	128
5	A variable reflectivity mirror for laser interferometers	133
5.1	Introduction to variable reflectivity mirrors	133
5.2	A variable reflectivity mirror	134
5.2.1	A low-frequency control system for the variable reflectivity mirror	136
5.2.2	A 'reflection-fringe' control system for the variable reflectiv- ity mirror	138
5.2.3	Conclusion	143
6	Conclusions and future prospects	144
A	Some properties of Fabry-Perot cavities	148
B	Laser stabilisation	153
C	Measurements of losses in high reflectance mirrors coated for $\lambda = 514.5$ nm	157
D	A measurement of ground displacement noise at one site	158

List of Figures

1.1	The effect of gravitational radiation on a ring of particles	3
1.2	Expected source strengths	9
1.3	A Michelson interferometer	13
1.4	Alternative optics for interferometer arms	14
2.1	Internal modulation	25
2.2	External modulation	29
2.3	Internal sine-wave modulation: amplitude spectrum	38
2.4	Internal modulation with a better waveform: amplitude spectrum .	38
2.5	Internal modulation with cavities	44
2.6	Recycling	50
2.7	The power recycling split-cavity	53
2.8	Dual recycling	61
2.9	The dual recycling split-cavity	63
3.1	The internal modulation system	72
3.2	The internal modulation electronics	75
3.3	A photodiode amplifier	77
3.4	Internal modulation control system 1	80
3.5	Internal modulation control system 2	81
3.6	Internal modulation frequency response	85
3.7	Internal modulation signal to noise ratio	87
3.8	External modulation	89
3.9	External modulation control system	91
3.10	Signal to noise ratio with external modulation	94
3.11	The automatic gain control	98

3.12	The power recycling servo-system	101
3.13	Signal to noise ratio with power recycling	101
3.14	The angle transducer	102
3.15	Power loss and misalignment	104
3.16	Dual recycling detail	106
3.17	Dual recycling control beam	108
3.18	Dual recycling frequency response	111
3.19	Signal to noise ratio with dual recycling	113
3.20	Misalignment and dual recycling	114
3.21	Modulation and measurement noise experiment	120
3.22	Modulation and measurement noise results	123
4.1	The mirror-heating experiment	131
5.1	Variable reflectivity mirror optics	135
5.2	The first control system	137
5.3	Coupled-cavity resonances	139
5.4	The reflection-fringe control system	141
A.1	An optical cavity	148
B.1	Frequency stabilisation	154
B.2	Frequency stabilisation loop gain	156
B.3	Laser noise	156
D.1	Seismic noise results	159

Acknowledgements

I would like to thank my supervisor Jim Hough for all of his help and advice throughout the period of this work. Thanks must go to Brian Meers for not only inventing dual recycling but helping me to understand it. All of the other members of the Glasgow gravitational waves group have more than earned my gratitude for all their advice, encouragement and friendship: Harry Ward, Gavin Newton, Norna Robertson, Graham Kerr, Norman Mackenzie, Peter Veitch, David Robertson, Caroline Cantley, Allan Carmichael, Euan Morrison and Jennifer Logan

I am grateful for the interest and support of Prof. I. Hughes and Prof. R.P. Ferrier.

Technical support was very competently provided by Jim Pittillo, Allan Latta, Angus McKellar and David Edwards.

I am grateful to SERC for financial support and to the University of Glasgow for general support.

Lastly I would like to thank my family and friends for all their help, encouragement and support.

This thesis was written using the \LaTeX document preparation system.

Preface

Chapter 1 contains an introduction to gravitational radiation and its detection. Astrophysical sources of gravitational radiation are considered briefly to allow the performance of a proposed detection method to be evaluated. The technique of laser interferometry between nearly-free test masses is introduced and the basic signal and noise properties discussed. This material is mainly a review of previous work.

In Chapter 2 two already proposed modulation and signal recovery schemes for laser interferometers (called ‘internal’ and ‘external’ modulation) are compared. The effect of the modulation schemes on the potential signal to noise ratio of the interferometer is evaluated. The application of one of these (internal modulation) to an interferometer with cavities in its arms is considered by the author to reveal likely problems with the control of such a system. A control method for an interferometer with external modulation is discussed. This was based on a method designed, by colleagues, for the proposed full-scale German-British detector.

The existing techniques of ‘power recycling’ and ‘signal recycling’ which should both allow the performance of an interferometer to be significantly enhanced are reviewed to introduce possible experimental tests of these systems. Possible control systems for interferometers with recycling are also discussed. This work was carried out in conjunction with colleagues at Glasgow.

Chapter 3 contains descriptions of experiments, carried out by the author, to test the ideas and techniques of Chapter 2. An interferometer with cavities in its arms was designed and tested. A series of experiments were then carried out to develop a test interferometer with dual recycling, the first implementation of this technique. Control systems were designed and built and the operation of the system investigated. The effect of internal modulation on measurement noise was

also measured.

Chapter 4 presents a series of measurements, carried out by the author in conjunction with Norna A. Robertson, to determine the losses of the very high quality mirrors required for a gravitational wave detector. An experimental test, by the author, of the predicted effect of mirror heating (due to the absorption of light) on a Fabry-Perot cavity is also described. (This effect had been predicted by several workers in the field of interferometric gravitational wave detectors.)

In Chapter 5 the use of a cavity as a mirror whose reflectivity can be varied is discussed and an experimental test, carried out by the author, of the properties of a cavity containing such a mirror is described.

Chapter 6 is a summary of the results of the earlier chapters and also relates these results to the development of a particular gravitational wave detector—the proposed German-British interferometer.

Summary

General relativity leads to the expectation of travelling gravitational waves which manifest themselves as strains in space. Massive relativistic systems are the only sources of gravitational radiation which ^{are} _^ expected to be detectable on earth. A range of such sources is reviewed in the first chapter in order to estimate the likely gravitational wave amplitudes at the earth. It is seen that in the frequency range accessible to ground-based detectors (tens of hertz to several kilohertz) the expected strain amplitudes are at most $\sim 10^{-21}$. At present the most promising technique for the detection of gravitational radiation is laser interferometry between nearly-free test masses. The signal and noise properties of the simplest configuration of this system are considered to show that the performance can approach that required to detect the predicted sources of gravitational radiation. In order to reach this level of performance more advanced optical techniques are needed and these are discussed in Chapter 2.

The lasers used to illuminate the interferometers have excess intensity noise at low frequencies and this forces all measurements to be made using high frequency (at least several MHz) modulation techniques. Two modulation and signal recovery schemes for laser interferometers (internal and external modulation) are compared. It is seen that external modulation should provide the same signal as internal modulation but without the need to add lossy modulation components to the arms of the interferometer. The effect of the modulation technique on the signal to noise ratio of the interferometer is evaluated and it is found that both the technique used and the particular modulation waveform can alter the potential signal to noise ratio slightly.

There is an optimum length of the arms of an interferometer designed to detect gravitational waves at a given frequency. The time the light spends in each

of the arms should be half of the period of the gravitational wave (i. e. several milliseconds). This can be achieved by multiple reflection of the light along arms (perhaps several km in length) using optical delay-lines or Fabry-Perot cavities. Some aspects of both of these schemes are considered in this thesis.

The application of internal modulation to an interferometer with cavities in its arms is considered. The signals which can be expected from this system are investigated to reveal if there should be any problems with the control of such an interferometer. It is found that there should be no unexpected control problems.

The very important techniques of power and dual recycling should both allow the performance of a basic interferometer to be enhanced considerably. Both of these are discussed in Chapter 2 in order to enable an experiment to be done to test the optical properties of these techniques and to test suitable control systems. Power recycling is concerned with the maximisation of the light amplitude in the interferometer for a given laser power by making the laser light resonant in the system. Dual recycling provides a method of enhancing the frequency response of the interferometer, especially at low frequencies or in a narrow range of frequencies, by resonating the signal sidebands. In this respect it can replace the need for cavities in the arms of the interferometer and also provides a method of optimising the detector response if the frequency of an expected signal is known.

The techniques presented in Chapter 2 were tested as described in Chapter 3. The results suggested that the behaviour of the optical systems were understood and that control systems could be made to operate these relatively complicated arrangements. The effects of internal modulation on measurement noise were also confirmed.

The above systems require extremely low loss mirrors. A method based on the measurement of the storage time of a Fabry-Perot cavity was adapted to allow the losses of such mirrors to be evaluated. This has revealed that sufficiently low loss mirrors are now becoming available in the large sizes required for gravitational wave detectors.

While the use of cavities in the arms of interferometers to increase the storage time is very attractive there is likely to be a problem with mirror heating due to

absorption of the some of the light by the mirrors. This problem is maximised in cavities since the power is concentrated on one spot on each mirror and only certain transparent materials can be used for the input mirror of the cavity. In a delay-line system the light enters each arm through a hole in a mirror and transparent mirrors are not required. An experiment was carried out by the author to test a simple, order of magnitude, prediction of the effect of mirror heating on the properties of a cavity.

It is likely that in any of the interferometer designs discussed it will be useful to have mirrors whose reflectivity can be varied. One possible use of this technique is to balance the storage times ^{of the} arms of an interferometer with cavities in the arms. Another application is in the control of the frequency response of an interferometer with dual recycling. The idea of using an optical cavity as such a variable reflectivity mirror was investigated experimentally, by the author. A variable reflectivity mirror was incorporated into a cavity and some of the optical properties were measured. Two different control systems, one of which obtained the two required control signals from the light reflected by the cavity, were tested.

In conclusion it is seen that the basic optical systems required to make interferometers which should be able to detect gravitational radiation have now been tested at least on a small scale. While it is clear that it will not be easy to extend this work to a full-scale system there is every indication to suggest that this will be achieved in the near future.

Chapter 1

Introduction to gravitational radiation and its detection

1.1 Introduction

In this chapter the nature of gravitational radiation is discussed and some likely sources are considered. Techniques for the detection of gravitational radiation are introduced. Further, the technique of ground based long baseline laser interferometry is discussed in some detail.

1.2 Some properties of gravitational radiation

The existence of gravitational radiation is a direct consequence of general relativity [1] or indeed any theory of gravitation which has local Lorentz invariance and, consequently, a finite propagation velocity for gravitational effects. General relativity places constraints on the properties of gravitational radiation, namely the type and number of polarisation states as well as the propagation velocity (the speed of light). It will be assumed that general relativity is correct in these respects for the remainder of this thesis. ¹

In essence any observed fluctuations in the local curvature of space-time which cannot be attributed to any direct induced gravitational field must be due to the passage of gravitational radiation. This phenomenon can be represented in general relativity by the fluctuating part of the Riemann curvature tensor ($R_{\alpha\beta\gamma\delta}^{GW}$) which is superimposed on the local static background curvature.

¹For a detailed background to the material in this section see e.g. [2, 4]

The simplest discussion of the effects of gravitational radiation is that set in the proper reference frame of an observer. This is a good approximation for regions of low background curvature (weak gravitation), and this is the situation of a detector in the solar system. It applies only to observed systems which are small compared to a wavelength of the gravitational radiation. This approximation is adequate for all of the detection schemes which are discussed below (section 1.4) .

The proper reference frame is a Cartesian co-ordinate frame (t, x, y, z) with the addition of non-Newtonian geodesic deviations due to gravitational radiation. The geodesic deviations are equivalent to the acceleration of adjacent test particles and these are obtained from the effect of $R_{\alpha\beta\gamma\delta}^{GW}$ on their relative positions. These deviations lead to changes in the separation of the two particles.

To quantify this put one test particle at the origin and one initially at rest at co-ordinates x_k . The apparent acceleration of the particle at x_k during the passage of gravitational radiation is then given by

$$\ddot{x}_j^{GW} = -R_{j0k0}^{GW}x_k, \quad (1.1)$$

where the dots represent differentiation with respect to time.

It is, however, conventional to use the dimensionless strain amplitude h_{jk} to describe the amplitude of the gravitational radiation. This is defined by

$$\ddot{x}_j^{GW} = \frac{1}{2} \frac{\partial^2 h_{jk}}{\partial t^2} x_k \quad (1.2)$$

and since the expected waves are of small amplitude $h \ll 1$ (see section 1.3) x_k is approximately constant and this can be integrated to give

$$\delta x_j^{GW} = \frac{1}{2} h_{jk} x_k \quad (1.3)$$

as the change in the relative positions of the two test particles under the influence of a gravitational wave.² Thus h_{jk} is dimensionless and is proportional to a strain in space. The nature of this strain is defined by general relativity and the symmetry properties of $R_{\alpha\beta\gamma\delta}^{GW}$. These imply that for a plane gravitational wave propagating

²The terms gravitational radiation and gravitational wave are used interchangeably.

in the z-direction (for convenience) the form of h_{jk} is traceless and represents a transverse wave. The only non-zero components are $h_{xx} = -h_{yy}$ and $h_{xy} = h_{yx}$. There are thus two polarisation states of the transverse wave and there is no longitudinal wave.

The polarisation states are called h_+ and h_\times and have associated test particle equations of motion given by

$$m\ddot{x} = \frac{1}{2}\ddot{h}_+x, \quad m\ddot{y} = -\frac{1}{2}\ddot{h}_+y$$

for the ‘plus’ polarisation

and

$$m\ddot{x} = \frac{1}{2}\ddot{h}_\times x, \quad m\ddot{y} = \frac{1}{2}\ddot{h}_\times y$$

for the ‘cross’ polarisation (where m is the mass of the test particle). Since all of the likely sources are at astrophysical distances the waves will be very nearly plane at Earth.

The effect of one cycle of a sinusoidal gravitational wave of the ‘plus’ polarisation on a ring of test particles is shown (figure 1.1). The effect on the embedded ‘L’ shape is worth noting. The cross polarisation would have a similar effect on the ring but rotated by $\pi/4$.

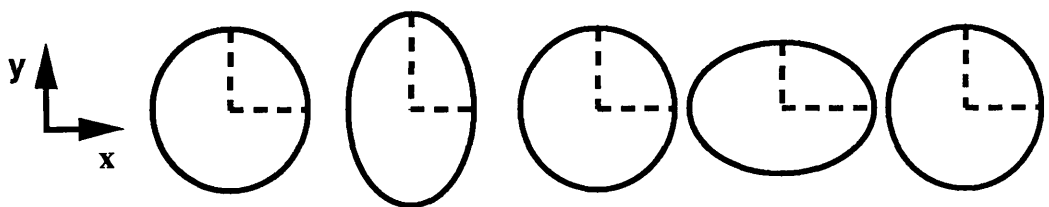


Figure 1.1: *The effect of one cycle of sinusoidal gravitational wave of the ‘plus’ polarisation propagating perpendicular to the page. The axes shown apply to each of the five equally spaced observation time instants which the separate rings represent.*

1.3 Some sources of gravitational radiation and predicted amplitude of the radiation

1.3.1 Production of gravitational radiation

The production of gravitational radiation will now be introduced and some sources, which have a reasonable probability of detection, identified.

The fact that there is one sign of mass and the conservation of momentum and angular momentum ensure that only quadrupole and higher moments can radiate. This fact along with the weak coupling between gravitation and matter is what renders gravitational radiation difficult to produce and detect. Since, as with most electromagnetic systems, the strength of the radiation falls quickly with increasing order of multipole, only the mass quadrupole moment term need normally be considered when estimating source strength.

Laboratory sources have been considered and rejected as being considerably too weak. The largest predicted radiated power of $\sim 10^{-30}$ watt [2], from a massive cylinder rotating at a rate which causes an internal stress close to the breaking stress for steel, would not produce a detectable strain amplitude. The only real hopes for detectable amplitudes of gravitational radiation lie with astrophysical sources, especially those associated with compact objects (for example neutron stars or black holes) where expected luminosities of order 10^{52} W more than compensate for the increased distances to the sources [2].

Some sources of gravitational radiation are now considered, especially those which can be expected to produce waves in the frequency range which should be accessible to ground based detectors (above ~ 10 Hz). This low frequency limit is set primarily by the presence of seismic noise (section 1.5.3). For a substantial review of expected sources see [4, 5].

For convenience sources are divided into three classes according to the form of the expected waveform of the gravitational radiation: burst or pulse sources, continuous periodic sources and stochastic background. It will be seen that it is difficult to predict some parameters of even the expected sources. This in itself provides motivation for the detection of gravitational radiation since more informa-

tion about the sources should result from direct observations. The following brief description of several possible sources is presented to allow the detection schemes which are described subsequently (section 1.4) to be evaluated.

1.3.2 Burst sources

Burst sources are characterised by a waveform which is dominated by up to several cycles of a characteristic frequency (or range of frequencies in the case of coalescing binaries). The two prime candidate sources in this category are pulses radiated during supernovae and the radiation emitted as the evolution of a binary system of compact objects reaches the point of coalescence.

Supernovae

There are understood to be two classes of supernovae. A supernova of ‘Type 1’ occurs either when an accreting white dwarf has a nuclear explosion (in which there may be a collapse of a remaining core to form a compact object) or perhaps when its mass exceeds the Chandrasekhar limit ($1.4M_{\odot}$) and it undergoes gravitational collapse to form a neutron star. A supernova of ‘Type 2’ is the last stage in the evolution of a giant star when the radiation pressure from the core nuclear reactions ceases to be sufficient to support the core against gravitational collapse to form a neutron star or a black hole.

The luminosity of such a source is strongly dependent on the extent to which the collapse is non-axisymmetric (i.e. on its quadrupole moment) and on the acceleration of matter during the collapse. The asymmetry in turn depends on the initial rotational state of the precursor star while the collapse may be slowed by the effect of radiation pressure (either electromagnetic or neutrino) countering the gravitational attraction. Both of these effects are difficult to quantify but an estimate of the gravitational wave amplitude at the earth is (from [3])

$$h \approx 10^{-21} \left[\frac{E}{10^{-2} M_{\odot} c^2} \right]^{1/2} \left[\frac{r}{15 \text{ Mpc}} \right]^{-1}, \quad (1.4)$$

where E is the energy emitted (as gravitational radiation) in the burst (in terms of the solar mass) and r is the distance of the supernova from the detector (in megaparsecs). The scale energy shown represents an estimate of the radiated energy which could be expected from a typical supernova. The occurrence rate for supernovae has an observed lower limit (since some may not be optically bright and may thus have missed detection) of, on average, around one of each type per galaxy per 40 years. The scale distance shown (15 Mpc) is approximately the distance to the centre of the Virgo cluster of galaxies (the highest nearby concentration of galaxies) and it is expected that there will be several events per year at the level shown [5].

Coalescing compact binaries

Two compact objects in close orbit will strongly radiate energy by gravitational radiation. The orbit will thus decay and the orbital period decrease. The last few cycles of such a system, just before the masses interact finally, would be accompanied by gravitational radiation of high luminosity. The expected signal for such a source is (from [3])

$$h \sim 10^{-23} \left[\frac{r}{100 \text{ Mpc}} \right]^{-1} \left[\frac{M}{M_{\odot}} \right]^{2/3} \left[\frac{\mu}{M_{\odot}} \right] \left[\frac{f}{100 \text{ Hz}} \right]^{2/3}, \quad (1.5)$$

where r is the distance from the source to the detector, M is the total mass of the source with reduced mass μ , the gravitational radiation has an instantaneous frequency f and M_{\odot} is one solar mass.

The waveform is also well predicted as it depends only on the masses of the orbiting bodies (until tidal forces begin to become important). In particular the change of the frequency of the radiation as a function of time can be predicted. The following relation describes the effect

$$\frac{f}{\frac{df}{dt}} \approx 7.8 \left[\frac{f}{100 \text{ Hz}} \right]^{-\frac{8}{3}} \left[\frac{M}{M_{\odot}} \right]^{\frac{2}{3}} \left[\frac{M_{\odot}}{\mu} \right] \text{ s}. \quad (1.6)$$

The predictability of the waveform allows the use of matched filters to examine the output of a (broadband) detector. This allows the detection threshold to be reduced considerably for a given detector noise (see [5]).

It is interesting to note that after an observation of such an event the above equations can be solved to yield the distance (r). Detection of such a source followed by optical identification of the galaxy in which the source was residing would allow determination of the distance to this galaxy as a result of the gravitational wave detection. If in addition the redshift of the galaxy could be measured then a few detections of this type of event in distant galaxies (in the hundred megaparsec range) should allow accurate determination of Hubble's constant.

The rate of such events occurring within a given volume is not well constrained at present due to the difficulty of electromagnetic identification of these systems in earlier stages of their evolution but estimates of several to several thousand per year within a distance of 500 Mpc have been made [5].

1.3.3 Periodic sources

Periodic sources are characterised by a continuous signal at one or more frequencies from a stable rotating system. The frequencies can be harmonics of the axial rotation frequency or can be altered by precession if the rotational axis and the mass distribution are not aligned [6]. The best examples are binary systems and rotating neutron stars. Gravitational radiation depends on the source being non-axisymmetric so that it has some quadrupole moment. While this is always true for a binary system it is only true for a neutron star if it is distorted to become non-axisymmetric.

For a binary system to be detectable by a ground based instrument it would have to have an orbital time of less than $\sim 1/10$ s (the radiation having half of this period). This is only possible for objects with a separation of less than $\sim 10^7$ m and these sources would then be coming close to the point of coalescence mentioned above and would not be continuous sources.

Even a small non-axisymmetry associated with a pulsar would cause signifi-

cant gravitational radiation [4] The frequency of the quadrupole radiation could be at twice the pulsar repetition rate (if the mass asymmetry is associated with the pulsar's magnetic field and the effects of precession are not important) and therefore well known for a pulsar which has been observed via its radio emissions [4]. The signal resulting from some values of non-axisymmetry associated with known pulsars is shown (figure 1.2).

1.3.4 Stochastic sources

A background of gravitational radiation could be formed by the addition of radiation from a large number of independent sources. Some example sources from the early history of the universe are vibrating cosmic strings or Population III supernovae [4]. If in a frequency band $\delta f \sim f$ about a frequency f the energy in the gravitational radiation background is a fraction Ω_{GW} of the closure density for the universe then the mean detectable amplitude is

$$h = 6 \times 10^{-26} \left[\frac{\Omega_{GW}}{10^{-10}} \right]^{1/2} \left[\frac{f}{100 \text{ Hz}} \right]^{-1}. \quad (1.7)$$

This indicates the detectability with a given detector. To look for such a signal it is necessary to correlate the output ^S of more than one detector. These instruments must then be separated by less than one quarter of the wavelength of the detected radiation if the correlations are to be maintained in the signals from each of the detectors [5].

1.3.5 Summary

A graph summarising the likely levels of gravitational wave signals is included for reference (figure 1.2). This gives an idea of the detector sensitivities and frequency response characteristics required to detect the range of sources described above. The data for this graph ^{have} been derived from the source strength equations stated or taken from [3].

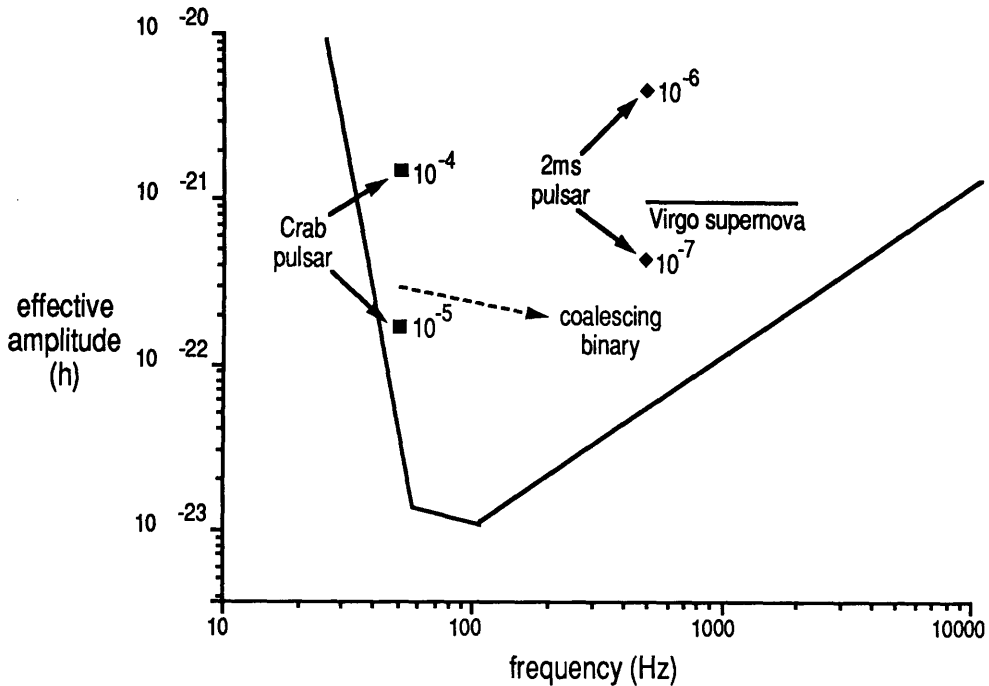


Figure 1.2: A graph of the expected strengths at earth of gravitational radiation from several probable sources as a function of frequency. This has been restricted to the frequency range which is accessible to ground-based observations. In order to allow the different classes of source to be shown the amplitudes have been multiplied by the square root of the number of cycles over which the source can be observed. For the case of pulsars an observation time of 10^7 seconds has been assumed. The non-axisymmetry of the pulsars have been indicated beside the marked points. The coalescence shown is for two 1.4 solar mass neutron stars at a distance of 100 megaparsecs. The line shown is an indication of the expected noise of one proposed detector (see Chapter 6) operated in a broadband mode. The rising part of the curve is due to photon shot noise and the noise here could be reduced by reducing the bandwidth of the detector (e.g. by dual recycling—see Chapter 2).

1.4 Introduction to the detection of gravitational radiation

Many methods of detecting gravitational radiation have been proposed (see [4, 2]). The most promising types which have been developed are resonant bar detectors and laser interferometers.

1.4.1 Resonant bar detectors

Resonant bar antennae were the first detectors to be developed [7] and their performance has been steadily improved over the past decades [4]. Such detectors consist typically of a massive right circular cylinder of a material with a high mechanical quality factor. This behaves much like two test masses with a connecting spring which form a system resonant at the intended detection frequency. The passage of a suitably oriented gravitational wave through such a detector causes a strain in the spring. The energy of vibration of the resonant mode of the mass-spring system may be increased or decreased because of this. The motion of the resonant mode (the fundamental axial mode of the cylinder) is monitored using a sensor consisting of a transducer and an amplifier. The passage of gravitational radiation would be detected by a change in the amplitude (or phase) of the output signal. The detector must be well isolated from external noise sources. This is achieved by careful vibration isolation and suspension of the detector in vacuum.

The signal from gravitational radiation competes with the random signals due to Brownian motion as a result of the thermal energy producing a stochastic driving force. The effect of this motion can be reduced by shortening the observation time but this corresponds to wider measurement bandwidth and so increases the noise from the sensor. There is therefore a compromise bandwidth set by these two noise sources. With current technology the bandwidth is around 1/100 of the resonant frequency so these detectors are rather narrow band.

The thermal noise can be reduced by cooling of the detector to low cryogenic temperatures but even if sensor noise can be reduced eventually quantum displacement fluctuations in the position measurement become important. Back-action

evasion techniques have been proposed to balance the uncertainties in the experimenter's favour [8] but these will probably take some time to develop. Until they are, the sensitivity of a bar detector designed to operate at 1 kHz will be at best $h \sim 10^{-20}$.

1.4.2 Broadband detectors

These detectors work by the principle that was demonstrated in figure 1.1. Masses which are free to move under the effects of gravitational radiation will respond in the manner indicated by this diagram. The separation of two such masses can be monitored using a laser beam. The result of this measurement will show the positional fluctuations due to the gravitational radiation. This technique is inherently broadband.

Ground-based observations are limited at low frequency by a background of seismic motions from which it is difficult to isolate the test masses. This sets a practical lower limit of tens of hertz for such apparatus.

Space-borne detectors have been proposed to investigate the lower frequency ranges. The separation of satellites or spacecraft could be monitored by laser interferometry or for the lowest frequencies and longest baselines (1 AU or more) by radar-doppler tracking [4].

The remainder of this thesis is, however, devoted to the more immediate problem of the design of ground based detectors using laser interferometry between essentially free test masses.

1.5 Laser interferometric gravitational wave detectors

A Michelson interferometer is well suited to the measurement of the relative lengths of two perpendicular arms. If these are aligned with the x and y axes of the proper reference frame then the system will be sensitive to the 'plus' polarisation of gravitational radiation propagating in the z direction. (The basic idea is shown by the effect of gravitational radiation on the 'L' shape in figure 1.1 where one arm

of the ‘L’ is lengthened as the other is shortened). The simplest implementation of such a detector is shown (figure 1.3).

The optical components of the interferometer are suspended as pendulums with a period (typically 1 s) much longer than the period of the gravitational waves being sought. The ‘test masses’ which respond to the gravitational radiation are either made to form the required optical components directly or have the optics (mirror etc.) fixed to them.

The relative phase, at the return to the beamsplitter, of the light traversing each arm leads to a change in the power on the output photodetector. The output power is given by

$$I = \frac{I_0}{2}(1 - \cos \Delta\phi), \quad (1.8)$$

where I_0 is the maximum (bright fringe) power and $\Delta\phi$ is the relative phase between the light from the two arms on returning to the beamsplitter.

The size of the output signal for a given gravitational wave amplitude and arm length can be increased by multiple reflection of the laser beams along each arm (until the storage time limit, defined below, is reached). This is achieved either using an optical delay line or by incorporating a Fabry-Perot optical cavity in each of the arms.

In the delay line the light is repeatedly reflected up and down the arms on non-overlapping paths. The delay line is illuminated via a hole in the mirror nearest the beamsplitter and the light must exit through this or a similar hole. The total transit time of the light is $\tau = Nl/c$ where N is the number of traverses of arm length l at velocity c .

In the cavity case the beams overlap on each traverse and the illumination is via a partially transmitting input mirror. There is now an effective number of bounces and an effective storage time. Both of these schemes are illustrated (figure 1.4), (Some properties of cavities are discussed in appendix A).

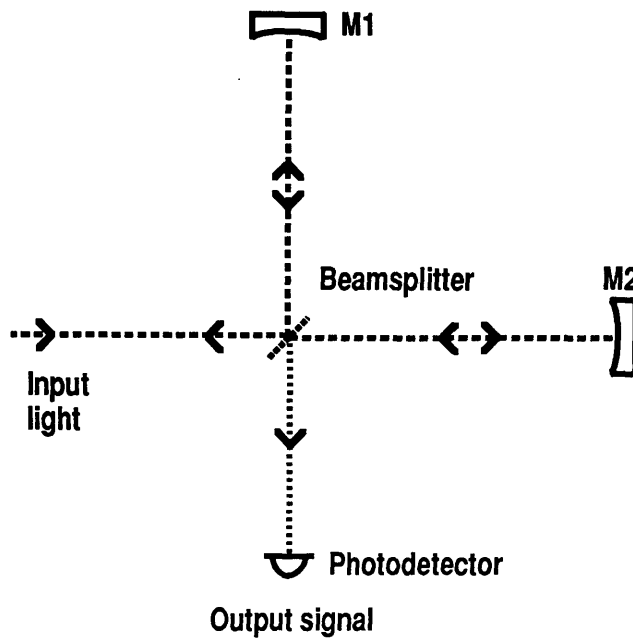


Figure 1.3: A basic Michelson interferometer in which the input laser light is split equally into two beams which traverse the arms and return to the beamsplitter. The two arms are represented by single traverses to the mirrors $M1$ and $M2$. The light power emerging from the output port is measured using a photodetector.

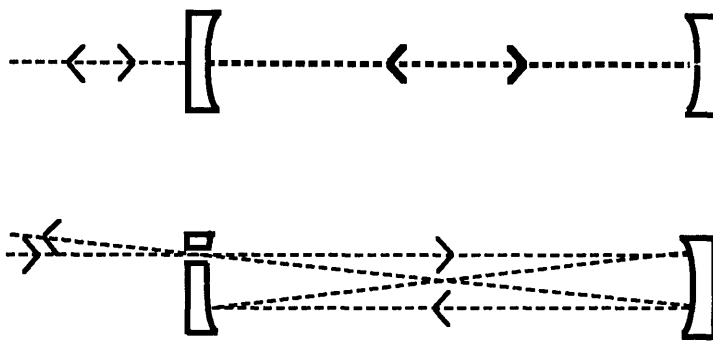


Figure 1.4: *An illustration of two systems which can be used to increase the storage time for light in the interferometer arms for a given arm length. The upper drawing shows a resonant optical cavity with a partially transmitting input mirror. The lower drawing shows the idea of the optical delay line with four traverses. In practice in a detector with arm lengths of a few km the number of traverses should be at least 30.*

1.5.1 The signal from a Michelson interferometer

Consider the effect of gravitational radiation of angular frequency ω_g wavelength λ and amplitude h on the length of one of the arms of a Michelson interferometer oriented in the xy -plane. There is gravitational radiation propagating in the z -direction with the plus polarisation aligned to the arms of the interferometer. The interferometer is illuminated with monochromatic coherent light of angular frequency ω propagating at velocity c . The initial length (l) is changed by an amount δl given by

$$\delta l = l \frac{h}{2} \cos \omega_g t, \quad (1.9)$$

where h is the peak amplitude of the components $h_{xx} = -h_{yy}$.

The phase shift on the light after traversing this path once in each direction is given by

$$\delta\phi = \frac{2\pi}{\lambda} \frac{hl}{\tau} \int_{t-\tau}^t \cos(\omega_g t) dt, \quad (1.10)$$

where τ is the time for the light of wavelength λ to traverse the arm and return to the beamsplitter. (This is only true if the arm length is less than the wavelength of the gravitational radiation.)

If the light makes a number of traverses of the arm then the phase shift imposed on each traverse must be added. It is then important to consider the changing length of the arm with time. If there are $2n$ traverses (where n is a natural number) then the total phase shift is given by

$$\delta\phi = \frac{2\pi}{\lambda} \frac{hl}{\tau} \left[\int_{t-n\tau}^{t-(n-1)\tau} \cos(\omega_g t) dt + \dots + \int_{t-2\tau}^{t-\tau} \cos(\omega_g t) dt + \int_{t-\tau}^t \cos(\omega_g t) dt \right]. \quad (1.11)$$

The common limits of the integrals cancel and this becomes

$$\delta\phi = \frac{h\omega}{\omega_g} \sin\left(\frac{\omega_g \tau}{2}\right) \cos \omega_g \left(t - \frac{\tau}{2}\right). \quad (1.12)$$

It can be seen from this that there is a maximum phase shift which can be obtained with a given optical wavelength and gravitational wave amplitude. This is as expected since if the light is stored in an arm for more than one half period of the gravitational wave then the sign of δl will have changed during the measurement

period and the phase signal will be reduced. (This argument applies to delay lines of several bounces or more where the total size of the apparatus is small compared to one wavelength of the gravitational radiation.)

The effect of the gravitational radiation of the ‘plus’ polarisation on the other arm is of the opposite phase to that on the first arm. The differential phase between the arms of the interferometer will then be twice the above value. The maximum or ‘storage time limited’ phase difference (setting $\tau = \tau_g/2$) will thus be

$$\delta\phi_{max} = \frac{2\omega h}{\omega_g} \sin \omega_g t. \quad (1.13)$$

The optimum way of operating the system illustrated is to maintain an operating point offset only slightly from the interference minimum. The power change for a given (small) phase shift $\delta\phi$ about the operating point offset from a null by small static phase angle ϕ is

$$\delta I = \frac{I_0 \phi \delta\phi}{2}. \quad (1.14)$$

The (storage time limited) maximum power change due to gravitational radiation would then be

$$\delta I_{max} = I_0 \phi \frac{\omega h}{\omega_g} \sin \omega_g t, \quad (1.15)$$

where I_0 is the maximum possible output power. (Any losses in the arms must be taken into account and this will restrict the choice of storage time for a given arm length—see [11]). In practice the long optical paths required to reach this storage time limited signal for low detection frequencies may be difficult to achieve.

1.5.2 Fundamental noise sources

The maximum power change derived above must now be compared to the minimum measurable power change. If all other noise sources are reduced to a suitably low level then this is set by vacuum fluctuations ^[9] which enter at the beamsplitter and are mixed with the laser light on the photodetector (which is always a square law amplitude detector and so acts as a mixer). This noise is equivalent to that

calculated from Poisson statistics on the counting of the detected photons [9] and is represented by

$$\delta I_{min} = \sqrt{\frac{2I}{\eta} \Delta f} = \sqrt{\frac{I_0 \phi^2}{2\eta} \Delta f}, \quad (1.16)$$

where η is the number of photons detected by the photodetector per unit incident light energy and Δf is the measurement bandwidth. Here the root mean square signal power is compared to the noise power in a given bandwidth due to the almost static light power I .

The minimum detectable relative phase change is

$$(\delta\phi_{min})^2 = \frac{2\Delta f}{I_0\eta} = \frac{4\pi\hbar c\Delta f}{\xi\lambda I_0}, \quad (1.17)$$

where \hbar is the reduced Planck constant and ξ is the quantum efficiency of the photodetector for light of wavelength λ . This is the optimum signal to noise ratio which can be achieved with the system described. The minimum detectable root mean square gravitational wave amplitude due to photon counting noise is therefore, from 1.12 and 1.17

$$(h_{min})^2 = \frac{\hbar\lambda\Delta f(\omega_g)^2}{2\pi\xi I_0 c}. \quad (1.18)$$

Expressing this numerically, the storage time limited sensitivity which can be obtained with an ideal interferometer with lossless mirrors is

$$h_{min} = 3.10^{-23} \left[\frac{\omega_g}{2\pi 100 \text{ Hz}} \right] \left[\frac{\xi I_0}{10 \text{ W}} \right]^{-1/2} \left[\frac{\lambda}{515 \text{ nm}} \right]^{1/2} \sqrt{\Delta f}. \quad (1.19)$$

This level of performance cannot be achieved in practice and optical systems designed to reach this or similar levels of performance in practice are considered in Chapter 2. (The above applies to normal coherent radiation only. The use of light in a squeezed or sub-Poissonian state, to replace the vacuum fluctuations entering at the unused port of the beamsplitter, would, in principle, allow this limit to be reduced [9].)

The application of the position-momentum uncertainty principle reveals a limit to the position sensing which is possible with a given mass of test mass [10]. This

is due to the balance between the increase in power reducing the error in phase (position) measurements but increasing the importance of radiation pressure fluctuations which move the test masses. The limit set by this, at a detection frequency ω_g (which is higher than the natural frequency of the suspension pendulums), is given by

$$h_{min} = \sqrt{\frac{8\hbar\tau_m}{M\omega_g^2 l^2}}, \quad (1.20)$$

where τ_m is the measurement time and M is the mass of each test mass. This is, however, only achieved with very high input laser powers. The diminishing importance of this noise source with increasing frequency and the relatively high noise levels at low frequency due to seismic and suspension thermal noise (see the next section) make this quantum limit very difficult to reach.

1.5.3 Technical noise sources

There are many other noise sources which have been considered in laser interferometric detectors [3, 11]. The most important of these (in relation to the work presented) are summarised below.

Laser noise

The input laser light will have power, frequency and geometry fluctuations. All of these can couple in various ways into the output signal from the interferometer. The argon-ion lasers currently used in gravitational wave experiments exhibit all of these noise sources with the noise concentrated at low frequencies (less than a few kHz). (See appendix B for the case of frequency noise.)

Frequency noise Frequency noise, where the laser's frequency varies on all timescales about its mean value can couple into the output signal from an interferometer in several ways, the most direct being through unequal arm lengths in

a delay line (unequal storage times if Fabry-Perot cavities are fitted in the arms). For a delay line system

$$h_{min} = \frac{\Delta l}{l} \frac{\delta\omega}{\omega}, \quad (1.21)$$

where $\Delta l/l$ is the fractional arm length difference, $\delta\omega$ is the magnitude of the angular frequency noise on light of angular frequency ω .

Much effort has been put into the frequency stabilisation of the lasers used in the present prototype interferometers [12, 3]. Levels of frequency noise of as little as 10^{-5} Hz/ $\sqrt{\text{Hz}}$ at around 1 kHz have been achieved at Glasgow.

Frequency noise can also be a problem if light scattered within the interferometer (for example from the mirrors—see Chapter 4) reaches the output photodiode. The scattered light could have a large path difference relative to the main interferometer light and so the phase changes caused by even a small frequency fluctuation could then be significant. Winkler [14] has found that with moderately low loss mirrors scattered light leads to a minimum detectable amplitude of

$$h_{min} \sim 10^{-4} \frac{\delta\omega}{\omega}, \quad (1.22)$$

where $\delta\omega/\omega$ is the relative frequency noise on the light in the interferometer.

Intensity noise Intensity variations of the laser light occur. These are generally concentrated below a certain frequency above which the intensity fluctuations reach the value expected from Poisson statistics on the number of photons present. All measurements must be made at such frequencies and this is the main reason for the use of the modulation techniques which are discussed in section 2.2.

There is still the possibility that low frequency intensity noise can couple into the interferometer output if the output is not held precisely on an interference minimum. The required intensity stability can be calculated from

$$\frac{\Delta I}{I} \sim h_{min} \frac{l}{\Delta l}, \quad (1.23)$$

where Δl is the absolute error in the arm length from its ideal value (modulo one wavelength of the light) this may be $\sim 10^{-12}$ m depending on the servo-system which is controlling the locking position [13].

Low frequency intensity fluctuations can be reduced by monitoring a fraction of the laser intensity and feeding back to some element which allows the intensity to be varied, for example, the laser power supply or a variable attenuator in the laser beam [15].

Laser beam geometry and orientation noise The third type of laser noise is beam position and orientation jitter. This can lead to changes in the path traversed by a beam and hence to a false output signal if there are any resulting (fluctuating) path differences between the two arms. Varying beam geometry and position can also lead to imperfections in the overlap of the output light from the two arms of the interferometer if there is any asymmetry between the two arms. The excess noise at the output due to this is caused by the intensity changes which occur as the imperfectly matched phasefronts move with respect to each other on the photodetector and at the beamsplitter.

The effects of such noise have been investigated [11] and methods of reducing them explored. These methods include the use of monomode optical fibres as spatial filters and the use of the spatial filtering effect of optical cavities to make mode-cleaners.^[39] (Mode cleaners have the additional benefit of reducing the frequency noise on the light at high frequencies and can be used to provide a frequency reference).

Excess noise associated with motion of the test masses

Vibrational motion of the test masses can arise from three sources. Two of these are of a thermal nature.

Test mass and suspension thermal noise In a system with a resonant mode at angular frequency ω_0 there will be a stochastic driving force of thermal origin. This has the form [16]

$$\Delta F^2 = \frac{4kTm\omega_0\Delta f}{Q}, \quad (1.24)$$

where Δf is the measurement bandwidth and Q is the mechanical quality factor of the resonance.

First the internal resonant modes of the masses themselves are thermally excited. If the masses are designed so that the lowest resonance is above the frequency range of interest and the internal Q (Q_{int}) is high then this leads to a spectral displacement noise power of

$$\Delta x^2 = \frac{4kT\Delta f}{m\omega_0^3 Q_{int}}, \quad (1.25)$$

where m is the mass of the test mass. If the mass is a right circular cylinder with similar length and diameter then the displacement noise is given by

$$\Delta x^2 \approx 2.5 \frac{4kT\Delta f}{\pi^3 \rho v^3 Q_{int}}, \quad (1.26)$$

where v is the velocity of acoustic waves in the material which has a density ρ . The factor 2.5 is included since there will be several resonances at frequencies low enough to contribute to this noise [3].

The limit on gravitational wave amplitude due to this, allowing for masses at the ends of each arm of the interferometer and adding the noise powers from all of these contributions, is given by

$$h_{min} \approx 6 \times 10^{-25} \left[\frac{\rho}{2330 \text{ kgm}^{-3}} \right]^{-1/2} \left[\frac{Q_{int}}{10^6} \right]^{-1/2} \left[\frac{l}{3 \text{ km}} \right]^{-1} \left[\frac{v}{8500 \text{ ms}^{-1}} \right]^{-3/2} \sqrt{\Delta f} \quad (1.27)$$

for silicon which has a density of 2330 kg/m³ and a sonic velocity of ~ 8500 m/s.

The second source of displacement due to thermal noise is the pendulum mode with quality factor (Q_s) of the suspended mass on its suspension wires. This is, again, thermally excited and since this mode will be at a low frequency (typically 1 Hz) this leads to a motion of

$$\Delta x^2 = \frac{4kT\omega_0\Delta f}{mQ_s\omega^4}, \quad (1.28)$$

where ω is the observation angular frequency.

The corresponding h_{min} is then

$$h_{min} = 5 \times 10^{-24} \left[\frac{\nu_g}{100 \text{ Hz}} \right]^{-2} \left[\frac{mQ_s}{10^{10} \text{ kg}} \right]^{-1/2} \left[\frac{\omega_0}{2\pi \text{ s}^{-1}} \right]^{1/2} \left[\frac{l}{3 \text{ km}} \right]^{-1} \sqrt{\Delta f}. \quad (1.29)$$

This suggests the need for massive test masses (at least 100 kg) and high Q suspensions if gravitational waves of low frequency are to be detected. Comparison of the above spectrum with the graph of source strengths presented earlier shows that the detection of coalescing binaries or the lower frequency pulsars may be limited by the mass thermal noise.

Seismic and Vibrational noise The final source of vibrational noise is any motion of the suspension point which will be partially transmitted to the test mass. Such motion would certainly be caused by seismic ground motion and may also be caused by the operation of vibrating mechanical systems nearby. (The use of an ultra high vacuum to eliminate significant refractive index fluctuations in the arms would provide excellent acoustic isolation of the test masses except via the suspension wires.) A measurement of seismic motion at one potential site is reported in Appendix D.

Detection with real interferometers

There is always the possibility that there will be periods of high noise levels due to the random nature of the noise sources. It is therefore necessary to use more than one interferometer when looking for gravitational radiation near the threshold of measurement of the individual apparatus. There is also motivation for the operation of several detectors to enable the properties of the radiation to be studied in more detail by providing sensitivity to both polarisations and directional information about the source.

Chapter 2

Advanced interferometry techniques applicable to gravitational wave detection

2.1 Introduction

Several prototype detectors have been built [3, 17] to evaluate the performance of the basic interferometry techniques described in the previous chapter. Currently these interferometers operate with strain sensitivities of at best $\sim 2 \times 10^{-18}$ for pulses where the energy is in a band centred on 1 to 2 kHz. This is perhaps four orders of magnitude from a sensitivity appropriate to a working detector. In this chapter some of the techniques which will be required if the interferometers are to become sufficiently sensitive are described.

Photon shot noise is usually viewed as the most important noise source in laser interferometers. Two techniques for improving the performance of laser interferometers by improving their gravitational wave sensitivity for a given input light power are described below (sections 2.4 and 2.5). In preparation for this two possible modulation schemes (called ‘internal’ and ‘external’ modulation respectively) for phase measurements in interferometers are introduced and compared. The effects of such schemes on the signal to noise ratio of the detector are considered. (The need for the modulation techniques was explained in section 1.5.3.) The application of one of these (internal modulation) to an interferometer with cavities in its arms is discussed.

2.2 Modulation schemes

2.2.1 Internal modulation

All interferometric measurements of phase changes in a Michelson interferometer, which is intended for use as a gravitational wave detector, have to be made at high frequency. The measurement frequency must be chosen such that there is no excess laser intensity noise in that region of the spectrum (see section 1.5.3). (For example with the argon-ion lasers used in the current prototypes, this implies measurements be made at frequencies above about 3 MHz.) A radio-frequency modulation and demodulation scheme can be used as the basis for the measurement system (compare with the laser stabilisation method of Appendix B).

In a Michelson interferometer with delay-lines in the arms the technique known as ‘internal modulation’ has been used [3, 16]. This technique consists of applying differential phase modulation to the light beams in each of the arms of the interferometer. The signal from the output photodiode is demodulated in phase with the modulation. This yields a signal which is a measure of the phase difference between the amplitudes returning to the beamsplitter from each arm. The internal modulation scheme is illustrated (figure 2.1).

Electro-optic phase modulators are normally used to provide the phase modulation. These devices are based on crystals which have a refractive index which is proportional to an applied electric field perpendicular to the propagation direction (for one polarisation). The effect, on suitably oriented linearly polarised light, is to cause a change in the transit time in the device which is proportional to the applied electric field. Modulation of the electric field therefore causes phase modulation on the transmitted light.

A delay-line system can be arranged so that the beams entering and leaving the arms are non-overlapping. In this case the modulator for each arm can be placed either in the beam as it enters the arm or as it leaves to return to the beamsplitter. If the beams entering and leaving the arms overlap then the modulator must be placed in the combined beam. In this case care is required to ensure that the modulation applied on each pass through the modulator is in phase with that

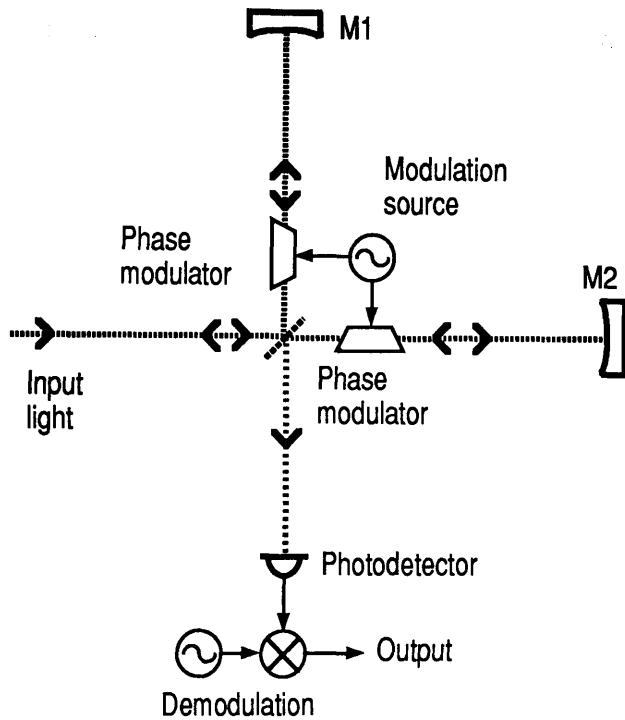


Figure 2.1: A Michelson interferometer with internal modulation. The delay-line arms are represented by showing one traverse each way. The mirrors $M1$ and $M2$ are highly reflecting. The phase modulation is applied differentially using the two modulators in the arms. The demodulated output signal is available for measurement and control.

applied on the other pass.

The signal which is expected from a single pass through an internal modulator in each arm is now considered. The amplitude (A_d) falling on the photodiode is given by

$$\frac{A_d}{\rho A_0 e^{i\omega_c t}} = \frac{1}{2} \left[\exp i \left(\delta_x + \frac{\beta \sin \omega_m t}{2} \right) - \exp i \left(\delta_y - \frac{\beta \sin \omega_m t}{2} \right) \right]. \quad (2.1)$$

This assumes a beamsplitter which has 50% transmittance and reflectance. The input amplitude has a magnitude A_0 and an angular frequency of ω_c . The phase modulation is sinusoidal with angular frequency ω_m and modulation index $\beta/2$. The modulation is applied differentially between the two arms labelled 'x' and 'y'. The phase shifts imposed on the light while traversing the arms are respectively δ_x and δ_y . The '-' sign for the second amplitude is chosen for convenience to give the output intensity minimum with zero phase difference between the light from the two arms. There are assumed to be intensity losses (L) associated with the mirrors and modulator in each arm. This leads to each arm having an amplitude reflectivity ($\rho = \sqrt{1-L}$) which is less than unity.

The signal from the photodiode is proportional to the power (I_d) on it. This is given by

$$I_d = A_d A_d^*, \quad (2.2)$$

where the star denotes complex conjugation. This gives the result

$$\frac{2I_d}{(1-L)I_0} = 1 - \cos(\delta_x - \delta_y + \beta \sin \omega_m t). \quad (2.3)$$

If the signal from the photodiode is demodulated coherently with the modulation only terms in $\sin \omega_m t$ remain and one obtains a signal voltage (S) with the form

$$S = \alpha I_0 (1-L) J_1(\beta) \sin(\delta_x - \delta_y), \quad (2.4)$$

where J_1 is the first order Bessel function of the first kind and α is a constant representing the size of the signal at the output of the demodulator for a given light power and phase shift (this constant includes the photodiode efficiency, the

transfer function of any amplifier before the demodulator and the insertion loss of the demodulator). This signal is of the same form as that previously obtained for the unmodulated interferometer (equation 1.15). The signal to noise ratio of this measurement system can closely approach that of the unmodulated system (as shown in section 2.2.3). Equation 2.4 can be used to calculate the signal to noise ratio for an internally modulated interferometer and it is used to this end in section 3.2.

General considerations related to the interferometer with internal modulation

It is interesting to consider some of the implications of internal modulation on the operation of the interferometer. This allows some of the limitations of the technique to be evaluated.

The interferometer may not have perfect balance between the arms. There will then be some non-interfered light at the output on the dark fringe. This light increases the power on the photodiode and hence the detection (photon shot) noise. The signal is not increased and so the signal to noise ratio is reduced. It is, therefore, necessary to ensure good symmetry of the arms to give good interference and to maximise the signal to noise ratio.

The output signal (equation 2.4) is bipolar in nature and is well suited to use in a control system designed to keep the interferometer output on a minimum. This requires control of the relative lengths of the arms and can be achieved by adjusting the positions of one or more of the interferometer mirrors or of the beamsplitter.

The electro-optic modulators available at present have some absorption (loss) and cause some wavefront distortion. The loss reduces the signal size for a given input power. The distortion, if unbalanced in the two arms, causes imperfect interference in the interferometer and so extra non-interfered light emerges from the output. It will be seen in the section (2.4) on recycling that the total losses in the interferometer must be minimised. The tolerable fractional intensity loss in a practical delay-line interferometer may be $\sim 10^{-3}$. Internal modulators could lead

to a loss in excess of this.

Conclusion to internal modulation

It has been shown that the signal produced at the output of the interferometer with internal modulation has a similar form to the signal produced in the unmodulated interferometer. This signal can be used to maintain the output of the interferometer on an interference minimum. It will be shown below that the signal to noise ratio which can be achieved with the internal modulation can approach that of the ideal unmodulated interferometer which has similar optical parameters. The losses introduced by the presence of the internal modulators may prevent the use of the recycling technique discussed below. It is therefore necessary to find a system which can provide the required signal without the need for modulators within the interferometer and the technique of ‘external modulation’ was proposed to satisfy this [18].

2.2.2 External modulation

In the external modulation system a reference beam is mixed with the output from the interferometer on the main photodiode. In practice a beamsplitter is used to add the reference and interferometer beams and so two photodiodes are required to detect all of the light. (The π phase difference between the internally and externally reflected beams at a beamsplitter requires that the signals from the two photodiodes are subtracted to form the desired output signal.)

The reference beam can, in principle, be any beam which has a simple phase relationship to the light in one of the arms of the interferometer. The best source of this beam is probably a beamsplitter which removes a small fraction of the amplitude from one of the arms. This ensures that the reference beam has the same frequency noise as the light in the interferometer. The reference beam (also called the local oscillator) is then phase modulated before addition to the interferometer output. One possible arrangement for external modulation is shown (figure 2.2). Here the reference beam is split off using the reflectivity of the otherwise unused

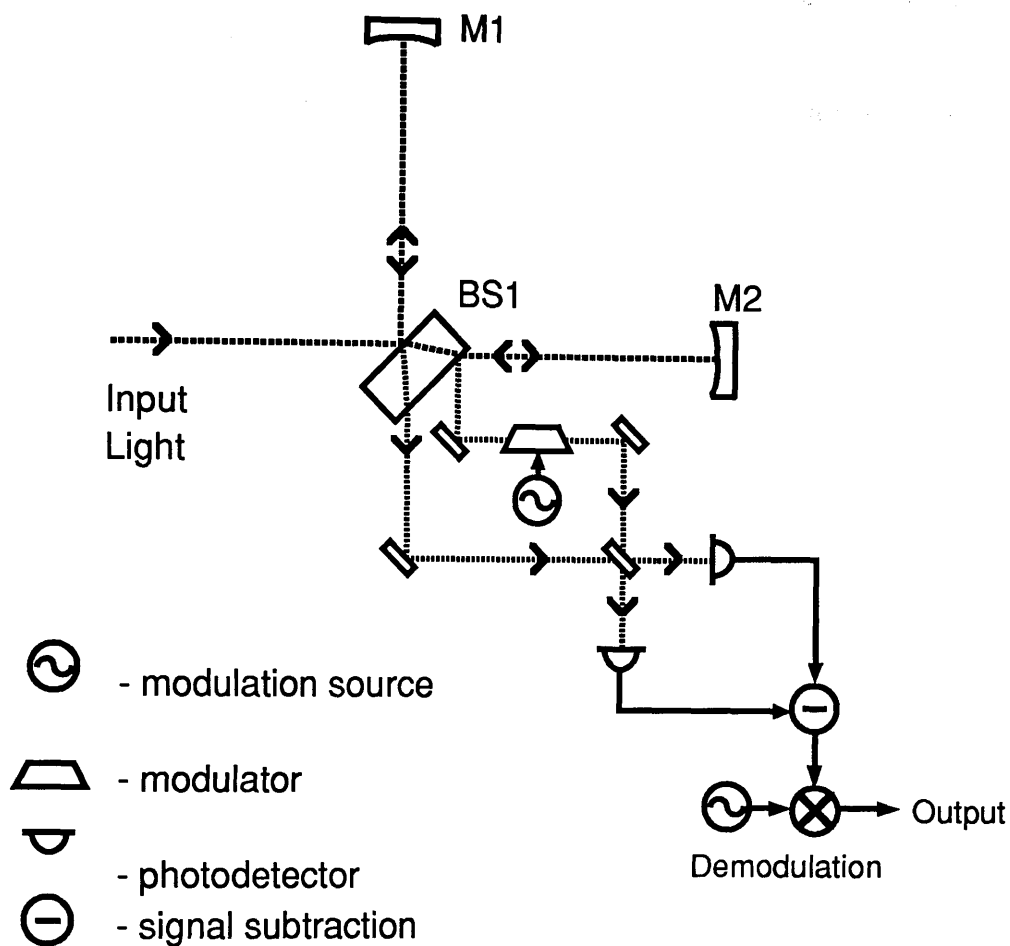


Figure 2.2: A Michelson interferometer with external modulation. The externally modulated reference beam is derived from the light in one of the arms of the interferometer and is added to the main output using the Mach-Zehnder arrangement shown. The main beamsplitter (BS1) has an anti-reflection coating on its rear surface. The finer dashes are used to represent low intensity light.

face of the beamsplitter. In practice the optimum amplitude of the reference beam will be obtained only with rather good anti-reflection coating of this surface (the anti-reflection coating may be required to have an amplitude reflectivity of ~ 0.03). An arrangement similar to a Mach-Zehnder interferometer is formed between the two beamsplitters. The modulator is no longer in the arms of the interferometer and in its new position higher losses can be tolerated.

The signal from an interferometer with external modulation is now calculated. It is assumed that the interferometer is again perfect except for some symmetrical losses in the arms. (The case of the imperfect interferometer is considered below.) The amplitude (A_d) on one of the output photodiodes is given by

$$\begin{aligned} \frac{\sqrt{8}A_d}{\rho A_0 e^{i\omega_c t}} &= \exp(i\delta_x) - \left(1 - \frac{1}{m^2}\right) \exp(i\delta_y) \\ &+ \frac{\sqrt{2}}{m} \left(1 - \frac{1}{2m^2}\right) \exp[i(\delta_y + \Delta + \beta \sin(\omega_{m1}t))]. \end{aligned} \quad (2.5)$$

The notation used is the same as for internal modulation. In addition Δ is the phase difference between the reference beam and the 'y' arm beam at the Mach-Zehnder beamsplitter. The fraction of the amplitude in the 'y' arm which is split off by the anti-reflection coating on the beamsplitter is $1/m$ (in each direction). One of the reflections from this coating is wasted. Again sinusoidal phase modulation is shown. The amplitude on the other diode is just the same expression multiplied by -1 .

The power on one diode (I_d) is (omitting some terms of order higher than $\frac{1}{m^4}$ in the small quantity $\frac{1}{m}$)

$$\begin{aligned} \frac{4I_d}{(1-L)I_0} &= 1 - \left(1 - \frac{1}{m^2}\right) \cos \delta + \frac{1}{2m^4} + \frac{1}{m^2} \\ &+ \frac{\sqrt{2}}{m} \left(1 - \frac{1}{2m^2}\right) \cos(\delta + \Delta + \beta \sin \omega_{m1}t) \\ &- \frac{\sqrt{2}}{m} \left(1 - \frac{2}{2m^2}\right) \left(1 - \frac{1}{2m^2}\right) \cos(\Delta + \beta \sin \omega_{m1}t), \end{aligned} \quad (2.6)$$

where $\delta = \delta_x - \delta_y$. The static terms in this expression show the expected power of the reference beam and the minimum power from the interferometer due to the

extraction of some light from one arm. The signal terms I_{dsig} can be extracted and re-arranged to give

$$\frac{\sqrt{8m}I_{dsig}}{(1-L)I_0} \approx \cos(\delta + \Delta + \beta \sin \omega_{m1}t) - \cos(\Delta + \beta \sin \omega_{m1}t) \quad (2.7)$$

$$+ \frac{1}{2m^2}[3 \cos(\Delta + \beta \sin \omega_{m1}t) - \cos(\delta + \Delta + \beta \sin \omega_{m1}t)].$$

Demodulation, coherent with the phase modulation, of the difference signal from the two output photodiodes, selects the terms in $\sin \omega_{m1}t$. This gives a signal (taking only the first two terms from equation 2.7)

$$S \approx \frac{I_0(1-L)\alpha\sqrt{2}J_1(\beta)}{m} [\sin(\delta) \cos(\Delta) + \cos(\delta) \sin(\Delta) - \sin(\Delta)], \quad (2.8)$$

where α is the same constant as for internal modulation. If δ is small (as it is when the interferometer is operating) the demodulated signal is

$$S = \frac{I_0(1-L)\alpha\sqrt{2}J_1(\beta)}{m} \left[\delta \cos \Delta - \frac{\delta^2}{2} \sin \Delta \right]. \quad (2.9)$$

This equation shows that the phase relationship between the reference beam and the interferometer output must be controlled. The signal from the main interferometer (δ) is multiplied by the cosine of the phase difference between the amplitude from the interferometer and the reference beam. This phase difference must be maintained close to zero (modulo π). This can be achieved by controlling the relative path length of the two halves of the Mach-Zehnder. When this is achieved the above signal has the same form as that obtained from the interferometer with internal modulation and from the unmodulated interferometer.

General considerations concerning external modulation

It is useful to consider some general aspects of the operation of the interferometer with external modulation in order to prepare for the design of a system which can be used to test the technique. The term ‘effective amplitude contrast’ is

introduced to allow the ideas below to be discussed. It is defined to be the ratio of the magnitude of the amplitude approaching the main beamsplitter from the input of the interferometer to the magnitude of the amplitude leaving the main beamsplitter and reaching the photodiode when the output of the interferometer is at a minimum. In external modulation the output amplitude which reaches the second beamsplitter is used since there are two photodiodes. The effective contrast is a measure of the quality of the interference in the interferometer.

In the section on recycling it will be seen that the total loss of power from the interferometer should be minimised (for a given output signal size). Since the reference beam represents a power loss the maximum value of m consistent with the optimum signal to noise ratio should be used. The value of m should therefore be chosen to be slightly less than the effective contrast. In this case the amplitudes on the photodiodes are dominated by the reference beam. (A typical value required for the effective contrast may be 100—see section 2.4). This justifies the above assertion that the anti-reflection coating used to split off the reference beam should have small reflectivity.

The signal to noise ratio achieved using the external modulation system depends on the total light on the photodiodes for a given output signal. If the intensity on the photodiodes is dominated by the local oscillator then increasing this increases the signal and the noise at almost the same rate. If the intensity is dominated by non-signal forming light then the signal to noise ratio is smaller. The signal to noise ratio is discussed further in section 2.2.3. (With the above choice of m the m^{-3} terms in equation 2.8 are small compared to any similar terms produced due to the finite effective contrast.)

The extent to which any motions (which change Δ) of the components of the external modulation system couple into the interferometer output signal is governed by the amplitude leaving the interferometer output. This can be seen by considering the case where the amplitudes from the two arms differ by an amount a . The amplitude on one photodiode is then

$$\frac{\sqrt{8}A_d}{(1-L)A_0e^{i\omega ct}} = (1-a)\exp(i\delta_x) - \exp(i\delta_y) \quad (2.10)$$

$$+ \frac{\sqrt{2}}{m} \exp[i(\delta_y + \Delta + \beta \sin(\omega_{m1}t))]. \quad (2.11)$$

If $\delta = 0$ the demodulated signal from the two photodiodes becomes

$$S = \frac{\alpha I_0(1-L)\sqrt{2}J_1(\beta)}{m} a \sin \Delta. \quad (2.11)$$

The dependence of the output signal on $a \sin \Delta$ can be seen and must be taken into account when designing an interferometer with external modulation.

Frequency noise on the reference beam is unlikely to cause excess noise in the detected output if the reference beam is obtained from inside the interferometer when the phase changes due to frequency noise in the Mach-Zehnder should be smaller than those occurring in the Michelson interferometer because of the same noise.

A method of deriving control signals for external modulation

Now that the principle of external modulation has been introduced it is necessary to consider the design of a suitable control system. In the above scheme two path lengths must be controlled. These correspond to control of the Michelson phase (δ) to keep the interferometer on a dark fringe and of the Mach-Zehnder phase (Δ) to ensure that the output signal is maximised and remains of consistent polarity. Control of the Michelson interferometer can be achieved in the same manner as with internal modulation (i.e. feedback of the main output signal to control the arm lengths).

One method of controlling the Mach-Zehnder involves first applying a small differential arm length modulation to the main interferometer. The angular frequency (ω_{m2}) of this modulation is chosen to be just above the expected gravitational wave angular frequencies. (So a frequency in the range $1 \sim 10$ kHz may be appropriate.) The signal (S') produced at the output of the original (ω_{m1}) demodulator is now (keeping only the interferometer signal term from equation 2.9 and assuming that a control system is maintaining $\delta \approx 0$)

$$S' = \frac{\alpha I_0(1-L)\sqrt{2}J_1(\beta)}{m} (\beta_2 \sin \omega_{m2}t) \cos \Delta, \quad (2.12)$$

where β_2 is the, small, modulation index of the ‘second’ modulation. If this is further demodulated at ω_{m2} then the output of the second demodulator is a measure of the size of the signal due to the interferometer modulation of the arm length at ω_{m2} .

The length of one of the arms in the Mach-Zehnder must be adjusted to maximise the test signal and hence any gravitational wave signal. The maximisation can be achieved by modulating the position of one of the mirrors forming the Mach-Zehnder at an angular frequency ω_{m3} . This modulation must be at a lower frequency than the second modulation to be correctly demodulated by the second demodulator. The last modulation must then be at a frequency slightly below that of the lowest expected gravitational wave signal. (It must not be within the signal band where it could then obscure a signal.) The signal from the output of the second demodulator is now

$$S' = \frac{\sqrt{8}\alpha' I_0(1-L)J_1(\beta)J_1(\beta_2)}{m} \cos(\Delta + \beta_3 \sin \omega_{m3}t), \quad (2.13)$$

where $\alpha' = \alpha$ if the demodulator has no insertion loss.

Subsequent demodulation of the output of the ω_{m2} demodulator at ω_{m3} produces a signal

$$S'' = \frac{\alpha''\sqrt{32}I_0(1-L)J_1(\beta)J_1(\beta_2)J_1(\beta_3)}{m} \sin \Delta, \quad (2.14)$$

where again α''/α' is a measure of the demodulator insertion loss. This signal can be used as the error signal in a control system designed to lock the Mach-Zehnder arm length to a zero of $\sin \Delta$. Full details of this control system are presented in Chapter 3. (The scheme is illustrated in figure 3.9.)

Conclusion

It has been shown that external modulation can produce a signal of the same form as internal modulation without requiring the addition of any lossy component to the interferometer. There is an extra degree of freedom (the relative path lengths in the Mach-Zehnder) which must be controlled if the system is to operate correctly.

Motions of the additional mirrors required can couple into the output signal and this coupling depends on the effective contrast of the interferometer. The presence of frequency noise can also cause excess noise in the output signal and this is best avoided by using a reference beam obtained from inside the interferometer as described above. The suggested method of control has been tested by the author (as reported in Chapter 3).

2.2.3 Modulation and measurement noise

Introduction

The modulation techniques discussed above yield signal to noise ratios close to that given for the unmodulated interferometer in section 1.5.2. (Where the noise is photon shot noise.) It was recently recognised [19, 20] that for many of the situations encountered in gravitational wave detection, including both of the above modulation schemes, sinusoidal phase modulation does not, in fact, provide the same signal to noise ratio as the unmodulated case.

An elegant method of calculating the effects of modulation on signal to noise ratio was suggested by Meers[21]. This method is described and used below.

The results of an experimental test of some of the predictions made in this section are presented (section 3.6).

Internal modulation

A photodiode measures power and so it is a square law detector of amplitude. This leads to mixing of the incident amplitudes with each other and with the white noise which can be considered as originating from the detection of vacuum fluctuations [9]. Application of this model allows calculation of the effects of modulation on the noise in the output signal from an interferometer.

In all of the cases considered below the modulation and demodulation waveforms are in phase and have symmetrical amplitude distributions about zero amplitude.

First consider internal sinusoidal phase modulation. In the frequency domain the amplitudes from the two arms approaching the beamsplitter consist of a component at the original laser frequency (ω_c) with phase modulation sidebands at $\omega_c + \omega_m$ and $\omega_c - \omega_m$. There will also be some other sidebands due, for example, to gravitational wave signals. These are not important to the argument if they are small (as they should be).

Perfect interference would allow the cancellation of the carrier light leaving only the sidebands which (for differential modulation) will add constructively. The amplitude incident on the photodiode can be represented by figure 2.3. The white noise in areas 'a' and 'b' in the figure are mixed with the modulation sidebands to give a signal. This signal shows these two uncorrelated noises near ω_m . In addition noise from region 'c' at $\omega_c + \epsilon$ mixes with each of the sidebands to give noise at both $\omega_m + \epsilon$ and $\omega_m - \epsilon$. These contributions originate from the same source and so noise at $\omega_m + \epsilon$ is correlated with noise at $\omega_m - \epsilon$.

If this signal is then demodulated by multiplication with a sinusoidal signal at ω_m (but not necessarily in phase with the modulation) then there are two cases worth consideration.

Case 1: demodulation with the phase which would maximise any signal. Any signals or noise at $\omega_m + \epsilon$ and $\omega_m - \epsilon$ are added together to produce the maximum signal. Remembering that noise powers must be added this leads to the addition of three uncorrelated sets of noise. There is one (arbitrary) unit of noise power originating from each of regions 'a' and 'b' and four units of noise power as a result of coherently adding the two amplitude units of noise from region 'c' before squaring to obtain the power. There are therefore a total of six units of noise power in the demodulated output in the signal band. The four of these which come from region 'c' would be measured by any system (with or without modulation) and correspond to the optimum detection case (as in the unmodulated interferometer). Sinusoidal modulation and demodulation therefore gives a signal to noise ratio worse than optimum by $\sqrt{3/2}$ (in amplitude).

Case 2: demodulation with the (quadrature) phase which would minimise any signal. In this case any signal sidebands yield no contribution in the demodulated

output. This is also true for the noise which originates at signal frequencies. There remain, however, the two units of noise mixed down by the modulation procedure. This case is interesting only as it provides a test of the predictions made by this calculation.

In practice

The above argument applies to an interferometer with a perfect null. There will be some unmodulated light coming out of the interferometer. The extra light is not correlated to the modulation sidebands and so behaves as a separate beam which causes normal unmodulated shot noise as expected. This noise tends to mask the excess noise due to the modulation if the extra light begins to dominate the total intensity on the photodiode.

If an interferometer is limited by the noise due to modulation then it is useful to know if another modulation and/or demodulation waveform could improve the signal to noise ratio. Schnupp[19] predicts that square wave modulation and demodulation would give the optimum performance.

The frequency domain argument above becomes a little messy when there are an infinite number of sidebands. Square waveforms can only be approximated experimentally in any case. It was therefore felt to be instructive to apply the frequency domain method to the two frequency approximation to the square wave, namely $\cos(\omega_m t) - (1/3) \cos(3\omega_m t)$.

Taking this as the modulation function and retaining sinusoidal demodulation the above process is repeated. The appropriate sideband diagram is shown (figure 2.4). The important point to note in this case is that the contributions in the signal from the photodiode from regions 'd' and 'e' due to mixing with first and third order sidebands partially cancel. This is due to the fact that the first and third harmonic components of the modulation waveform have the opposite sign and lead to signals with the opposite signs. The noise power in the signal band of the demodulated output is (in the same units as above) $(1/3)^2 = 1/9$ from each of regions 'a' and 'b'; $(1 - 1/3)^2 = 4/9$ from 'd' and 'e' and finally the same 4 from region 'c'. The total is $46/9$ which is an improvement on the sine-wave case. Looking at the above the optimum level of the third harmonic in the modulation is $1/2$ of the fundamental. (It can be seen that the sum of the above terms is

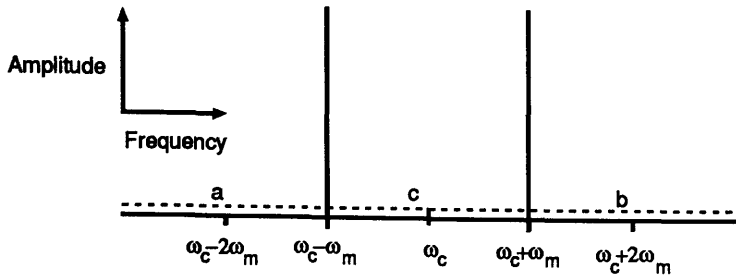


Figure 2.3: *The spectrum of the light amplitude incident on the photodiode at the output of an internally sinusoidally modulated interferometer. The magnitudes of the components are indicated. The spectrum is shown over a few modulation frequencies (ω_m) either side of the carrier (ω_c). The vacuum fluctuations lead to the white noise represented by the broken line above the frequency axis.*

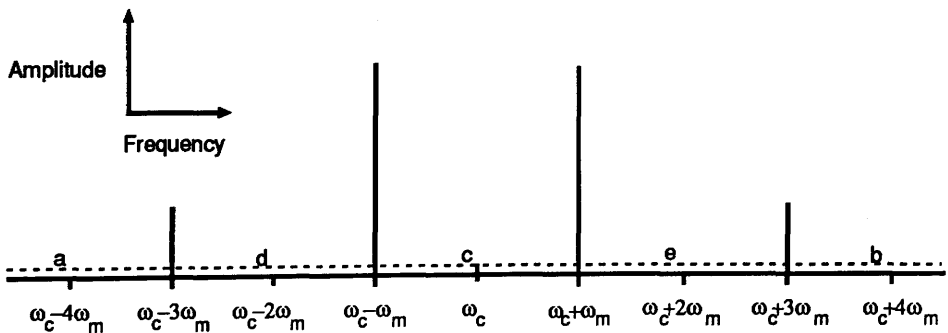


Figure 2.4: *The amplitude spectrum approaching the photodiode in an interferometer with internal modulation with the waveform which is the best two harmonic frequency approximation to a square wave.*

minimised if the third harmonic amplitude is $1/2$). There are then 5 units of noise power at the output.

It should be noted that if the modulation and demodulation waveforms are interchanged then the result is unaltered. This can be seen in the above case by considering the effect of demodulating at the third harmonic (with only sine wave modulation). The signals from regions 'a' and 'b' are then introduced by the demodulation. The signals from both regions 'd' and 'e' demodulated by each of the demodulation frequencies partially cancel to give the same result as above.

As further harmonics are added to the modulation and/or demodulation waveforms and these waveforms approach square waves the signal to noise ratio approaches the optimum (unmodulated) value.

External modulation

In the situation of external modulation there are two essential differences. First the instantaneous size of the signal from the photodiode depends on the sine of the phase modulation angle of the local oscillator and this implies that the modulation angle should be large ($\pm\pi/2$). Secondly the intensity on each photodiode is constant if the output is dominated by the local oscillator. (Since then only phase modulated light is present.) In the case of square wave external modulation it can be shown that the amplitude spectrum of the light on the photodiodes is the same as for square wave internal modulation. The same, optimum, signal to noise ratio can therefore be achieved with this type of modulation and square wave demodulation.

The amount by which the signal to noise ratio is decreased from the optimum for any given pair of modulation and demodulation waveforms can be calculated by comparing the signal power produced by the modulation ($M(t)$) and demodulation ($D(t)$) functions and the noise power which depends only on the demodulation function. The instantaneous signal from the photodiode is proportional to the sine of the phase of the modulation waveform (this can be seen from the earlier discussion of external modulation). This signal is weighted by the demodulation

waveform and must then be averaged over a multiple of the period of the modulation waveform to give the size of the output signal (S). The signal power is then proportional to the square of this and is therefore

$$S^2 = \overline{D(t) \sin M(t)}^2 \quad (2.15)$$

so that a power of unity would be obtained with square-wave modulation and demodulation (the averaging is denoted by the overline).

The noise power is independent of the modulation waveform (since the intensity of the light is constant at the photodiode) but the signal from this is weighted by the demodulation waveform. The resulting output noise power (N^2) is given by

$$N^2 = \overline{D(t)^2}, \quad (2.16)$$

where this is again averaged over a multiple of the period of the modulation waveform. This also evaluates to unity for square wave demodulation.

For sine wave modulation and square wave demodulation the signal to noise ratio, compared to the optimum, therefore becomes

$$\frac{1}{2\pi} \int_0^{2\pi} \sin(\beta \sin \theta) d\theta. \quad (2.17)$$

This is maximised when the modulation index (β) is chosen to maximise $J_1(\beta)$ (i.e. $\beta \approx 1.8$) yielding a signal to noise ratio ≈ 2 dB worse than the optimum. The use of sinusoidal demodulation can be shown to give marginally better signal to noise ratio than square wave demodulation in this case.

Conclusion

The above discussion of the effects of modulation techniques on the signal to noise ratio of the internal modulation and external modulation measurement systems reveals several interesting features. In both cases the signal to noise ratio can reach the ‘optimum’ value due to photon shot noise if the correct modulation and demodulation waveforms are used. The required square wave modulation may be

2.3 A Michelson interferometer with cavities in the arms and internal modulation

2.3.1 Introduction

In Chapter 1 the need to increase the time that the light spends in the arms of an interferometer to obtain improved detector sensitivity at low frequencies was outlined. One method which could be used to achieve this, the use of optical cavities in the arms of the interferometer, was introduced. An interferometer with cavities in its arms could have one important advantage over a delay-line system. If the desired storage time of the arms implies that the light must make many traverses then a cavity system has the advantage of requiring a smaller mirror area. The size of mirror which is required in either system is set by the allowable diffraction losses and the distribution of the light on the mirror. In a cavity system there is only one spot on each mirror; in a delay-line there may be several tens of spots. Since these spots are of the same order of size the delay-line mirrors must be considerably larger.

The 10 m prototype detector at Glasgow[3] is an interferometer with cavities in its arms. At one time the light from each of the cavities was interfered in order to obtain the output signal. A polarisation scheme was used to separate the light for the two arms before it entered the interferometer where orthogonal polarisations were directed into the arms by a polarising beamsplitter. This allowed the use of modulators outside of the interferometer since each polarisation could be modulated individually. This scheme was not absolutely successful as is reported by Kerr [22]. A scheme where the beams returning toward the beamsplitter from the cavities were directly detected, rather than being interfered, was then implemented. This system, which was successful, does not allow the use of the ‘recycling’ techniques discussed below (section 2.4). It was therefore thought to be worthwhile to study an interferometer with internal modulation and cavities in its arms as a step on the path from the present prototype to one possible design of working detector. The expected properties of such a system are evaluated below.

2.3.2 The signal from an interferometer with cavities in its arms

The proposed modulation scheme is illustrated (figure 2.5). Here the delay-lines are replaced by cavities. The beams entering and leaving the arms overlap. Linearly polarised light is used to illuminate the system.

The amplitude of the light reflected from one of the cavities can be considered to consist of a component (A) directly reflected from the ‘inboard’ mirror (M_2, M_1) and a component (C) due to the transmission by the inboard mirror of some of the amplitude which has built-up in the cavity. (These amplitudes are calculated in detail in Appendix A.) The former amplitude components illuminate only the Michelson interferometer formed by the inboard mirrors and the beamsplitter. This light will be modulated on each pass through the modulator. The net result of this double modulation depends on the phase change in the modulating signal between the two passes of the light and also on the relative phases of the sidebands and the carrier on return to the modulator. If the distance between a modulator and an inboard mirror is small compared to the speed of light multiplied by the period of the modulation waveform then the significance of the double modulation is determined by the properties of the cavity.

As for the case of frequency stabilisation of a laser to a cavity the cavity is arranged to be resonant for the original laser (carrier) frequency. The modulation frequency is chosen to be much higher than the corner frequency of the cavity integration but not at a free spectral range of the cavity and so the phase modulation sidebands do not resonate in the cavity.

If the cavity has perfect visibility¹ then the cavity amplitude has the same magnitude but opposite sign to the directly reflected carrier. The carrier amplitudes cancel to leave the sidebands due to phase shifts in the cavity and any modulation sidebands. In practice the visibility will depart from unity. If the cavity amplitude is less than the directly reflected amplitude the cavity is said to be ‘undercoupled’ and there is a net component of the carrier which has suffered a π phase change on reflection from the cavity. The second modulation pass will then tend to enhance the total modulation sideband amplitude. In the case of an ‘overcoupled’

¹Visibility is defined in Appendix A.

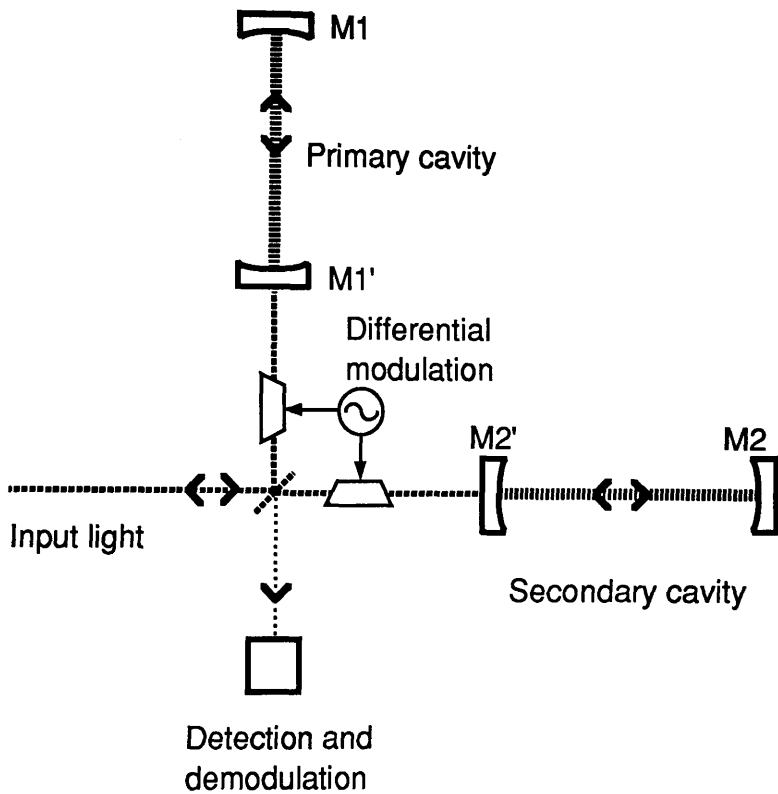


Figure 2.5: *An interferometer with cavities in its arms and internal modulation. The modulation is applied differentially. The cavities are formed by the mirror pairs and the input mirrors are partially transmitting.*

cavity, the cavity amplitude exceeds the directly reflected one and there is a net carrier component reflected with no phase change. The second modulation pass then reduces the amplitude of the modulation sidebands on this beam.

The cavity amplitudes have their first modulation removed by the integrating action of the cavity (Appendix A). These amplitudes are therefore modulated once only. The phase shifts (from whatever source) are labelled as (a) and (c) in the inboard Michelson interferometer and (b) and (d) in the respective cavities. The amplitude incident on the photodiode is then

$$-A_x \exp i(a+2\beta) + C_x \exp i(a+b+\beta) + A_y \exp i(c-2\beta) - C_y \exp i(c+d-\beta), \quad (2.18)$$

where the 'x' and 'y' subscripts identify the arms. β represents the phase modulation appropriate to one pass through the modulator and is of the form $\beta_0 \sin \omega_m t$. The signs have been chosen to give the expected results with zero values of the phase shifts (for example minimum output from the interferometer).

The components of the output intensity which, when demodulated, can contribute to a signal are

$$\begin{aligned} -A_x A_y \cos(a - c + 4\beta) & \quad -A_x C_x \cos(b - \beta) & (2.19) \\ -A_y C_y \cos(d + \beta) & \quad +A_x C_y \cos(a - c - d + 3\beta) \\ +A_y C_x \cos(a - c + b + 3\beta) & \quad -C_x C_y \cos(a + b - c + d + 2\beta) \end{aligned}$$

and the demodulated signal is proportional to

$$\begin{aligned} -A_x A_y J_1(4\beta_0) \sin(a - c) & \quad +A_x C_x J_1(\beta_0) \sin(b) & (2.20) \\ -A_y C_y J_1(\beta_0) \sin(d) & \quad +A_x C_y J_1(3\beta_0) \sin(a - c - d) \\ +A_y C_x J_1(3\beta_0) \sin(a - c + b) & \quad -C_x C_y J_1(2\beta_0) \sin(a - c + b - d). \end{aligned}$$

If the modulation indices are small ($\beta_0 \ll 1$) then $J_1(\beta_0) \approx \beta_0/2$. Also if all of the phase shifts are close to zero (the case for an operating detector with the cavities on resonance and the output intensity a minimum) the output signal

reduces to

$$\begin{aligned}
 & -A_x A_y 4(a - c) \quad + A_x C_x (b) \quad - A_y C_y (d) \quad (2.21) \\
 & + A_x C_y 3(a - c - d) \quad + A_y C_x 3(a - c + b) \quad - C_x C_y 2(a - c + b - d),
 \end{aligned}$$

where the factor $\beta_0/2$ has been extracted for clarity.

If the phase changes are due to gravitational waves (or frequency noise) then those associated with the cavities will be larger than the others by the the effective number of bounces in the cavity times the ratio of the lengths of the cavities to the length of the inboard Michelson interferometer arms. This should be at least several hundred in a working detector. If the reflectivities $\frac{ie\omega}{\hbar}$ of the inboard mirrors are equal then the signal due to gravitational radiation is, to a good approximation, proportional to

$$b[4AC_x - 2C_x C_y] - d[4AC_y - 2C_x C_y], \quad (2.22)$$

where the substitution $A = A_x = A_y$ has been made (these quantities depend only on the beamsplitter and inboard mirror reflectivities). The size of the signal for a given cavity phase shift is therefore determined by the ratio of the magnitude of the cavity amplitude to that of the directly reflected amplitude. This ratio can range from zero through one to a maximum of two. The respective signal sizes are zero, increasing to two and decreasing back to zero (in the units used in equation 2.22). This expression is used to calculate the expected signal size for a differential arm length change in the interferometer on which the system was tested (section 3.2).

It is interesting to note that if the cavity phase shifts (b, d) are of the same sign and magnitude then, if the cavities have identical properties, the signal cancels completely. This would be the case if the phase shifts were due to frequency noise on the input laser light and is the property of ‘subtraction’ which gives rejection (at the output) of any common mode phase signals in the two arms. If there is some imbalance between the properties of the two arms then the fidelity of subtraction is reduced.

It is important to consider the implications of the above output signal for a control system used to keep the cavities on resonance and the output on an

interference minimum. The phase shifts can now be replaced by the equivalent mirror motions which would cause them. It is reasonable to consider only one arm. Then the output signal becomes (with the same assumptions as 2.22)

$$2G(\omega)k(x' - x)[4AC_x - 2C_xC_y] + 2kx[-4A^2 + 3AC_y + 3AC_x - 2C_xC_y], \quad (2.23)$$

where k is the wavenumber of the light, x is the round-trip distance of the inboard mirror from the beamsplitter (modulo one wavelength of the laser light) and x' is twice the distance of the outboard mirror from the beamsplitter. $G(\omega)$ is the amount by which the phase shift is enhanced by the multiple reflections in the cavity. It decreases at high frequencies. The other arm has an equivalent expression.

Motions of the outboard mirror appear only in the cavity term and there is nothing surprising about the behaviour of the signal from this (in that above the cavity corner frequency the signal declines with increasing frequency as does the signal from any cavity). Motions of the inboard mirror may appear with opposite signs in the two terms depending on the degree of coupling of the cavity and there can be a situation where the sign of this signal reverses as the signal frequency increases. This occurs in the overcoupled case.

This effect could make design of a control system difficult if the control system was required to operate above the frequency of the sign reversal which depends on the relative magnitudes of the terms in equation 2.23. In practice the Michelson interferometer term is relatively small compared to the cavity term, with the substitution $G = 1$, for all values of overcoupling $1 < C < 2$. The sign reversal therefore occurs at a frequency comparable to the free spectral range of the cavity at which the control system would fail to operate in any case.

Control of an interferometer with cavities in the arms

In order to control the interferometer with cavities it is necessary to derive three independent control signals. One signal is required to keep each cavity on resonance with the laser light and one is required to maintain the output on a minimum.

There must also be a signal which represents the differential phase shifts produced by gravitational radiation.

Signals which give information about one cavity are obtained if some of the light reflected from the cavity is split off before its return to the beamsplitter. Detection and subsequent demodulation gives the required signal. There is, however, a compromise between the amount of light which is removed for the purpose of control and that which is left to give the important interferometer output signal (and the amount left to be 'recycled' if the technique described below is to be implemented). If the laser frequency is stabilised to the length of one of the cavities using a small amount of light then frequency noise will be imposed on the light due to the relatively high shot noise on the small amount of light detected. Whether this amount of frequency noise is important depends on the common mode rejection (or subtraction) of frequency noise by the interferometer as a whole.

An experimental test of control systems for internal modulation with cavities is described below (section 3.2).

2.4 Recycling

The technique known as ‘recycling’ was proposed by Drever [23] to make efficient use of the available illuminating laser power. It is presented here as an important idea in its own right and also as an introduction to ‘dual recycling’ a related technique (discussed in section 2.5).

2.4.1 Introduction to recycling

Choice of a storage time for the arms of an interferometer (either delay-lines or cavities) determines the number of traverses of the arms required of the light if the arm length is fixed. The arms should be long to reduce the importance of noise sources which do not scale with arm length. The number of traverses required may therefore be quite small for a detector optimised for gravitational wave frequencies of above a few hundred hertz (e.g. ~ 30 for a detector with 3 km arms). If the mirrors are of sufficiently low loss then most of the light will emerge from the arms. When the output of the interferometer is at the interference minimum most of the laser light is reflected back out of the input port of the interferometer.

In the above picture the light reflected by the interferometer appears to be wasted. However, it can instead be ‘recycled’. A partially transmitting mirror (M0—figure 2.6) is placed in the path of the light entering the interferometer. This is made to form a resonant optical cavity with the virtual mirror formed by the highly reflecting interferometer. This cavity is split into two arms M0 to M1 and M0 to M2 (where the two paths need not be exactly the same length). The round trip phase shift on the carrier must be identical for the two paths (this is the condition for the interferometer output to be at a minimum). This round trip phase shift (δ_c) must be controlled to maintain the cavity on resonance with the laser light when the light amplitude within this cavity, and hence within the arms of the interferometer, is maximised.

Comparison with a normal cavity (Appendix A) shows that the magnitude of

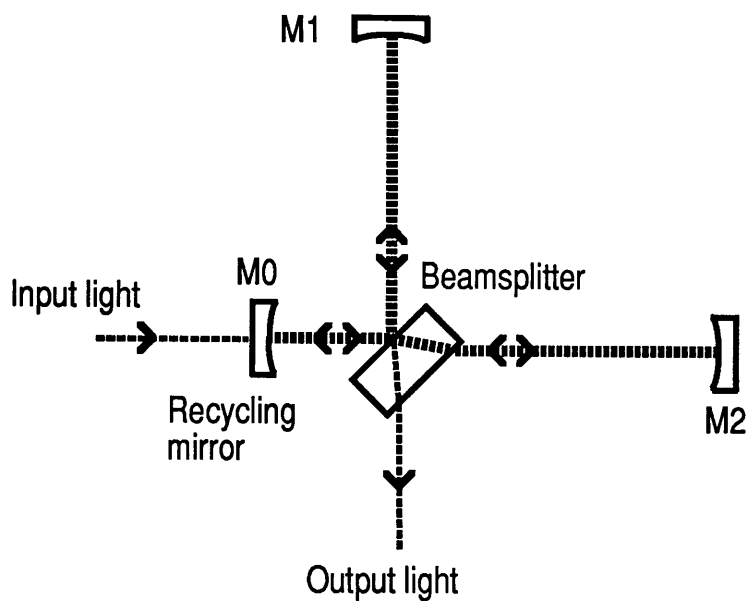


Figure 2.6: *The basic principle of power recycling. The recycling mirror $M0$ is added to the interferometer. This mirror is positioned so that the light reflected from the interferometer is resonant in the cavity formed.*

the amplitude approaching the beamsplitter from M0 is given by

$$\frac{A_i}{A_0} = \frac{t_c \rho}{1 - r_c \rho}, \quad (2.24)$$

where A_0 is the magnitude of the amplitude in an arm with no recycling, A_i the new amplitude in that arm with recycling, t_c is the amplitude² coefficient of transmission of M0 and r_c its reflectivity, ρ is the reflectivity of each of the arms of the interferometer and the phase shift (δ_c) imposed on the carrier light on one round trip of the cavity is zero. (It is assumed that the arms have identical losses and that the losses from the output of the interferometer are small.)

As an example of the application of recycling consider an interferometer with 3 km arms which are delay-lines which the light traverses 15 times in each direction and assume that on each reflection at a mirror 5×10^{-5} of the light intensity is lost. The total losses associated with each arm are thus 1.45×10^{-3} and if the interferometer is otherwise perfect the amplitude in the arms can be increased by up to ≈ 27 .

The light which is stored in the recycling cavity will have any frequency noise components above the cavity linewidth attenuated by the integrating effect of the cavity (as shown in Appendix A). The recycling cavity then behaves ^{as} a low pass filter with the frequency noise on the light within the recycling cavity falling as $\sim 1/f$ above the corner frequency of the integration. This corner angular frequency (ω_f) is (from Appendix A) given by

$$\omega_f = \frac{1}{2\tau_c}, \quad (2.25)$$

where τ_c is the storage time of the recycling cavity. For the above example the storage time is ~ 0.6 seconds.

2.4.2 The split-cavity argument applied to power recycling

It is useful to explicitly calculate the gravitational wave sensitivity of a recycled interferometer especially since the method used is well suited to the analysis of the more complicated dual recycling system which is described below.

²All coefficients of transmission and reflection in this thesis are amplitude coefficients unless otherwise stated.

The recycled interferometer can be modelled as a ‘split-cavity’ system. The light is considered to be composed of an original carrier frequency and a set of sidebands which are due to phase changes imposed on the light. Considering the phase changes due only to gravitational radiation equation 1.12 can be restated as

$$\delta\phi = \frac{h\omega \sin(\omega_g\tau/2)}{2\omega_g} [\exp(i\omega_g(t - \tau/2)) + \exp(-i\omega_g(t - \tau/2))]. \quad (2.26)$$

This is the expression for the phase shift imposed on the light which traverses one arm of an interferometer once each way taking a round trip time τ . The amplitude resulting from this is proportional to $e^{i\delta\phi}$. The two sideband nature of this signal can be seen by expanding this exponential. Since the phase changes due to gravitational radiation are always small the effect of the phase shift is to multiply the carrier by $1 + i\delta\phi$ to give the two sideband amplitudes explicitly.

The interferometer is composed of two arms which each lead to a similar set of sidebands which if produced by gravitational radiation of the ‘plus’ polarisation are out of phase. If the interferometer is set to operate such that the output is at an interference minimum for the carrier light then the carrier will leave the input port while the sidebands will leave the output port. The sidebands from the two arms will add constructively to give a relative sideband amplitude

$$\frac{A}{A_0 e^{i\omega t}} = i\Delta, \quad (2.27)$$

where, for clarity,

$$\Delta = \Delta_0 [\exp i\omega_g(t - \tau/2) + \exp[-i\omega_g(t - \tau/2)]] \quad (2.28)$$

and in turn

$$\Delta_0 = \frac{h\omega \sin(\omega_g\tau)}{\omega_g}. \quad (2.29)$$

The effect of M0 and the consequent multiple reflections of the carrier light within the system can be dealt with in the same manner as the summation of the components of the light amplitude emerging from a normal cavity (Appendix A). This is sketched in figure 2.7. This leads to a sum for the carrier after n round

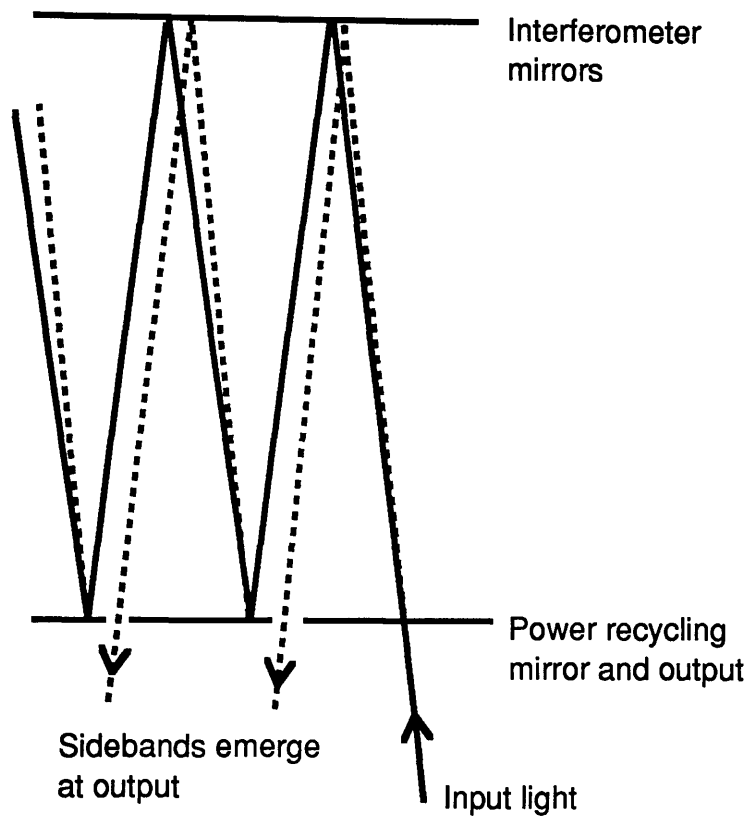


Figure 2.7: A diagram showing the contributions to the amplitudes in the recycling split-cavity which represents the recycling system. The sidebands (dashed) emerge from the output. The carrier (solid line) persists in the resonant system. The beams have been tilted and only a few cycles are shown.

trips of

$$t_c \rho e^{i\delta_c} + t_c \rho r \rho e^{i2\delta_c} + \dots + t_c \rho [r\rho]^{n-1} e^{in\delta_c}. \quad (2.30)$$

Each of the above terms leads to the production of a pair of sidebands which appear at the output. The sum of these sideband amplitudes at time (t) is given by Δ multiplied by the carrier sum.

The sideband amplitudes are given by

$$\frac{A}{A_0 e^{i\omega t}} = it_c \rho \Delta \sum_{n=1}^{\infty} [r\rho]^{n-1} e^{in\delta_c} \quad (2.31)$$

which can be summed to give

$$\frac{A}{A_0 e^{i\omega t}} = it_c \rho \Delta \frac{e^{i\delta_c}}{1 - r\rho e^{i\delta_c}}, \quad (2.32)$$

or with the same transformation as used in Appendix A

$$\frac{A}{A_0 e^{i\omega t}} = it_c \rho \Delta \frac{e^{i\delta_c} - r\rho}{(1 - r\rho)^2 [1 + F'_c \sin^2 \frac{\delta_c}{2}]}, \quad (2.33)$$

where F'_c is the coefficient of finesse of the recycling cavity. The sidebands produced can be detected, for example by mixing with a small amount of light (amplitude A_L) at the carrier frequency. This gives an output power

$$\delta I = A_L A^* + A_L^* A, \quad (2.34)$$

which gives, with $\delta_c = 0$ to maximise the signal,

$$\delta I = \frac{2A_0 A_L t_c \rho \Delta_0}{1 - r\rho} \cos[\omega_g(t - \tau/2)]. \quad (2.35)$$

This shows the same enhancement of the signal as in the simple case outlined above (equation 2.24) and with no recycling mirror reduces to the response expected from the non-recycled interferometer (e.g. equation 1.15 with the substitution $A_L = \frac{A_0 \phi}{2}$).

In order to determine the signal to noise ratio increase due to recycling it is necessary to consider the effect of this technique on the photon shot noise. The

noise performance of a recycled system depends on the effective contrast of the interferometer. The local oscillator should still dominate the output intensity. Since the power in the interferometer is higher the power emerging from the output due to imperfect interference is proportionately increased. The local oscillator amplitude should therefore be increased by the same factor as the amplitude increase within the arms of the interferometer. The noise depends on the amplitude on the photodiode while the signal depends on the product of the local oscillator amplitude and that of the sidebands from the interferometer output. The signal to noise ratio is therefore increased by the amplitude enhancement due to recycling.

2.4.3 Interferometer contrast and recycling

It is useful to consider the implications of the loss of power from the output of a interferometer with recycling. The particular case of loss of power due to the misalignment of one of the interferometer arms is used as an example. This allows the degree of misalignment which can be tolerated in a given interferometer to be calculated. It also provides the basis for an experimental comparison of recycling and the new technique, dual recycling, which is considered in section 2.5.

The power build-up in recycling is sensitive to loss of power through the output port of the interferometer. Such losses may be due to poor interference caused by some imbalance between the light returning to the beamsplitter from the two arms. The loss of power here reduces the build-up of power in the recycling cavity. It also increases the light intensity on the photodetector and hence the detection noise without increasing the signal size. The loss of power from the output should certainly be less than the loss due to absorption in the arms.

One important cause of poor interference is misalignment of one of the mirrors in one of the arms from its optimum orientation. This causes a misalignment of the laser beam in that arm and so poor overlap of the beams from the two arms at the beamsplitter. The effects produced by misalignments are studied by considering the mode structure of the light within the recycling cavity.

The light amplitude in a cavity can be represented by a set of normal modes [24].

Here only the case of spherical mirrors is considered. Cartesian co-ordinates are a good choice (z is along the cavity axis joining the centres of curvature of the mirrors, x and y are then orthogonal to this). The transverse modes, for a known amplitude distribution ($A(X, Y)$), are then represented by the set of Hermite-Gaussian functions such that

$$A(X, Y) = \sum_{m=0}^{\infty} \sum_{n=0}^{\infty} A_m h_m(X) A_n h_n(Y), \quad (2.36)$$

where the transverse co-ordinates are normalised to the Gaussian beam size w ($X = \sqrt{2}x/w$ and $Y = \sqrt{2}y/w$.) For all of the effects of interest here only one transverse dimension (x) need be considered, remembering that there are similar expressions for the other dimension. The ‘mode amplitudes’ A_m are a measure of the contribution of mode (m) which has a spatial amplitude distribution given by

$$h_m(X) = \frac{\Gamma(\frac{m}{2} + 1)}{m + 1} e^{-\frac{X^2}{2}} H_m(X), \quad (2.37)$$

where H_m are the Hermite polynomials of order m . The A_m are evaluated from

$$A_m = \gamma \int_{-\infty}^{\infty} A(X) H_m(X) e^{-\frac{X^2}{2}} dX, \quad (2.38)$$

where γ is the normalisation

$$\gamma = \frac{\sqrt{2/\pi}}{\Gamma(\frac{m}{2} + 1) 2^m}. \quad (2.39)$$

(There is such a set of transverse modes corresponding to each of the longitudinal resonant modes of the system.) These modes propagate with constant amplitude but their phase (ϕ) with respect to a plane wave is [24]

$$\phi = (m + 1) \arctan \left(\frac{\lambda z}{\pi w_0^2} \right), \quad (2.40)$$

where w_0 is the size of the waist in the cavity and the z -co-ordinate is measured from this waist. The modes thus have different phase velocities and hence different

resonant frequencies within the cavity. The resonant frequency of a given mode is different from that of the fundamental ($m = 0$) mode by

$$\delta\nu = \frac{c}{2l}C \Delta m, \quad (2.41)$$

where l is the cavity length and Δm the difference in the number which labels the modes. The effect of the cavity geometry is described by

$$C = \frac{1}{\pi} \arccos \left[\sqrt{\left(1 - \frac{l}{R_1}\right)\left(1 - \frac{l}{R_2}\right)} \right], \quad (2.42)$$

where R_1 and R_2 are the radii of curvatures of the two mirrors which are separated by a distance l .

Mode (m) has a round trip phase shift (δ) in a cavity. The amount by which this mode is suppressed or enhanced ($g_m(\delta) > 1$ corresponding to enhancement) by the action of the cavity is (from Appendix A, equation A.10)

$$g_m(\delta) = \frac{t}{1 - r\rho} \left(1 + F' \sin^2(\delta/2)\right)^{-1/2}, \quad (2.43)$$

where F' is the coefficient of finesse of the cavity. Any suppression or enhancement of these modes is then dependent on the cavity geometry which determines the phase shift for a particular mode.

Consider an input beam which is initially correctly matched to the fundamental mode of a cavity. If one of the mirrors is rotated by a small angle then the resulting mode amplitudes can be calculated. The rotation is in general equivalent to a displacement δX in the X direction and a rotation of the cavity axis [11]. The displacement leads to mode amplitudes

$$\frac{A_m}{A_a} = \frac{e^{-\frac{(\delta X)^2}{4l}}}{\Gamma\left(\frac{m}{2} + 1\right)} \left(\frac{\delta X}{2}\right)^m, \quad (2.44)$$

where A_a is the initial amplitude in the original mode.

The rotation of the cavity axis about the waist leads to a phase shift across the beam. This gives mode amplitudes

$$\frac{A_m}{A_a} = \frac{(i\theta_n)^m e^{-(\theta_n)^2}}{\Gamma(\frac{m}{2} + 1)}, \quad (2.45)$$

where the normalised angle is $\theta_n = \theta\pi w/\sqrt{2}\lambda$ (this assumes that the curvature of the phase front over the beam diameter is small compared to the spot size).

Consider the cavity representing one arm of an interferometer with recycling. A rotation of this mirror by an angle (θ) leads to the production of the first order mode amplitude (A_1) in the arm where

$$\frac{A_1}{A_a} = \frac{2}{\sqrt{\pi}}\theta_n e^{-(\theta_n)^2}, \quad (2.46)$$

where A_a is the initial amplitude in the cavity (to be distinguished from $\sqrt{I_0}$ below). The amplitude of the fundamental mode is changed by an amount

$$\frac{\Delta A_0}{A_a} = 1 - e^{-\theta_n^2}. \quad (2.47)$$

The loss of power from the fundamental mode is dominated by the generation of the first order mode. The change in the power of the fundamental mode in the imperfect arm is

$$A_a^2 - [A_a - \Delta A_0]^2 = 2A_a\Delta A_0 - (\Delta A_0)^2. \quad (2.48)$$

The loss of power (ΔI) from the output of the recycling system for a given change in the fundamental mode amplitude in one arm is then given by

$$\frac{\Delta I_i}{I_0} \approx \frac{\Delta A_0}{A_a}, \quad (2.49)$$

where I_i is the power emerging from the output, A_a is the initial amplitude in each arm (from a power I_0 approaching the beamsplitter from M0 ($I_0 = 2A_a^2$)). ΔA_0 is the (small) change in the fundamental amplitude in the imperfect arm.

For the case of misalignment of one arm by rotation about a waist the above expression becomes

$$\frac{\Delta I_i}{I_0} = 1 - e^{-\theta_n^2} \approx \theta_n^2. \quad (2.50)$$

This can be used to set a limit to the allowable misalignment angle of one of the mirrors in the arm of an interferometer. An experimental test of the effects of such a mirror rotation in a recycling interferometer are discussed in section 3.4.4 where the above expression is used to predict the power lost from the recycling interferometer.

It should be noted that other imperfections can lead to loss of power from a recycled system. Examples are deviations from spherical mirror surfaces due to the manufacturing process or to thermal effects (see section 4.2) or mismatch of the curvatures of the mirrors in the two arms.

2.4.4 Conclusion

It has been seen that the use of recycling should allow the signal to noise ratio of an interferometer, in which the arms have high reflectivity, to be increased for a given input laser power. One possible limitation to this technique is the loss of power from the output of the interferometer. The extent to which this can happen in the particular case of the misalignment of one arm of the interferometer was calculated. These aspects of recycling have been tested by the author (as reported in Chapter 3).

It will be seen in Chapter 4 that mirrors with intensity losses of $\sim 5 \times 10^{-5}$ should be available. If an interferometer in which the light makes 30 double traverses of the arms is to be limited by the mirror losses then the effective contrast will have to approach ~ 100 . This may be very difficult to achieve with power recycling but it will be seen that the technique, dual recycling, discussed below should allow this effective contrast to be attained more easily.

2.5 Dual recycling

2.5.1 Introduction to dual recycling

Dual recycling is an extension of recycling. Another ‘recycling’ mirror is added. This mirror, the ‘signal recycling mirror’, is placed between the output of the interferometer and the photodiode (or second beamsplitter with external modulation). This mirror is made to form a resonant cavity with the interferometer in a manner similar to that in which the original recycling cavity was formed.

Dual recycling was proposed [25] as a technique which allows tuning of the frequency response of an interferometric detector. It turns out that there are also significant advantages with respect to the potential power build-up in the recycling system. (Recycling will be referred to as ‘power recycling’ from now on to avoid confusion.)

The tuning of the frequency response is especially important. It will be demonstrated that dual recycling allows a recycling detector with a short storage time in the arms to approach the low frequency behaviour of an interferometer with much longer storage time. This could be valuable if one desired to use delay-lines in the arms but mirrors of sufficient size to contain the number of spots required for a long storage time could not be obtained.

A diagram of an interferometer with dual recycling is shown (figure 2.8). The addition to the power recycling system is mirror M3—the signal recycling mirror. This is another partially transmitting mirror which is placed so as to form a cavity with the output of the interferometer. The mirror reflects light which has emerged from the beamsplitter back into the interferometer with a phase shift which is determined by the position of the mirror (M3) with respect to the interferometer mirrors (M1,M2). (In a similar manner to that previously described for M0.) The sidebands, which previously emerged from the output of the interferometer can then resonate in this cavity according to their round trip phase shift (δ_s).

The split-cavity analysis can be extended to this system. Now the contributions to the output amplitude from multiple reflections of the sidebands within the dual recycling cavity must be considered. The carrier and sidebands share

The input light enters from the left, passes through mirror M0, and is split by the beamsplitter into two paths. One path goes up to mirror M1, and the other goes right to mirror M2. Both paths reflect back to the beamsplitter, recombine, and pass through mirror M3, which is labeled as the signal recycling mirror. The light then exits as output light.

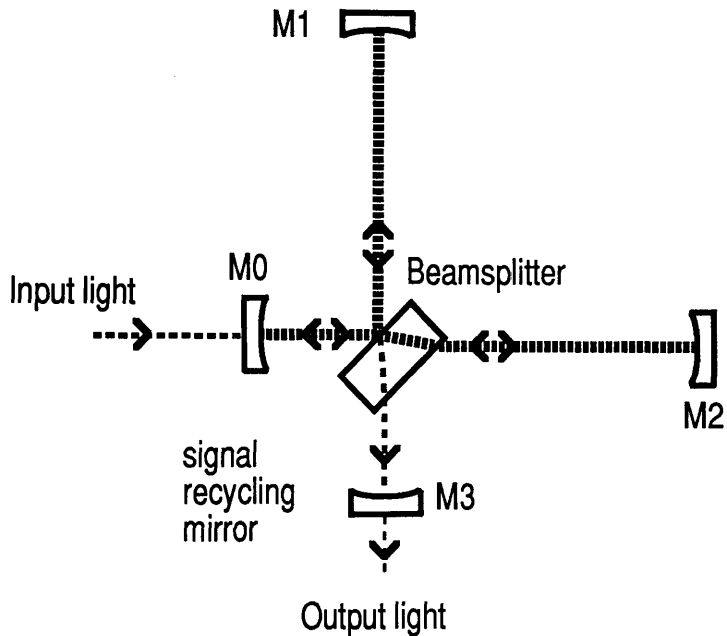


Figure 2.8: An interferometer with dual recycling. The signal recycling mirror M3 is added to the power recycling interferometer to form a cavity on the output of the interferometer.

the same optics in the arms of the interferometer but they are separated at the beamsplitter and see different mirrors at the beamsplitter end of the system (M0 and M3 respectively). The position of M3 determines the phase with which the sidebands re-enter the system at the beamsplitter.

The various amplitudes circulating in the cavity are shown (figure 2.9), The amplitude emerging through M3 due to one of the signal sidebands (the one at $\omega_c + \omega_g$) resonating in the signal recycling cavity is given by

$$A_0 e^{i\omega t} \times i t_c t_s \rho \Delta_0 [\exp i\omega_g(t - \tau/2)] \times$$

$$\left(\begin{array}{cccc} e^{i(\delta_c + \delta_s)} & + [r_c \rho] e^{i(2\delta_c + \delta_s)} & + \dots & + [r_c \rho]^{n-1} e^{i(n\delta_c + \delta_s)} \\ + [r_s \rho] e^{i(\delta_c + 2\delta_s)} e^{-i\omega_g \tau} & \vdots & \vdots & \vdots \\ \vdots & \vdots & \vdots & \vdots \\ + [r_s \rho]^{m-1} e^{i(\delta_c + m\delta_s)} e^{-i(m-1)\omega_g \tau} & + \dots & + \dots & + [r_c \rho]^{n-1} [r_s \rho]^{m-1} \\ & & & e^{i(n\delta_c + m\delta_s)} e^{-i(m-1)\omega_g \tau} \end{array} \right),$$

where r_s is the reflectivity of M3 and t_s it's coefficient of transmission. The $e^{i\omega_g t}$ factors allow for the change in the phase of the gravitational wave during the time the light spends in the system. This can be summed to give

$$\frac{A}{A_0 e^{i\omega t}} = \left[\frac{i t_c t_s \rho \Delta_0}{1 - r_c \rho} \right] \left[\frac{e^{i\delta_s}}{1 - r_s \rho e^{i(\delta_s - \omega_g \tau)}} \right] \times \exp(i\omega_g(t - \tau/2)), \quad (2.52)$$

where the notation is the same as in power recycling. This represents the enhancement of the sideband amplitude due to dual recycling. It can be seen that the signal from this sideband is maximised when $\delta_s = \omega_g \tau$. There is a similar expression for the enhancement of the other sideband. This can be obtained by substituting $-\omega_g$ for ω_g in the above expression.

The above allows the enhancement of the signal from dual recycling to be found for any set of optical parameters. This has been done by Meers [26]. Two limiting cases of the possible frequency responses are considered here.

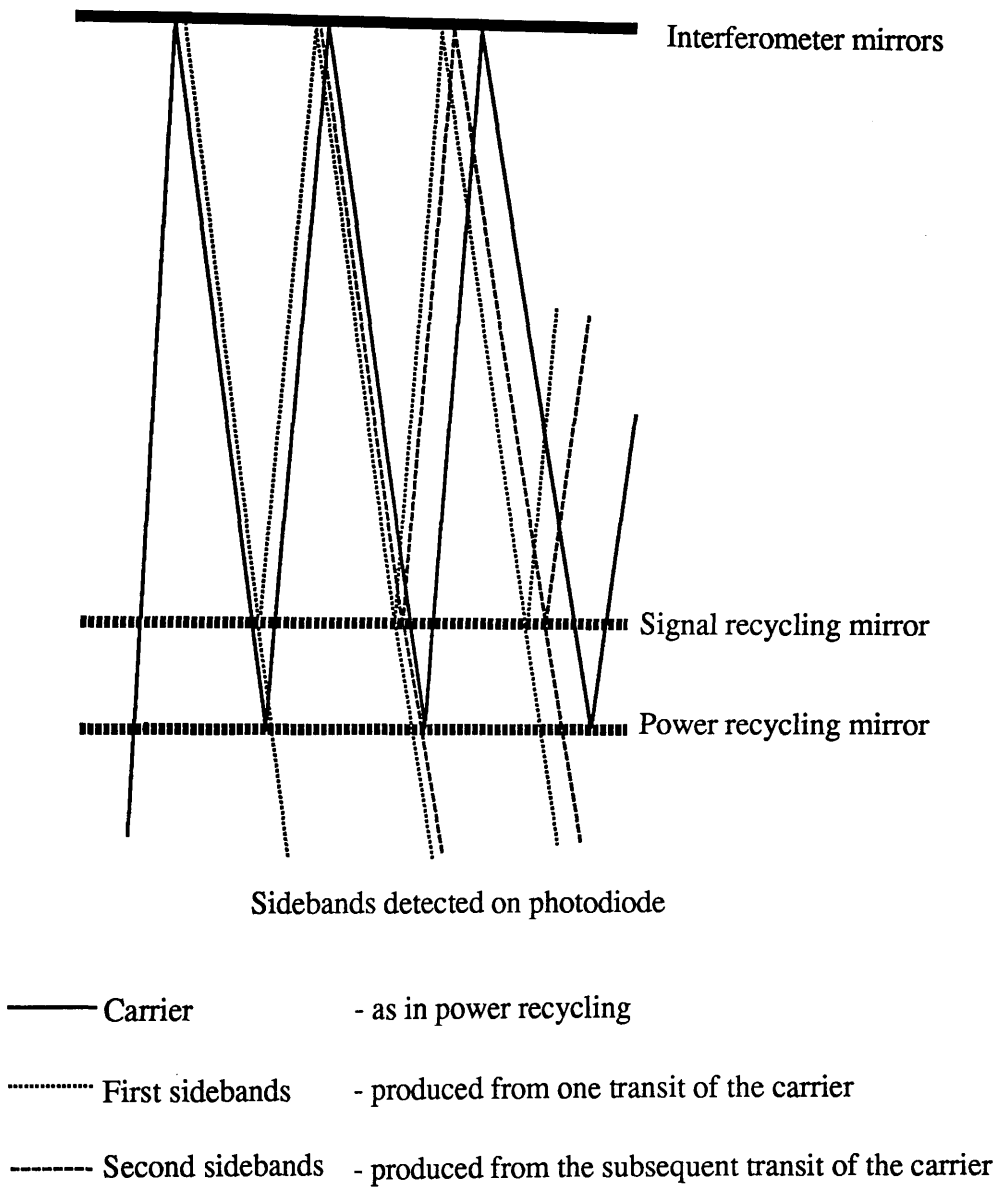


Figure 2.9: *The set of amplitudes which are found in the split-cavity appropriate to dual recycling. The upper mirror is shared by all of the light while the lower mirrors represent $M0$ for the carrier and $M3$ for the sidebands. For clarity, only a few cycles are shown.*

Tuned or narrowband dual recycling

The signal recycling mirror may be adjusted so that one of the sidebands produced by a particular gravitational wave frequency is resonant in the signal recycling cavity. If the linewidth of the signal recycling cavity is small compared to half of the gravitational wave frequency then the other sideband will not resonate significantly and does not contribute to the signal. In this case, called ‘narrowband’ or ‘tuned’ dual recycling, the response of the detector is centred on this resonant ‘tuning’ frequency.

The signal from this configuration is determined by the build-up of the amplitude of the signal sideband in the signal recycling cavity. Half of the potential signal is lost since only one sideband is resonant. The peak enhancement of the signal over power recycling is therefore, for signals with periods much greater than the storage time of the arms,

$$\sim \frac{t_s}{2 - 2r_s\rho}. \quad (2.53)$$

The width of the tuning peak is determined by the length of the arms and the coefficient of transmission of M3 (these set the free spectral range and linewidth of the signal recycling cavity). The noise is again dependent on the light incident on the output photodiode. (The effect of dual recycling on the contrast of the interferometer is discussed below.)

The narrowband response could be useful if the frequency of a suspected source of gravitational waves was known (e.g. a pulsar).

Broadband dual recycling

If M3 is positioned so that $\delta_s = 0$ the frequency response of the detector is maximum at low frequencies. This is known as ‘broadband’ dual recycling. Now both signal sidebands are resonant for signal frequencies less than the linewidth of the signal recycling cavity. In this case the frequency response of the detector is not predominantly determined by the storage time of the arms but by the storage time of the signal recycling cavity. The low frequency response of a detector can

therefore be enhanced without increasing the length or number of traverses of the arms.

In the broadband case the two signal sidebands experience approximately the same phase shift on one round trip of the signal recycling cavity. The amplitudes emerging through M3 are therefore enhanced in the same way as any light with this round trip phase shift would be in a cavity with the optical properties of the signal recycling cavity. The signal enhancement (G) in this case is given by

$$G = \frac{t_s}{1 - r_s \rho} \left(1 + F'_s \sin^2(\delta_s/2) \right)^{-1/2}, \quad (2.54)$$

where F'_s is the coefficient of finesse of the signal recycling cavity. An experimental measurement of this interferometer response is reported in Chapter 3.

2.5.2 A control system for dual recycling

In order to operate an interferometer with dual recycling it is necessary to control the position of the signal recycling cavity to maintain the desired sideband phase shift (δ_s). This can be achieved by illuminating the signal recycling cavity, via M3, with a ‘control’ beam derived from the main carrier light but with the orthogonal polarisation within the interferometer. This light will resonate in the signal recycling cavity and will provide a control signal via the reflection fringe method used elsewhere.

In order to control the signal phase shift the frequency of the control beam can then be offset by the required tuning frequency. The control system will then move M3 until the control beam (and hence the correct sideband frequency) is fully resonant in the signal recycling cavity.

It is necessary to consider some of the implications of the use of this control signal on the performance of the interferometer. In order to allow this to be quantified it is useful to define the ‘internal contrast’ of the interferometer. The internal contrast is the magnitude of the amplitude approaching the beamsplitter from M0 divided by the magnitude of the amplitude approaching M3 from the beamsplitter.

The effect of moving the signal recycling mirror is to generate sidebands on the light reflected from it. The amplitude of each sideband is proportional to the amplitude incident on this mirror. This amplitude is related to the amplitude incident on the beamsplitter by the internal contrast. The sidebands produced by motions of the signal recycling mirror are smaller than those produced by the same motion of the beamsplitter by the internal contrast.

Frequency noise on the control beam at gravitational wave frequencies will cause phase changes for this beam in the signal recycling cavity. These phase changes will lead to signals being applied to the position of M3 as the control system attempts to keep the cavity on resonance. The motion of M3 will then produce sidebands on any light incident on it. These sidebands would then ^{be} detected in a manner similar to those generated by gravitational wave. This implies that light with the lowest possible frequency noise should be used to form the control beam. In the interferometer with recycling this implies removing a fraction of the (main) light from within the recycling cavity.

The required power of the dual recycling control beam can be calculated by considering the effects of motions of M3 due to the control system feeding back noise due to shot noise in the detection process. The motions of the signal recycling mirror can be larger than those of the beamsplitter by the internal contrast of the interferometer. The motion of the beamsplitter can, in turn be larger than that of the interferometer mirrors by the number of traverses of the light in the arms in one direction. The power can therefore be weaker than that in the interferometer by, at most, the square of the internal contrast times the square of this number of traverses. (The ability to measure a phase shift, and hence a displacement, depends on the amplitude of the light used if the limit is photon shot noise.) This allows the required power of the dual recycling control beam to be calculated.

The practicalities of the operation of such a system are discussed with the experimental test of the technique (in section 3.5).

2.5.3 Contrast and dual recycling

The description of the effects of imperfections in the arms producing higher order modes in the power recycling system can be extended to dual recycling. The non-interfered light emerging from the beamsplitter is now in a resonant system. The effect of this is to suppress (or enhance) the different mode amplitudes emerging through M3 due to imperfect interference.

In the case of the misalignment of one arm the fundamental and first order modes are important. The suppression factors for the modes are (from equation 2.43)

$$g_m = \left[\frac{t_s}{1 - r_s \rho} \right] \left[\frac{1}{1 + F'_s \sin^2(\delta_m/2)} \right]^{1/2}, \quad (2.55)$$

where δ_m is the round trip phase shift for mode m in the signal recycling cavity and the other quantities apply to the dual recycling system described above.

The overall power loss is given by two related terms. The production of higher order modes by the distortion mechanism reduces the power in the fundamental. The higher order modes have nothing with which to interfere at the beamsplitter and so will lead to light emerging from the output. The amplitudes of the fundamental mode from each arm at the beamsplitter are now different and this will also lead to imperfect interference. The fractional loss of amplitude from the fundamental mode due to some asymmetry in one arm is for one round trip of the dual recycling cavity

$$\frac{\Delta A_0}{\sqrt{2} A_a}. \quad (2.56)$$

The relative power loss from the fundamental on one round trip is therefore

$$\frac{2\Delta A_0}{A_a} - \frac{(\Delta A_0)^2}{A_a^2} \quad (2.57)$$

which is therefore the power gain in the modes produced by the distortion.

The sidebands emerging from the beamsplitter on each round trip are within the dual recycling cavity and it is therefore necessary to allow for the enhancement or suppression of these sidebands in this cavity. If all of the higher order modes which contain a significant share of the distortion amplitude have similar suppression

factors in the dual recycling cavity then the loss from the system as a whole is given by

$$\frac{2\Delta I}{I_0} = g_0^2 \left[\frac{\Delta A_0}{A_a} \right]^2 + g_m^2 \frac{\Delta A_0}{A_a} \left[2 - \frac{\Delta A_0}{A_a} \right]. \quad (2.58)$$

Putting in the angular misalignment case this result becomes for small misalignments

$$\frac{2\Delta I}{I_0} \approx g_0^2 \theta_n^4 + 2g_1^2 \theta_n^2. \quad (2.59)$$

For broadband dual recycling the power lost in the fundamental mode is enhanced since it is resonant in the dual recycling cavity ($g_0 = t_s/(1 - r_s\rho)$). This is therefore the dominant loss for all but the smallest misalignment angles $\theta_n < \sqrt{2}g_1/g_0$. In tuned dual recycling the fundamental is no longer fully resonant and for moderate misalignments there can be a significant reduction of the power loss. The effects of dual recycling on the power loss from an interferometer are demonstrated in the section (3.5.2) on the experimental test of the contrast properties of dual recycling.

There is still the possibility that the new fundamental mode within the recycling cavity will differ from the illuminating mode to such an extent that the overlap between the two is small. For the case of a small misalignment ($\theta_n \ll 1$) only a small fraction of the amplitude is initially removed from the fundamental mode and the new mode formed should therefore overlap very well with the original mode.

2.5.4 Conclusion

Dual recycling is predicted to allow a variety of frequency responses to be obtained from a single interferometer. Importantly it should allow a detector with relatively short storage time in the arms to approach the low frequency performance of a detector with much longer storage times. It has also been claimed that dual recycling should allow the effective contrast of a recycling interferometer to be increased. This would allow the power build-up and the signal to noise ratio of such a system to be increased. The effective contrast of > 100 , mentioned in section 2.4, should be more easily attained with the addition of signal recycling to

Chapter 3

Experimental tests of advanced interferometry techniques

3.1 Introduction

In this chapter experimental tests, conducted by the author, of the interferometry techniques discussed in Chapter 2 are presented. The experiments were designed to measure the optical properties of the various interferometer designs and to test the predictions made in the previous chapter. In addition the control systems required for each of the optical arrangements were developed. It was felt to be important that there was nothing, in principle, that would prevent the control methods used here being applied to a full-scale detector.

To minimise the complexity it was decided that the tests would be carried out on a rigid apparatus with the optical components fixed to an optical bench (as opposed to a suspended system). The apparatus would also be in air (not in an evacuated enclosure) to enable a number of configurations to be tested in a relatively short time. The inevitable penalty was relatively large amounts of low frequency vibrational and acoustic noise. The amplitude of this noise does, however, fall quite rapidly with increasing frequency. The noise performance of each of the interferometers was, therefore, measured in the frequency band between 10 kHz and 100 kHz (rather than the 100 Hz to 10 kHz appropriate to a gravitational wave detector).

3.2 A Michelson interferometer with internal modulation and cavities in its arms

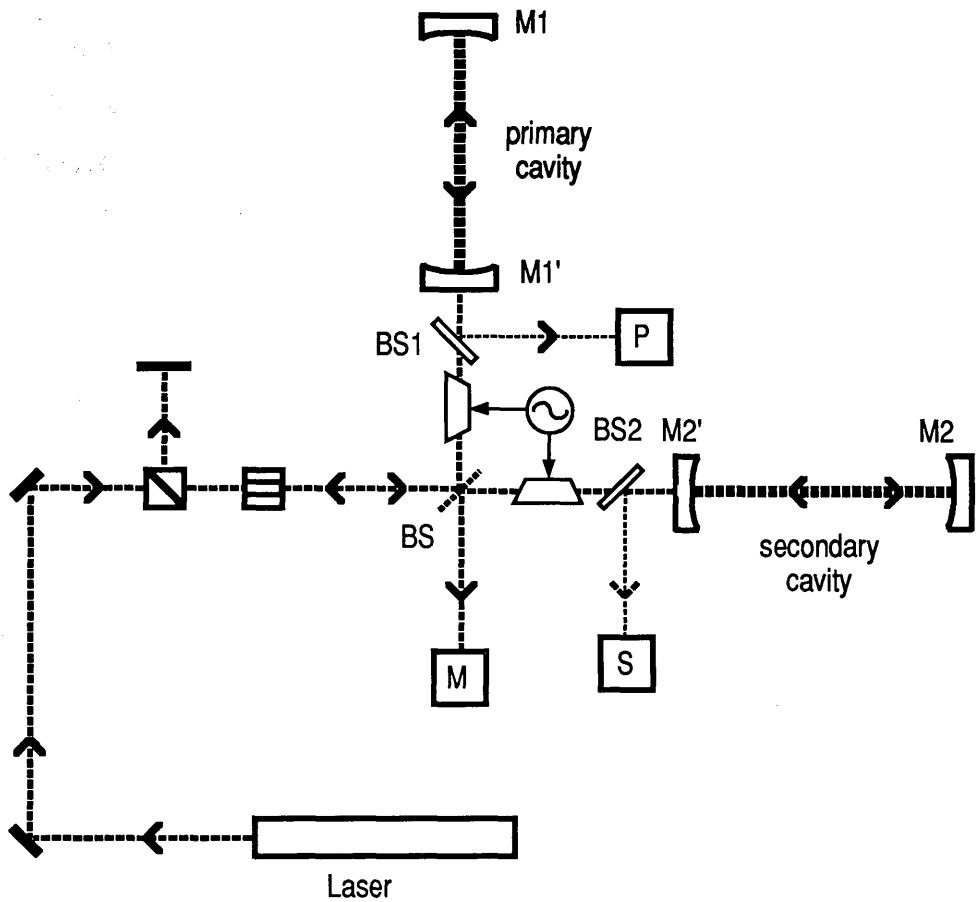
The main objective of the experimental test of an internally modulated Michelson interferometer with cavities in the arms was to confirm that it was possible to design a reliable method of controlling such a system. In order to evaluate the performance of the control systems it was necessary to ensure that the interferometer would operate in a predictable manner and that there was no evidence of any excess noise due to the action of the control system. Overcoupled cavities (as described in section 2.3.2) were chosen to simulate those which would be used in a full-scale detector where the long arms would allow the desired storage time to be achieved with low total cavity loss.

Another experiment with an internally modulated interferometer has since been carried out, elsewhere, with similar results [27].

3.2.1 Optics

The basic elements of an interferometer with internal modulation and cavities in the arms were shown in section 2.3.2. A diagram of the optical layout used is shown (figure 3.1). The cavities were chosen to be 0.45 ± 0.01 m long for convenience. The mirrors which were nearest the ^{main} beamsplitter (the ‘inboard’ mirrors) were plane with a measured ^{intensity} transmittance of 0.0051 ± 0.0003 . The mirrors at the other end of the cavities (the ‘outboard’ mirrors) were chosen to have a radius of curvature of 0.7m and a negligible transmittance. The outboard mirrors were placed with their concave face into the cavity to give a stable mode.

The mirrors which formed the main interferometer components had very low loss (typical power loss of $< 2 \times 10^{-4}$). (Low loss mirrors are discussed in some detail in Chapter 4. The methods which were used to evaluate the losses of the mirrors are also described there.) The finesse (F) of each of the two cavities was measured and they were found to be similar with a finesse of 1200 ± 100 . This determined the signal enhancement property of the cavity (that is the effective number of traverses $G(0) = F/\pi$ as shown in Appendix A). The large coeffi-



KEY

- M1 - outboard primary mirror
- M1' - inboard primary mirror
- M2 - outboard secondary mirror
- M2' - inboard secondary mirror
- BS - main beamsplitter
- BS1 - primary 4% beamsplitter
- BS2 - secondary 4% beamsplitter

-  - Differentially driven electro-optic modulators
-  - polarising beamsplitter
-  - 45 degree Faraday effect rotator

Laser - argon-ion laser

Figure 3.1: *The optics for the interferometer with internal modulation and cavities in the arms. The three control signals originate from the photodiodes: 'M' from the main output; 'P' and 'S' from the primary and secondary cavities, respectively.*

cient of transmission of the inboard mirror prevented an accurate measurement of the (absorption and scattering) losses associated with the cavity since these were comparable to the experimental error on the transmission measurement. It was, however, possible to set an upper limit to the total power losses at $\sim 3 \times 10^{-4}$. Previous measurements suggested that the total losses could be expected to be $\sim 20 \times 10^{-5}$ and it was thought that this loss could be used as an estimate of the loss in the interferometer cavities unless there was some evidence that this was not reasonable. The expected magnitude of the cavity amplitude relative to that of the directly reflected amplitude (C/A from section 2.3.2) had a value of 1.92 ± 0.03 . The cavities were therefore overcoupled.

The beamsplitter used to form the Michelson interferometer was a high quality dielectric coating on a fused-silica substrate. The transmittance and reflectance were both $50 \pm 2\%$ for 's' polarised light. This defined the polarisation used in the whole interferometer. The internal phase modulators were of a type known to have relatively low losses and small wavefront distortion. The final optics within the interferometer were a pair of fused silica windows which were used to reflect a small fraction (4% in the experiment) of the light returning from each cavity on to photodiodes.

The remainder of the optical system consisted of the components required to transfer the light from the argon-ion laser to the interferometer and prevent light reflected from the interferometer returning to the laser. The latter aim was achieved using 45° Faraday effect rotators and polarising beamsplitters to make optical diodes. The light was mode-matched to the fundamental modes of the cavities. The argon-ion laser (Spectra-Physics 165) was equipped with a prism and etalon to give single-mode operation. The laser was modified (using the methods described by Kerr [22]) by mounting the laser mirrors on a separate rigid structure based on 'Invar' low expansion alloy rods and extensive use of damping materials. This allowed the laser mirrors to be isolated from the vibration due to the cooling water in the laser. The modified laser provided up to 200 mW of single mode light at 514.5 nm. Due to losses in the optics delivering the laser light to the interferometer the power available at the input to the interferometer was about 20 mW.

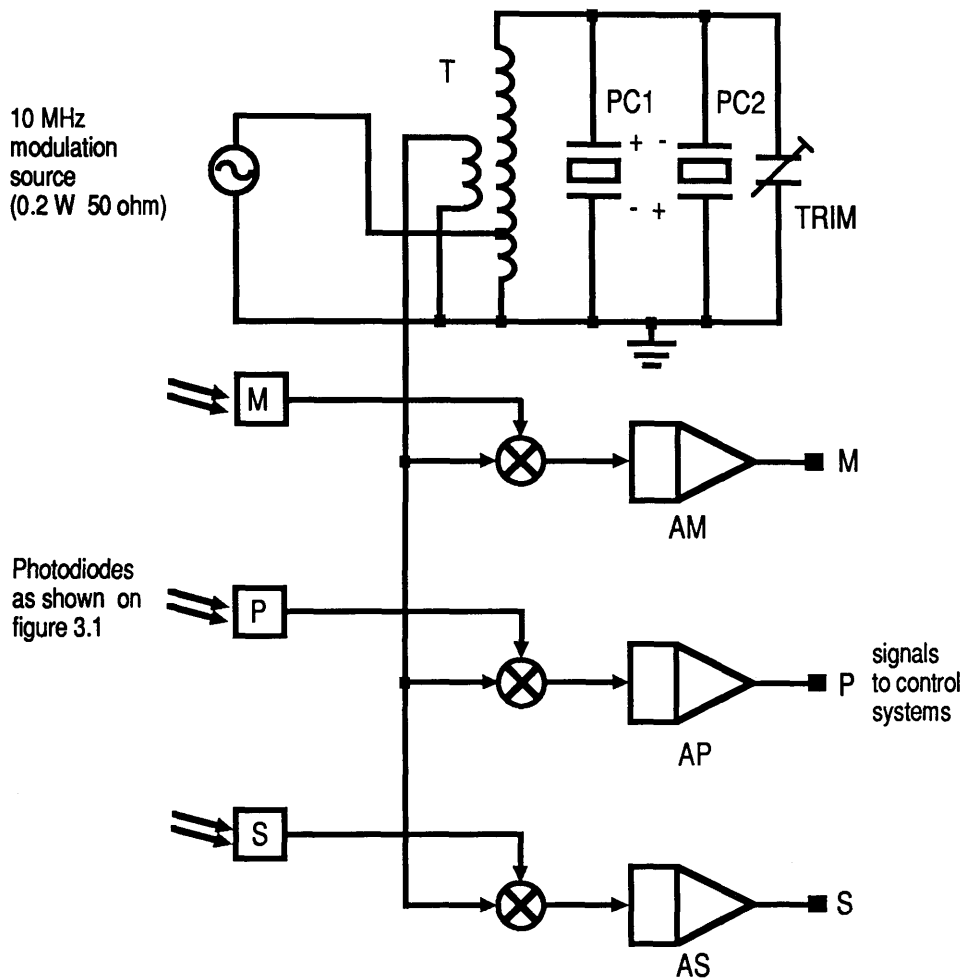
It was necessary to make the interferometer quite rigid to avoid excessive relative motions of the components. It was also desirable to use a material with a reasonably low coefficient of thermal expansion to define the lengths of the two arms to improve the long-term operation of the system. In order to achieve this the components which formed the interferometer were mounted on a structure made from rods of fused silica. The mounts used to hold each of the interferometer mirrors and the beamsplitter were connected by using three of these rods (each 0.65 m long by 18 mm diameter) for each arm. The rods were covered in viscous damping material to damp their resonant modes. This structure and the rest of the optics were mounted on a metal optical bench.

3.2.2 Signals, feedback elements and control systems

It was necessary to obtain or construct the required electronics to provide the modulation, amplify the signals from the photodiodes and perform the demodulation to obtain the phase signals. The design of the modulation and detection electronics is shown in figure 3.2.

The electro-optic modulators used provide one half wavelength (at 515 nm) of retardation for an applied voltage of $\sim 810\text{V}$. A phase modulation index of ~ 0.2 was chosen to provide signals of a reasonable size with the small light powers available without significantly reducing the power remaining at the carrier frequency. This determined the required radio-frequency drive power to be supplied to the modulator ($\sim 0.15\text{ W}$) at the modulation frequency of 10 MHz and the modulation level was checked by using a 'Tropel' optical spectrum analyser to confirm the presence and size of the modulation sidebands. (This method was used to check the modulation index produced by the radio-frequency phase modulators used in all of these experiments).

Two types of photodiodes were used according to the expected incident light power. Both were EG&G types (FND100 and SGD200) with small capacitance allowing high speed operation. The latter type was used where the incident power was likely to exceed 10 mW. The radio frequency signal from each photodiode



KEY

M - main photodiode
 P - primary photodiode
 S - secondary photodiode

⊗ - demodulator

A_x - amplifier with filtering to remove unwanted radio-frequency signals

PC_n - electro-optic modulator in circuit resonant at the modulation frequency

T - tuned auto-transformer for impedance matching (1:7 step up) with pick-off coil for demodulation references

$n=1$ or 2 , $x=M, P$ or S

Figure 3.2: *The radio frequency electronics for internal modulation with cavities. The modulation is applied differentially via the two phase modulators. The signals from the three photodiodes are demodulated and amplified to provide the three required control signals i.e. the main interferometer signal (M), and the cavity signals (P and S).*

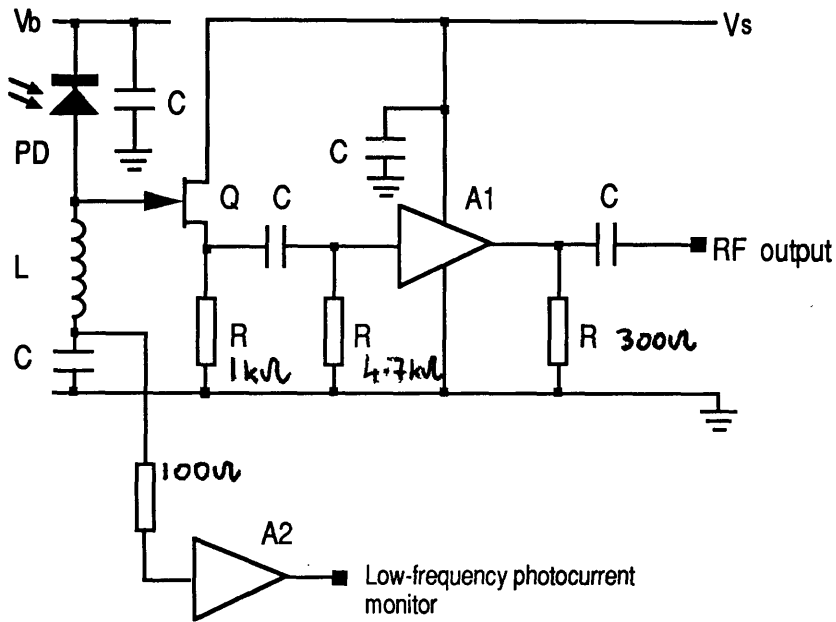
was amplified using the circuit shown below (figure 3.3). A tuned circuit is used to enhance the signal voltage before active amplification. The finite 'Q' of the tuned circuit and the electronic noise of the active components set a limit to the smallest light power in which photon shot noise can be seen above electronic noise. This was important in those experiments which were designed to reach shot noise limited performance. The signals from the photodiodes were demodulated using double-balanced radio-frequency mixers.

The control of the path lengths within the interferometer and the laser were provided by piezo-electric transducers at low frequency and an electro-optic modulator where high frequency feedback was required (in the laser frequency stabilisation servo-system). The piezo-electric transducers provide position control over $\sim 1\mu\text{m}$ but are limited in usable frequency response by internal resonances (at frequencies from a few kHz to $\sim 100\text{kHz}$ depending on design). Position transducers were fitted to both of the inboard mirrors. These were usable in control systems at frequencies up to $\sim 10\text{kHz}$. One of the outboard mirrors (in the cavity which will be referred to as the secondary cavity) was also mounted on a transducer. This required more drive voltage to achieve a given displacement but was usable up to 30kHz .

The system was built as described and most of the important parameters confirmed by measurement (e.g. mirror transmittances, cavity storage times and transducer behaviour). The transducers were calibrated against the wavelength of the laser light in a Michelson interferometer by finding the voltage required to cause a mirror to move one half wavelength.

The first step in operating the interferometer was to stabilise the laser frequency to one of the cavities (the 'primary' cavity). The signal to do this stabilisation was obtained from the light reflected from the primary cavity on to the photodiode associated with that arm. The signal produced was used in the manner described in Appendix B to control the laser frequency. This servo-system remained unchanged throughout the experiment.

In order to measure the important differential phase signal from the cavities it was necessary both to stabilise the length of the secondary cavity to the stabilised



KEY

- C - coupling or decoupling capacitor (0.1μF)
- R - bias resistor
- Q - low noise FET (BFW10)
- PD - photodiode
- L - inductor to form tuned circuit (~10μH)
- A1 - RF amplifier (SL 560)
- A2 - transimpedance amplifier (output voltage proportional to input current)
- V_s - supply voltage (+9V)
- V_b - photodiode reverse bias (50 V)

Figure 3.3: An amplifier for the radio frequency photodiode signals. The main signal appears at the radio-frequency (RF) output. The other output provides a useful measure of the average photocurrent.

laser light and to maintain the output of the Michelson interferometer on a dark fringe. Two control systems which were intended to achieve this were tested and compared.

It is first useful to recall the nature of the two signals which were available. The main Michelson interferometer signal contains both information about the Michelson interferometer and about each cavity. Since the light frequency was stabilised to the primary cavity there should have been little signal from this cavity at the main output. The output should then be dominated by a combination of information about the phase changes in the secondary cavity and the path difference between the two arms of the small Michelson interferometer formed by the beamsplitter and the inboard mirrors.

The size of the cavity signal (at the main output) produced by a given, low frequency, mirror motion is large compared to the Michelson interferometer signal due to a similar motion of an inboard mirror because of the signal enhancement property of the cavity. The degree to which these signals are changed by the double modulation can be calculated from equation 2.23. The signal component from the cavity is 0.15 ± 0.02 of the maximum which can be obtained with a perfectly coupled cavity of the same finesse and with no reduction due to double pass modulation. These estimates are used below to calculate the expected displacement sensitivity of the interferometer. (Any of the problems, mentioned in section 2.3.2 caused by sign reversal of the output signal due to motions of the inboard mirror would occur at ~ 30 MHz. This is very far above the unity gain frequency (~ 200 Hz) of the relevant servo-system.)

The second signal, which is obtained from the photodiode illuminated by a small fraction of the light reflected from the secondary cavity, contains information about only this cavity. Since a small amount of light is used to obtain this signal it does not have as large a signal to noise ratio as the main output signal. This signal must therefore be used for control purposes only at frequencies at which the differential output signal is not required. If 4% of the light was used the signal to noise ratio, for signals produced by cavity phase changes, would be worse than that of the main output by > 14 dB (if the noise was dominated by photon shot

noise) even if the contrast of the interferometer was very poor. If the contrast of the interferometer is high then the cavity signal represents an even poorer signal to noise ratio.

The first feedback scheme is shown (figure 3.4). Here the entire signal from the main output is amplified, filtered and applied to the transducer controlling the position of the secondary outboard mirror. The control system formed by this must have sufficient bandwidth to ensure stable locking of the cavity when the system is fully operational. It seems reasonable that due to the phase enhancement property of the cavity the main output signal will be dominated by the cavity component. While the Michelson interferometer output is close to an interference minimum this signal should, therefore, allow the cavity length to be adjusted to keep the laser light on resonance, at least for short periods. In order to complete the control system the secondary cavity signal was filtered, amplified and applied to the transducer controlling the position of the secondary inboard mirror. The filtering was arranged so that the unity gain point of the control system formed was below the lowest desired differential phase measurement frequency. This servo-system should have the correct operation to counteract any, low frequency, signal component from the Michelson interferometer which when applied to the outboard mirror of the cavity tends to prevent stabilisation of the cavity to the laser light. In this scheme the differential phase signal is proportional to the voltage applied to the secondary outboard mirror at frequencies where the loop gain of the main output servo-system is high and where the loop gain of the low frequency cavity servo-system is well below unity.

The second feedback scheme is shown in figure 3.5. Here the main output signal is split into low and high frequency components. The high frequency component is applied to the transducer controlling the outboard mirror. The low frequency component is directed to the inboard mirror. The reasoning behind this is that the Michelson interferometer will be maintained near its correct operating point independent of the state of operation of the cavity control systems. The low frequency signals from the secondary cavity photodiode are then added to the outboard mirror to correct for the error due to the relative motions of the inboard

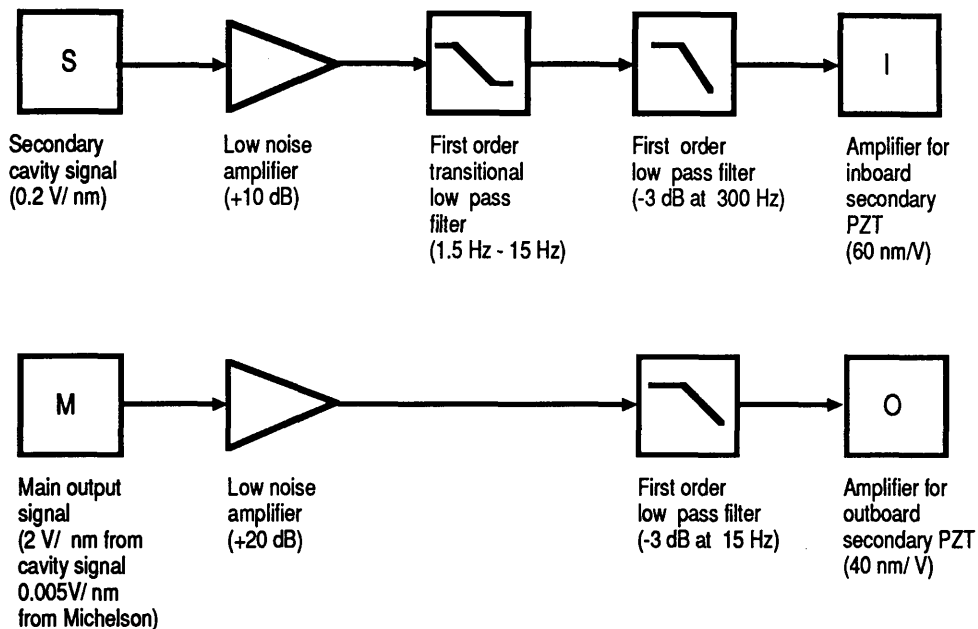
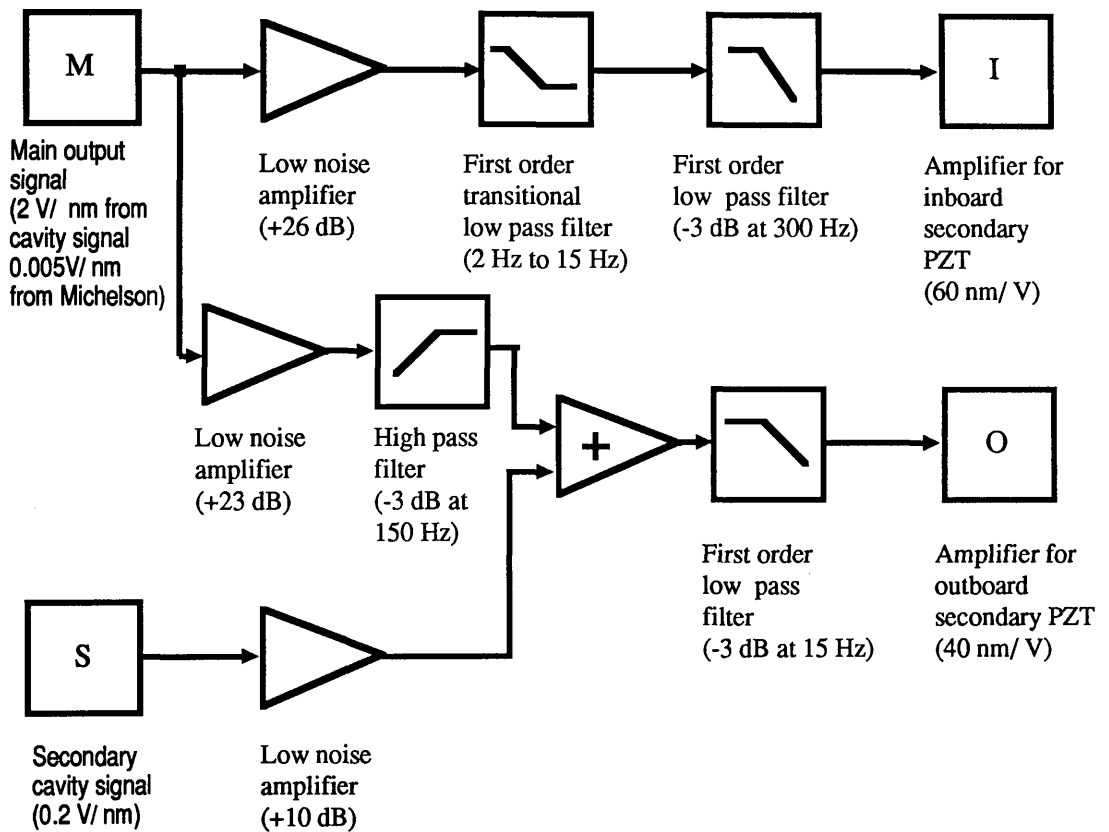


Figure 3.4: A control system for internal modulation. The signals from the demodulators are shown on the left with the typical signal size as a function of mirror motion about the operating point. The servo-systems are represented by a single amplifier (gain independent of frequency) and the appropriate filters. The resulting signal is further amplified and used to control the positions of the mirrors as indicated on the right. 'PZT' is used as an abbreviation for piezo-electric transducer.



The notation used is the same as in the previous figure.

Figure 3.5: A different control system for internal modulation. The properties of this system should be similar to those of the system in the previous figure.

mirrors and maintain the cavity at the correct length. The differential phase output signal is obtained in the same way as for the first system.

In a detector with suspended masses there will always tend to be some motion of the mirrors at the suspension pendulum frequencies and so it was important to consider the effects of moderate amounts of low frequency motion of the main mirrors. This was done by moving the primary inboard mirror sinusoidally with an amplitude of $\sim \frac{1}{2}$ wavelength peak to peak at ~ 5 Hz.

3.2.3 Results

The primary cavity servo-system allowed the laser to be stabilised to the length of the primary cavity. The error signal in this type of system is a measure of the residual frequency deviations of the laser with respect to the resonant frequency of the cavity. This signal was calibrated from the known properties of the cavity and the size of the cavity fringes at the error point. The residual noise level at the error point corresponded to a frequency noise of $\approx 0.15 \text{ Hz}/\sqrt{\text{Hz}}$ in the region from 50 kHz to 100 kHz. This was approximately 3 times the limit set by photon shot noise as calculated using equation A.19 of Appendix A.

The two Michelson interferometer and secondary cavity control systems were then tested. It was very difficult to distinguish between the operation of these systems. Each remained operational until thermal expansion or increased disturbance caused one of the transducers to reach the end of its range. The addition of the low frequency motion to the primary inboard mirror caused the expected behaviour with this motion being imposed on the inboard secondary mirror by the control systems. Again this failed if one of the amplifiers driving the transducers reached the end of its range.

The bandwidth of the secondary cavity length servo-system was set to about 20 kHz. This was adequate to maintain the cavity on resonance in the presence of the ambient vibrational noise.

It now remained to measure the signal and noise properties of the system. This was done for both control systems. There was no discernible difference between

their noise performances and so only one set of results is presented. When either of the cavities was resonating the reflected power was 0.88 ± 0.02 of the incident power. This was compatible with the calculated visibility of 0.15 ± 0.02 and the measured modulation index of ~ 0.2 if the efficiency of the mode matching to the cavity was close to unity.

With a total input light power of ~ 16 mW the light power at the output of the Michelson interferometer with the system operating was measured to be 3.0 ± 0.8 mW. This cannot be explained by the constructive interference of the modulation sidebands at this point. There must also have been some residual unmodulated light at the output due to an imbalance between the arms. This light on the photodiode sets a lower limit to the displacement sensitivity. This is discussed below.

The degree of common mode rejection of frequency noise was measured by imposing a frequency noise peak on the laser and comparing the signals produced by this at the outputs of the secondary cavity signal demodulator and the main output signal demodulator. The estimate (0.15 ± 0.02) of the reduction of the cavity signal at the main output due to the double modulation, was assumed. The size of the two signals to be compared should also depend linearly on the light power used to make each measurement (with 4% used to produce the cavity signal the main output signal potentially could be 25 times larger). The main output signal (due to differential cavity phase shifts) would therefore be expected to be $25 \times 0.15 = 3.75 \pm 0.5$ times the other signal if there was no common mode rejection. The experimental measurement of the two signals due to the frequency noise peak showed that the signal at the main output was 0.41 ± 0.04 of the signal directly from one cavity. The degree of common mode rejection of frequency noise was therefore 9 ± 2 . The lack of better cancellation was probably due to some imbalance between the two arms of the interferometer (either of the storage times or of the signal size due to mode-matching or modulation index). Together with the measured residual laser frequency noise the subtraction sets a limit to the detectable relative arm length changes. The equivalent displacement noise spectral density due to this would be $\approx 2 \times 10^{-17}$ m/ $\sqrt{\text{Hz}}$.

Another possible limit to the performance of the interferometer is the photon shot noise in the total detected light power. This can be calculated by comparing the signal produced by a given mirror motion to the photon shot noise. For the cavity properties given above ($G(0) \approx 380$) the signal size is enhanced by a factor ($E = 0.15G(0)$) of ~ 55 compared to the signal produced in an internally modulated Michelson interferometer which has an arm length the same as the length of each cavity. The absolute size of the signal for a given small phase shift (δ) is therefore (from equation 2.4)

$$\eta I_0 E J_1(\beta) \delta \quad (3.1)$$

where η is the photocurrent produced per unit of power incident on the photodiode and I_0 is the power mode matched into the two arms of the interferometer. With the optical parameters given above this gives an equivalent photocurrent signal due to small relative arm length changes of $\sim 2 \times 10^5$ A/m

The photon shot noise due to the detected light is given by the shot noise on the photocurrent. This should be modified by the factor 1.22 to allow for the use of sinusoidal modulation and demodulation (as described in section 2.2.3). With the measured average photocurrent of 0.7 ± 0.2 mA the equivalent photon shot noise limited spectral displacement should be $\sim 1 \times 10^{-16}$ m/ $\sqrt{\text{Hz}}$. (The uncertainty on this value originates from the lack of knowledge of the true cavity parameters and modulation index.)

The feedback signal to the secondary outboard mirror was examined at frequencies where the loop gain of the servo-system was high (< 20 kHz). A sinusoidal voltage was applied to the transducer which controlled the inboard primary mirror. The resulting signal applied to the outboard secondary mirror was monitored. The response to this gravitational wave simulation is shown (figure 3.6). The bandwidth of the part of the control system controlling the Michelson interferometer was therefore ~ 200 Hz. This moderate bandwidth was required due to relatively high levels of background vibrational noise in the laboratory. The presence of this excess noise prevented the observation of any more fundamental noise at these low frequencies.

In order to allow measurement of the signal to noise ratio of the interferome-

the control system. The control system was designed to cancel the low-frequency noise and to provide a flat response at higher frequencies. The control system was designed to cancel the low-frequency noise and to provide a flat response at higher frequencies. The control system was designed to cancel the low-frequency noise and to provide a flat response at higher frequencies. The control system was designed to cancel the low-frequency noise and to provide a flat response at higher frequencies.

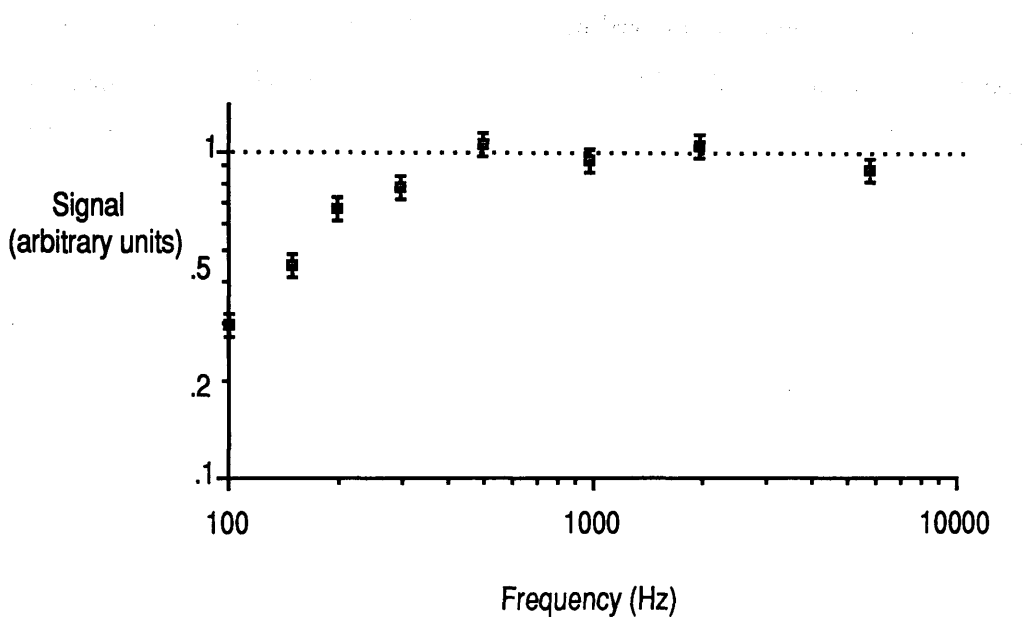


Figure 3.6: *The loss of gravitational wave signal at low frequencies due to cancellation by the control system. The reduction has the expected form indicating the loop-gain of the secondary inboard mirror control system. The signal is reduced by 3 dB in the region of 200 Hz.*

ter a high frequency calibration peak corresponding to a known displacement was produced by applying a 45 kHz signal to the primary inboard mirror. (The motion produced by this signal was calibrated by monitoring the power on the main output photodiode with the outboard mirrors removed. The small Michelson interferometer so formed could be locked to a dark fringe and the output power investigated. The output power is then proportional to the square of the phase offset in the interferometer and the size of the resulting 90 kHz signal was measured to reveal the amplitude of arm length modulation. The motion per applied voltage for the transducer in question was then calculated.)

The spectrum of the residual noise at high frequency is shown (figure 3.7). The root mean square displacement to which the calibration peak corresponded was $(1.3 \pm 0.4) \times 10^{-12}$ m. To achieve the highest signal to noise ratio the interferometer had to be shielded against acoustic noise. In addition the ambient noise level in the laboratory was reduced to a minimum. The background noise corresponds to a displacement of $(2.0 \pm 0.8) \times 10^{-16}$ m/ $\sqrt{\text{Hz}}$ above 50 kHz.

3.2.4 Conclusion

The control systems each appeared to perform satisfactorily and there was no apparent operational difference between them even with the added low frequency mirror motions. It is possible that in a fully suspended apparatus one of the control systems may be simpler to implement. This would have to be tested on a suspended interferometer. Both of the control systems allowed photon shot noise limited displacement sensitivity to be approached at high frequencies (> 50 kHz) where the other noise sources were sufficiently reduced.

3.3 External modulation

The experiment described here was intended to test one possible control system for the externally modulated interferometer. (Colleagues in France have tested a similar system and the results have recently appeared in the literature[28].) It was considered important that the system used could be applied to a full-scale detector

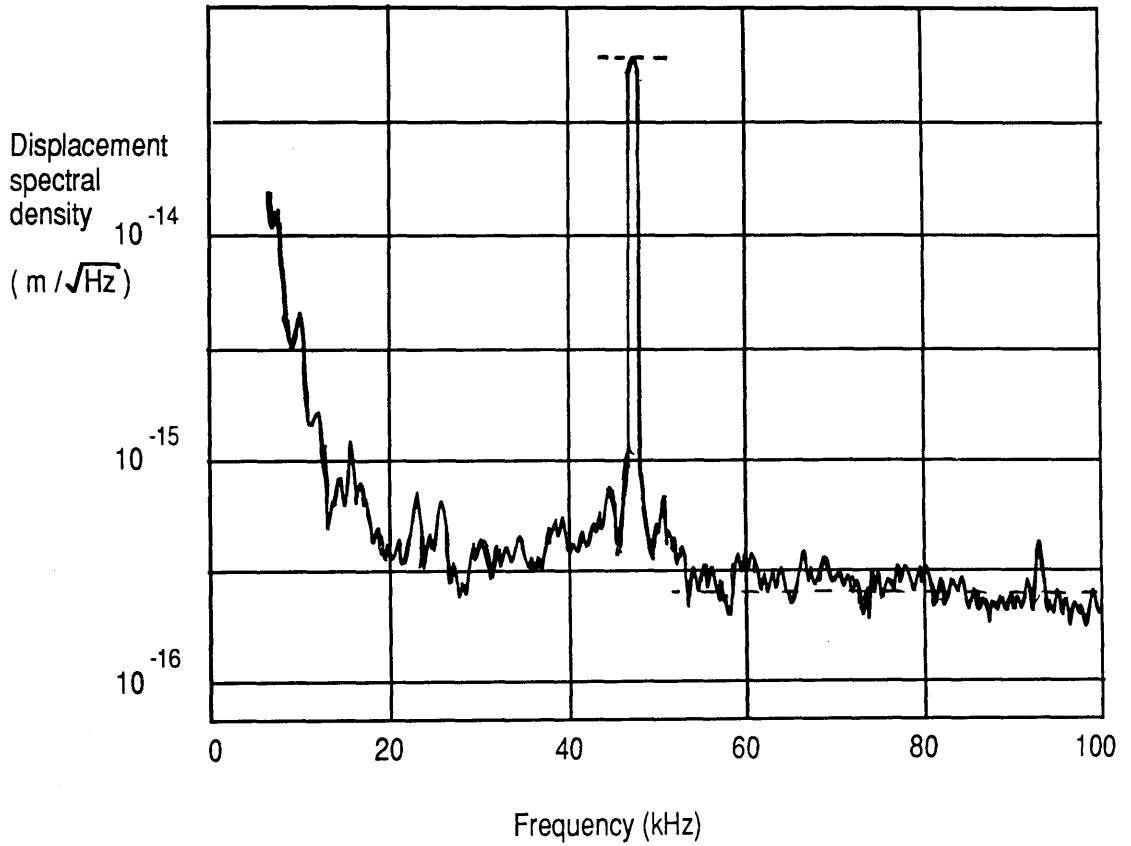
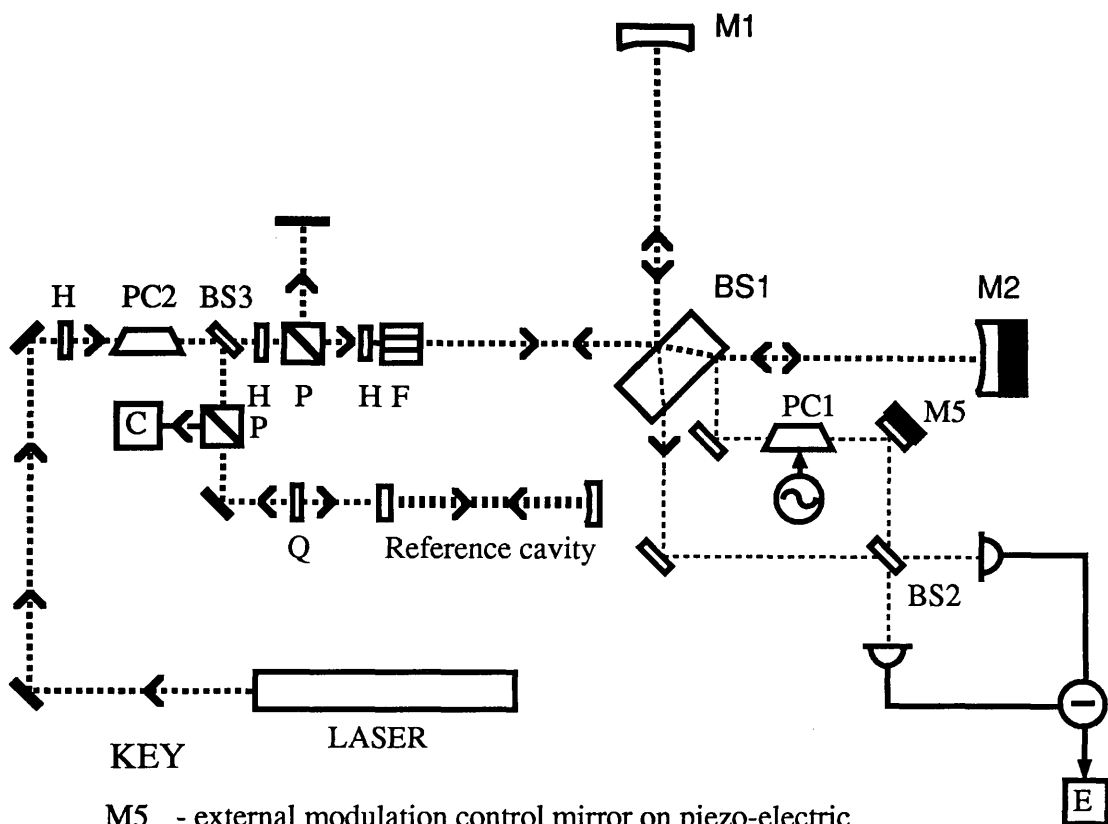


Figure 3.7: *The equivalent displacement spectrum of the signal at the error point in the internal modulation experiment. The peak near 45 kHz is the calibration peak described in the text. The spectrum analyser measurement bandwidth was 477 Hz.*

and that the apparatus produced would be a suitable basis to which recycling and dual recycling systems could be added. Optics of a similar quality to those described in the internal modulation experiment were used. Due to the complexity inherent to some of these systems it was decided that all of these tests would be carried out on a Michelson interferometer with a single traverse of the arms (in each direction). The results of these experiments could therefore be applied to interferometers with delay-line arms but not, directly, to systems with cavities in the arms.

It was realised that the physical layout of the external modulation system would be more complicated than the internal modulation scheme due to the need for the Mach-Zehnder interferometer used to combine the reference beam with the main output from the Michelson interferometer. A granite optical bench (1200 mm \times 700 mm \times 110 mm) was obtained. It was thought that, as well as offering considerable rigidity, the large thermal inertia of this bench would reduce thermal expansion effects to a minimum (to allow sustained operation with the limited range of the position transducers available). The beam paths in the sensitive parts of the system were enclosed by glass tubes to provide some isolation from acoustic noise and air currents. High quality mounts were used to hold all of the main optical components. These mounts were fixed directly to the optical bench to maximise the rigidity of the system. The whole optical bench was mounted on six small pieces of soft rubber to give some isolation from vibration. All of this was done in an effort to allow measurements to be made at as low a frequency as possible.

A diagram of the optical system used is shown (figure 3.8). The interferometer mirrors (M1,M2) were each spaced 0.50 m from the beamsplitter. Their radii of curvature were 5.0 m. The reference beam, a small fraction of the light returning to the beamsplitter from M1, was directed through one half of the external modulation optics. The Michelson interferometer output beam was made to overlap correctly with the reference beam at the second beamsplitter. This was done with the output of the Michelson interferometer far from an interference minimum to ensure that the output light was dominated by the fundamental mode (rather than the



KEY

LASER

M5 - external modulation control mirror on piezo-electric transducer

BS2 - second beamsplitter (50%)

BS3 - 20 % beamsplitter

PC1 - main electro-optic modulator for external modulation

PC2 - electro-optic modulator for cavity locking (12 MHz)

E - main output signal

C - laser stabilisation signal

Q - quarter wave retardation plate

H - half wave retardation plate

▨ - 45 degree Faraday-effect rotator

▧ - polarising beamsplitter

BS1 - main beamsplitter (50%) with anti-reflection rear coating as described in the text

Figure 3.8: *The optical system used to test external modulation. Only the essential elements are shown, for clarity. The piezo-electric transducers are shown as solid black rectangles. The control systems are described in the text.*

complicated mixture of modes found at the minimum). Fine adjustment of the angle of the overlapping beams, with the system operational, allowed the signal size to be maximised. The two output beams from the second beamsplitter were directed on to two photodiodes. A fraction of the light from the laser ($\sim 20\%$) was used to illuminate a reference cavity to which the laser frequency could be stabilised. Optical diodes were again used to prevent reflected light returning to the laser.

Modulation and feedback system for external modulation

The modulation and control systems used to operate the interferometer with external modulation are shown (figure 3.9). The modulation index required for optimum signal to noise ratio with external modulation is quite large (~ 1.8 —from section 2.2.3). A phase modulator which was rated for high power was used to obtain a measured modulation index of ~ 1.3 . This was considered to be adequate representing a signal loss of only about 15% compared to the optimum modulation index. The modulation frequency was again 10 MHz. Piezo-electric transducers were provided to control the lengths of one of the arms of the Michelson interferometer and one of the arms of the Mach-Zehnder.

In order to reduce the frequency noise of the laser, especially at high frequencies (> 1 kHz), it was stabilised to a reference cavity (length 0.46 m, finesse 6000 and input mirror transmittance of $\sim 3.6 \times 10^{-4}$) which was mounted on the bench close to the Michelson interferometer using the method described in Appendix B. The residual frequency noise spectral density, relative to the reference cavity, in the region from 10-30 kHz was measured to be $\leq 0.2 \text{ Hz}/\sqrt{\text{Hz}}$.

The design of photodiode amplifier was changed to subtract the signals from two diodes before amplification and demodulation as required for the external modulation system. The subtraction was done at radio-frequency using a broadband transformer with opposed primary windings to subtract the signal from two tuned photodiodes. The signal from the main photodiodes was demodulated at 10 MHz. The resulting signal was amplified, filtered and used to control the position of one

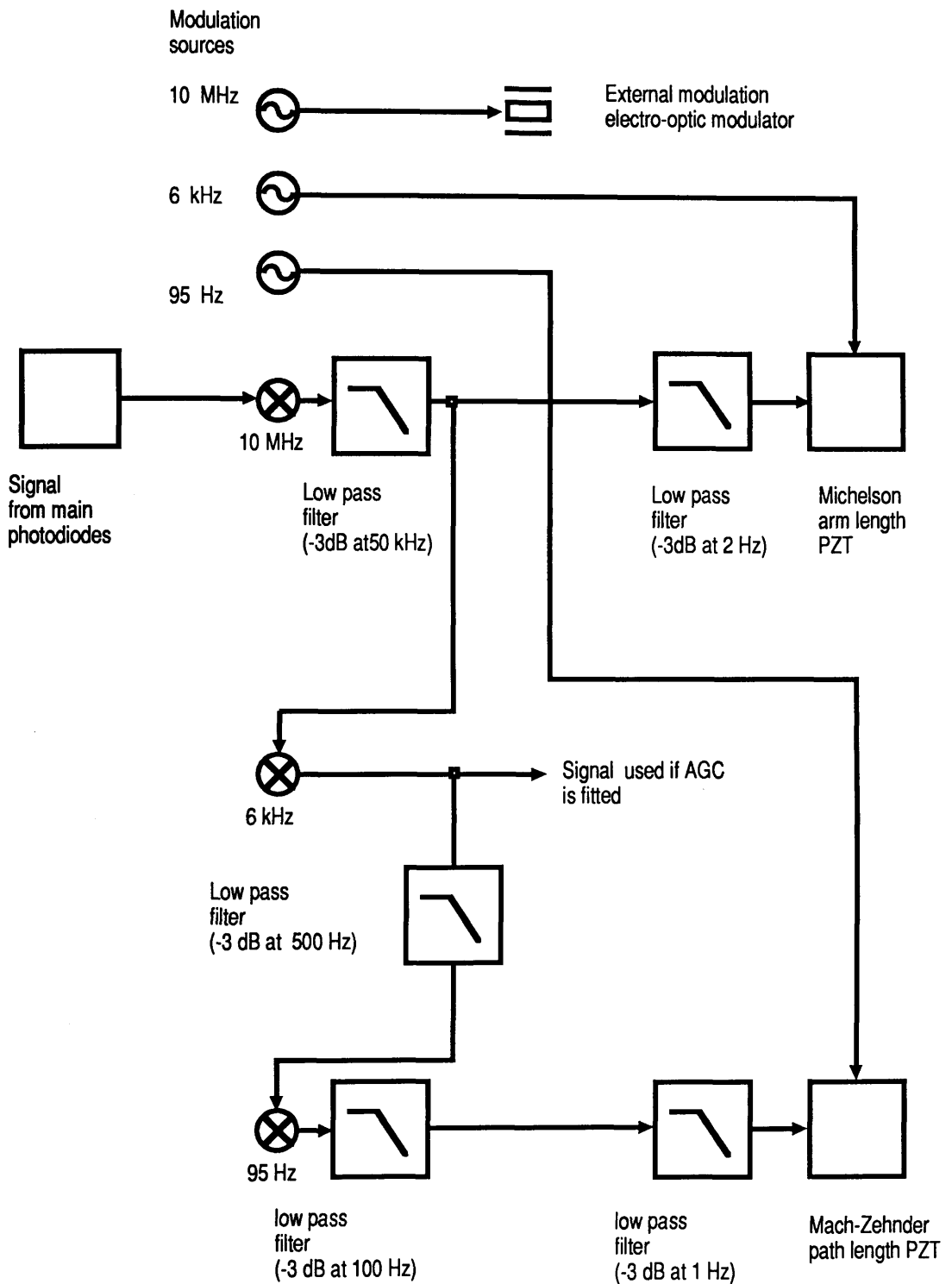


Figure 3.9: *The modulation, demodulation and control systems for external modulation. The properties of the control systems are given in the text. The output from the 6 kHz demodulator was used to provide the signal for the automatic gain control (AGC) when it was implemented.*

of the interferometer mirrors (M1).

The second modulation was applied to the arm length transducer. The frequency of the modulation was chosen to be 6 kHz. The modulation index of this modulation was chosen to be small ($\sim 10^{-3}$). The modulation index is limited by the need to ensure that the loss of power from the interferometer due to the presence of this modulation is small compared to other causes of power loss from the output. It was chosen to give a workable signal to noise ratio in the external modulation system with a very small illuminating power (effectively the case when the recycling system described below is attempting to acquire correct operation). The output of the 10 MHz mixer was amplified, filtered and demodulated coherently with the 6 kHz modulation (using a lock-in analyser). This provided a measure of the signal resulting from the second modulation.

The third modulation was applied to the Mach-Zehnder arm length transducer. The frequency chosen, 95 Hz, was a little higher than that which would be used in a full-scale detector intended to work at the lowest practical frequencies. This was because it was felt that a control system bandwidth of several tens of hertz would be necessary in the benchtop experiment to allow compensation for the effects of air currents. The index of this modulation should be large to provide a large signal. This could have the undesirable side-effect of non-linearity of the transducer causing some mixing of the modulation with the main output signal. A compromise modulation index of ≈ 0.1 was chosen and was found to be satisfactory.

The output of the 6 kHz demodulator was filtered and was demodulated by multiplication with a sine wave (in phase with the 95 Hz modulation) in an analogue multiplier. The resulting signal was amplified and fed to the Mach-Zehnder arm length transducer. An optional inverter was included to select the sign of the feedback for the whole system.

3.3.1 Results

The external modulation control system was found to work satisfactorily. The bandwidths of the two control systems were measured by noting the suppression

of added test signals. The Michelson interferometer system was operated with a bandwidth of about 2 kHz and a low frequency gain (< 2 Hz) of 60 dB. The external reference beam path control servo-system had a bandwidth of ~ 40 Hz and a low frequency gain of about 20.

The arm lengths were carefully equalised (allowing for the optical thickness of the beamsplitter). The lengths of the arms were balanced to about 0.5%. This should give a common mode rejection of frequency noise of 46 dB. The measured rejection, using a frequency noise peak applied via the electro-optic modulator in the laser, was found to be ~ 43 dB. The measured frequency noise would therefore produce an equivalent displacement noise of $< 2 \times 10^{-18}$ m/ $\sqrt{\text{Hz}}$.

The amplitude reflectivity of the anti-reflection coating was measured to be 0.022 ± 0.003 for the 's' polarisation. This determined the amplitude of the reference beam and hence the size of the signal and minimum light power at the main photodiodes. The effective contrast of the Michelson interferometer was later measured to be 30 ± 2 . (This was improved to 45 ± 3 by more careful alignment of the arms of the interferometer when an angle transducer was added to allow control of the orientation of one of the interferometer mirrors.) The reflectivity of the anti-reflection coating was therefore a little less than optimum but there was no alternative coating available. (It is interesting to note that, if the power recycling mirror had been chosen to maximise the displacement sensitivity of the interferometer then the reflectivity of the anti-reflection coating would have been close to the optimum [36].)

The signal from the interferometer was analysed. At low frequency, < 2 kHz, the gravitational wave signal is proportional to the feedback signal to the Michelson interferometer arm length. At higher frequency the error point in the arm length servo-system loop has the correct information. Calibration of this measurement used the known size of the 6 kHz arm length modulation. At this stage the position modulation was $(2.0 \pm 0.6) \times 10^{-10}$ m peak to peak.

A Fourier spectrum of the output signal is shown (figure 3.10). With the input power of 10 mW and the effective contrast ~ 30 the measured photon shot noise limited spectral displacement noise was very close to that expected

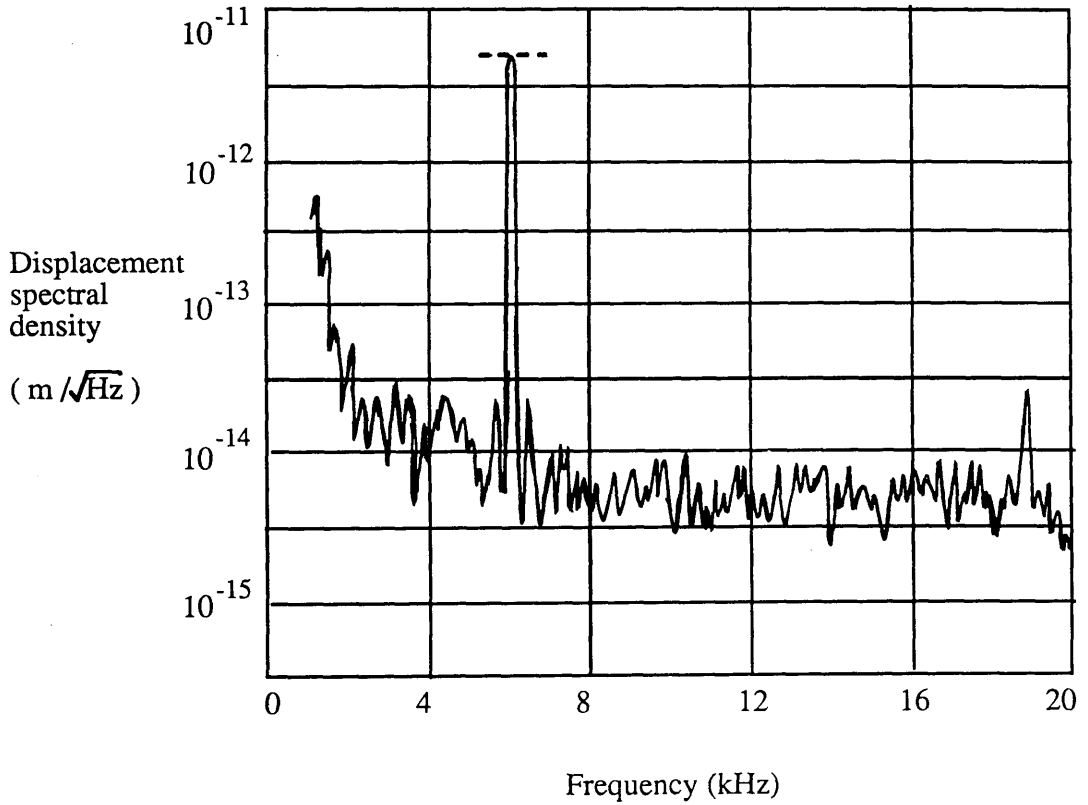


Figure 3.10: *The equivalent displacement spectral density of the error-point signal in the external modulation system. The peak at 6 kHz represents a displacement of $\sim 2 \times 10^{-10}$ m peak to peak. The measurement bandwidth of the spectrum analyser was 96 Hz.*

($\sim 6 \times 10^{-15} \text{ m}/\sqrt{\text{Hz}}$) given the known parameters of the interferometer and equation 2.9.

3.3.2 Conclusion

The interferometer with external modulation operated as predicted in the previous chapter. The control system worked very reliably to keep both the Michelson interferometer output on the dark fringe and to maintain the correct phase of the reference beam at the second beamsplitter. The measurement noise was dominated by photon shot noise at frequencies above 10 kHz. The results indicate that the system was operating correctly and that the signals were understood.

correctly until the cavity was an axial mode of a laser. In this case, the laser does not behave as a highly coherent source of radiation as assumed in the basic model of a control system, therefore a phase-locked loop will not be able to lock the receiving cavity.

In the next step test of recovery there was the addition of a laser to align the reference beam with the frequency of the signal to be measured. Zero frequency was used. With a power level of approximately 10 mW, the reference beam could be used to align the laser to the laser cavity. The alignment was done from the output of the laser. The laser was used to align the laser to the laser. The non-linearities in the laser were not to have intensity, noise

2% level over the range of frequencies. It could be expected that the signal level in the output of the laser would change by about 10%.

3.4 Power recycling

In order to implement power recycling on the interferometer it is necessary to add the power recycling mirror between the laser and the input to the interferometer. This mirror must be correctly aligned with the interferometer to form a cavity. A servo-system to control the length of this cavity to maintain the maximum internal amplitude must also be provided.

3.4.1 An automatic gain control for power recycling.

The main potential difficulty with recycling is that if the recycling cavity is not resonant the light amplitude within the interferometer will be very small, the signals used to control the external modulation system will be small and the control systems may not operate. This is likely to be a problem if the power recycling mirror has a ^Q small coefficient of transmission, in order to achieve a large power increase, or if the input power is small. The recycling cavity cannot resonate correctly until the interferometer is close to its operational condition. Only then does it behave as a highly reflecting mirror. Correct operation of the external modulation control system is, therefore, a prerequisite to amplitude build up within the recycling cavity.

In the bench top test of recycling there was the additional problem of aligning the reference beam with the interferometer output beam at the Mach-Zehnder beamsplitter. With a power recycling mirror transmittance of $< 1\%$ the reference beam could not be seen sufficiently clearly to allow it to be correctly aligned with the output from the Michelson interferometer. A 4% transmittance mirror was chosen. This mirror had been previously measured to have intensity losses of $\sim 2\%$ Even with this, quite large, transmittance it could be expected that the signal sizes at the output of the interferometer would change by almost 60 dB. In order to overcome this difficulty it was decided to include an automatic gain control system to counter the changing signal size. This was achieved by monitoring the size of the 6 kHz modulation at the output and feeding back to control the gain of the radio-frequency amplifier connected to the main photodiodes.

The automatic gain control was based on standard radio-frequency integrated circuit amplifiers with gain control inputs (Plessey SL1610). This device can be regarded as a low noise radio-frequency amplifier with a fixed gain followed by a stage with an attenuation dependent on a control voltage. The transfer function of gain against gain control input voltage can be approximated by

$$G = Ke^{-V_g}, \quad (3.2)$$

where K is the fixed gain and V_g is related to the voltage at the gain control input.

The circuit which was used for the automatic gain control is shown (figure 3.11). The operation of this control system can be evaluated by considering the attenuation part of the transfer function as a function of input voltage

$$V_{out} = V_{in}e^{-H(V_{ref}-V_{out})}, \quad (3.3)$$

where V_{out} is the size of the output voltage as measured by the 6 kHz demodulator and V_{in} is the size of the input voltage as would be measured by a similar demodulator. V_{ref} is a control voltage and H is set by the transfer function of the automatic gain control amplifier and the gain of the operational amplifier circuit shown. Differentiating equation 3.3 with respect to the input voltage gives

$$\frac{dV_{out}}{dV_{in}} = \frac{A}{1 - HV_{out}}, \quad (3.4)$$

where A is the attenuation ($V_{out}/V_{in} < 1$). If the product $HV_{out} \gg 1$ and there is some attenuation then $\frac{dV_{out}}{dV_{in}} \rightarrow 0$ and the output voltage is almost independent of input voltage.

If, initially, the signals are small and the gain high then when the power begins to increase the automatic gain control must reduce the gain quickly as the power increases. If this is not so there is the possibility that the bandwidths of the servo-systems will increase until they oscillate. The time-scale for the power build-up should be determined by the response time of the Michelson interferometer and power recycling mirror servo-systems. In the experiment the power increase

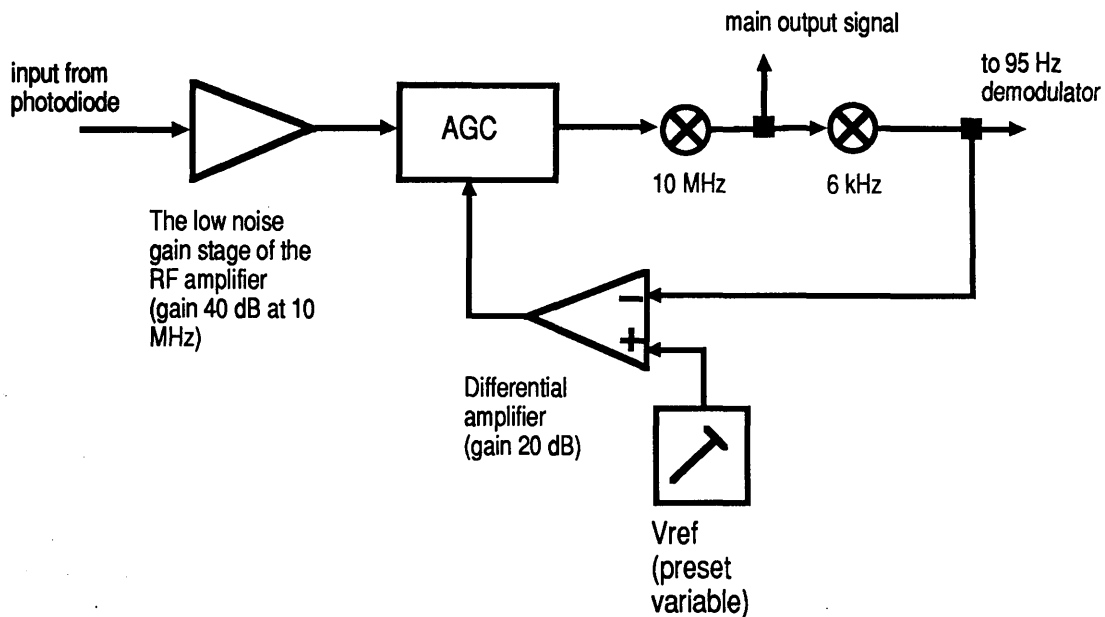


Figure 3.11: *The automatic gain control circuit. The gain of the differential amplifier was chosen to give a loop gain of about 26 dB for the automatic gain control at the maximum input signal operating point. The output signal size was chosen by setting the reference voltage V_{ref} to the desired value.*

occurred over periods of a few milliseconds. The automatic gain control was operated with its unity gain frequency at about 4 kHz. This proved an adequate arrangement.

The automatic gain control system has the disadvantage that it will reduce the size of the signal from the 95 Hz modulation used to control the Mach-Zehnder. The extent to which this happens depends on the loop gain of the automatic gain control at 95 Hz. The loop gain of the automatic gain control servo-system was measured to be ~ 20 at 95 Hz and the gain of the Mach-Zehnder control system was, therefore, increased by this amount.

3.4.2 The power recycling mirror control system

The control signal for the power recycling mirror was obtained by detecting and demodulating the fringes reflected from the recycling cavity. The output from the demodulator was amplified, filtered and applied to the piezo-electric transducer on which M0 was mounted. This servo-system was designed to have a high gain at low frequency (60 dB at up to 2 Hz) followed by a long range of first order (frequency⁻¹) roll-off. This produced a control system which was stable over a wide range of gain. The intention was that this would then begin to function even if the interferometer was not operating with its output on a dark fringe. The circuit used for this system is shown schematically (figure 3.12).

3.4.3 The experimental test of power recycling

The recycling system was tested both with and without the automatic gain control implemented. The system would operate in either case but the automatic gain control allowed generally more rapid recovery of correct operation after any disruption.

The power within the interferometer was measured by monitoring a small fraction of the reference beam on a low frequency photodiode monitor. This showed a power increase of 35 ± 3 with recycling (after allowing for the known fraction of the phase modulated light which could not resonate). This compares reasonably

The output signal was analysed in the same way as for the external modulation system. The spectrum of the output signal is shown (figure 3.13). This spectrum shows an enhancement of signal to noise ratio by a factor of ~ 3 compared to figure 3.10. The amplitude in the fundamental mode of the power recycling cavity would be expected to increase by a factor of about $\sqrt{34}$ modified by the reduction in input power due to the fact that the modulation sidebands on the input light ($\sim 33\%$ of the power) cannot resonate. The observed increase in signal to noise ratio thus approaches the expected increase of ~ 5 . (For this measurement the contrast and input power were similar to those used to measure the signal to noise ratio without recycling.)

to the expected increase of 43 (calculated from equation A.1). The discrepancy between these figures was probably due to the imperfect mode matching of the input laser beam to the fundamental mode of the recycling cavity.

In order to allow the test of dual recycling presented below it was necessary to use a different power recycling mirror. This was due to a desire to keep the curvature of the two recycling mirrors equal (at 0.70m) to allow simple mode matching of the parts of the interferometer. The mirrors which were available in pairs had 10 % transmittance. The power recycling experiment was repeated with one of these mirrors as M0. The power increase due to recycling was now 34 ± 3 . This again compares quite well with the expected value (37) for the given optical parameters.

(PLEASE REFER LEFT)

3.4.4 The effects of misaligning one of the arms in the power recycling interferometer

The effects of misaligning one of the arms of the interferometer were measured. In order to allow this the system was modified to include an angle transducer on one of the interferometer mirrors and a power monitor on the light from the main output.

The angle transducer was based on a Burleigh PZAT80 piezo-electric transducer. This has three separate longitudinal transducers spaced at 120 degree intervals around a cylinder. The application of differential signals to this unit allows one end of the transducer to be tilted with respect to the other. The geometry of this is illustrated (figure 3.14). Only one element of this transducer was used. A

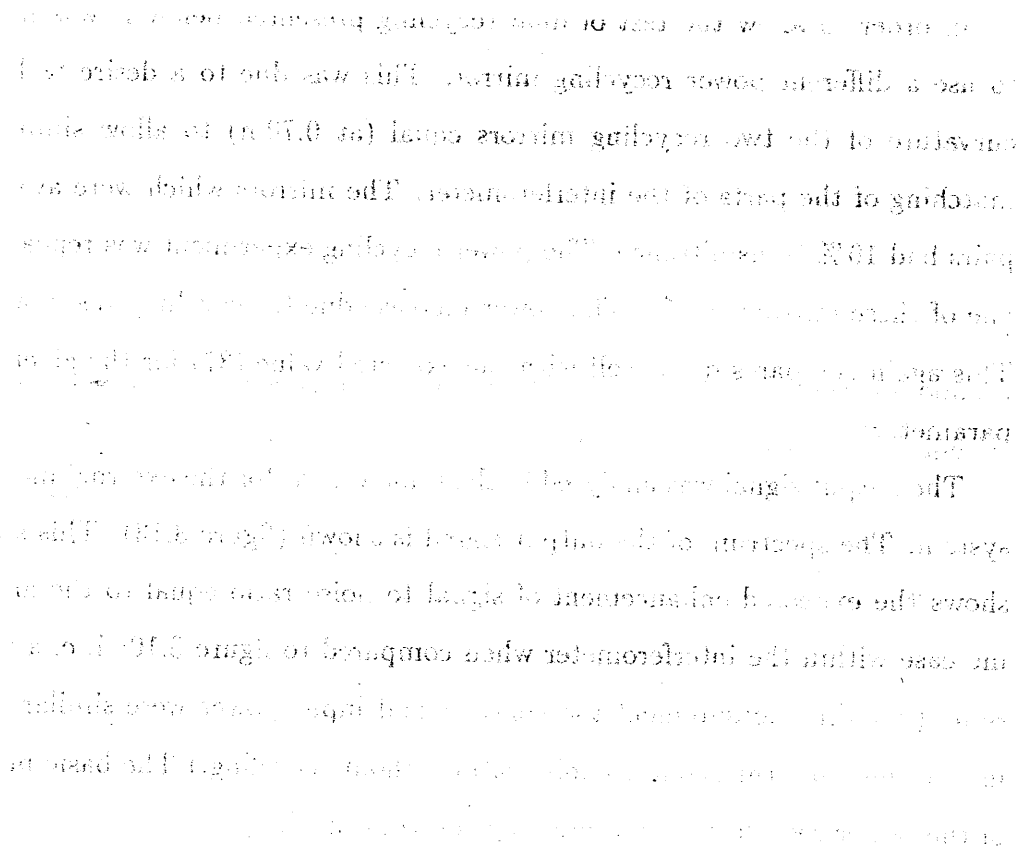


Figure 3.13: A spectrum of the error-point signal from power recycling. The peak at 6 kHz was used as calibration. The presence of harmonics of this frequency were almost certainly due to the action of the automatic gain control which could have led to modulation of the gain by $\sim 10\%$ at a frequency of 6 kHz. The harmonics were not observed when the automatic gain control was inoperative. In practice, since the automatic gain control was only required for acquisition, its bandwidth, and the resulting nonlinearities, could be reduced when the interferometer was operating correctly.

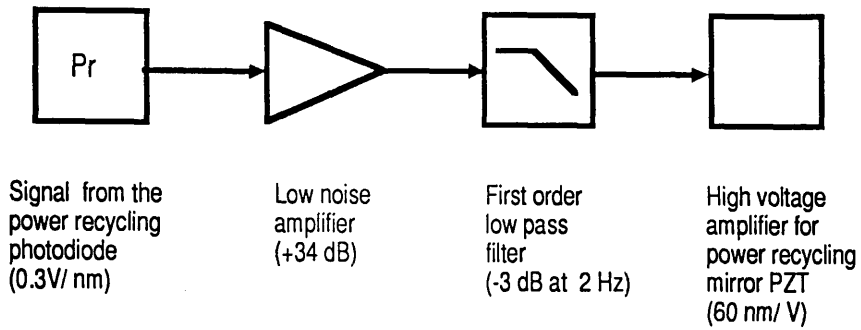


Figure 3.12: *The circuit of the recycling servo.*

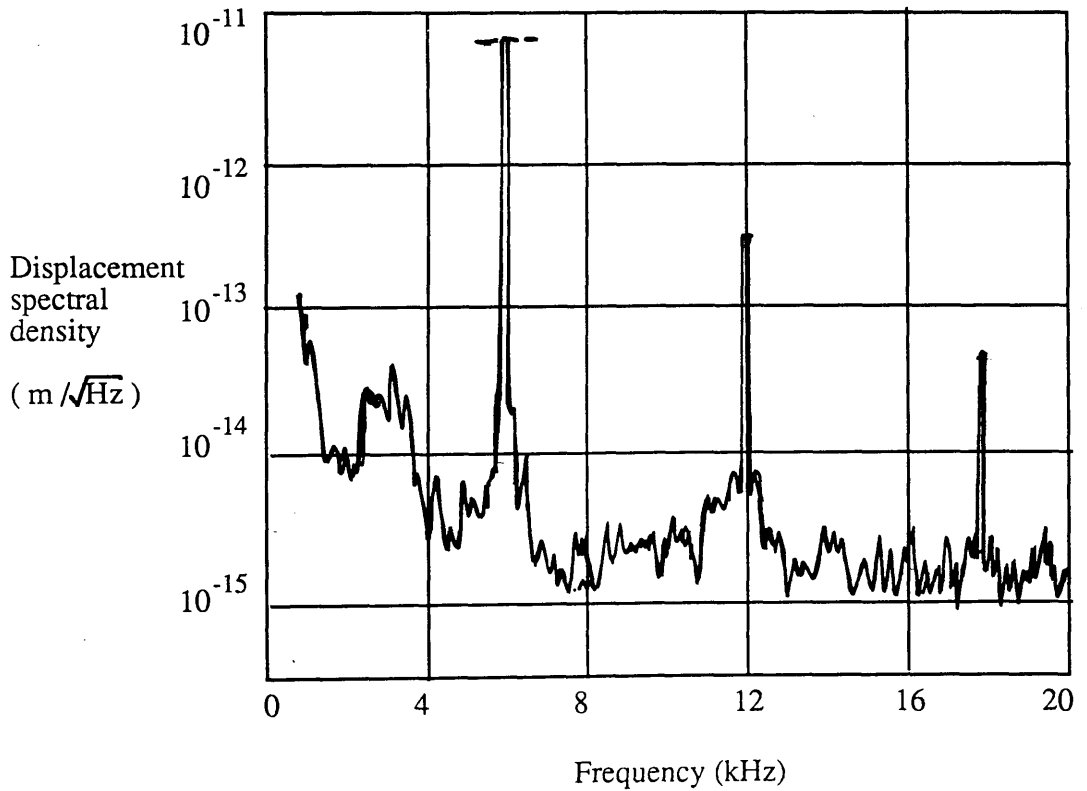


Figure 3.13:

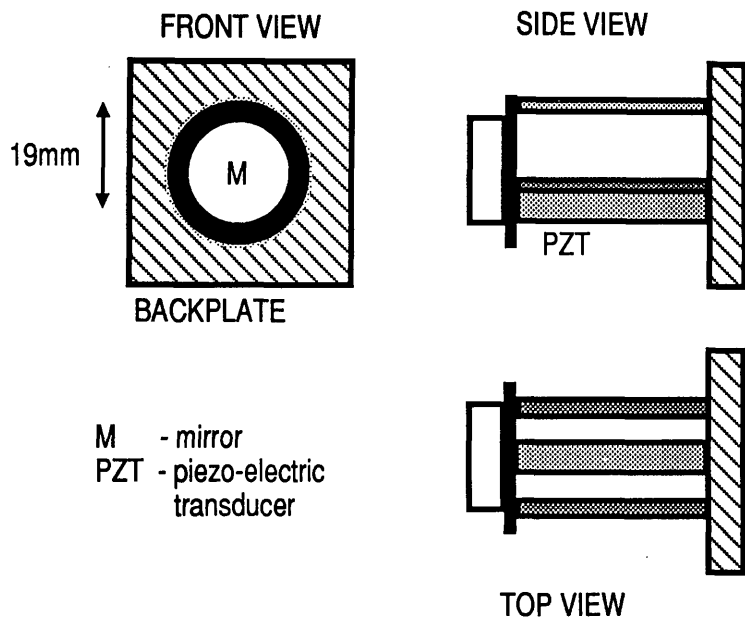


Figure 3.14: *The geometry of the angle transducer. Application of a voltage to one of the piezo-electric (PZT) elements tilts the mirror.*

variable (0-1 kV) power supply was connected to the transducer. Variation of the voltage allowed the angle of the mirror attached to the transducer to be altered. This type of transducer does have some hysteresis and the manufacturer's calibration of this effect was used to calculate the absolute relationship between angle and applied voltage.

The size and position of the beam waist in the recycling cavity were calculated from the curvatures and positions of the mirrors which formed this cavity. There are two waists, one in each arm, each ~ 12 mm from the interferometer mirrors (M1,M2). The predicted beam size at the mirror is 0.21 mm. This allowed the 'normalised misalignment angle' (θ_n —defined in section 2.4.3) to be related to the voltage applied to the angle transducer.

The interferometer was aligned until the output light power was a minimum. The corresponding effective contrast (the ratio of the amplitude in the interferometer to that emerging from the output) was 45 ± 3 . The angle of M2 was then changed and the power emerging from the interferometer was measured relative to the power within the interferometer. The result of this measurement is shown (figure 3.15) along with the predicted power loss as a function of angle. The power uncertainty was due to the fluctuations in the laser power. The uncertainty on the angle originates from an estimate of the precision of the hysteresis curve for the transducer and the stability of the high voltage supply. The predicted quadratic dependence of loss against angle (equation 2.50) is followed over most of the range of misalignment angles. At the smallest angles ($\theta_n \leq 0.02$) the loss is independent of angle. It was thought that this loss was probably due to distortions in the shapes of the mirrors or beamsplitter leading to second or higher order modes in the recycling system. The best fit to the experimental data was obtained by assuming an angle independent loss of 4×10^{-4} added to $(0.96\theta_n)^2$. The discrepancy between the expected and apparent angles is reasonable given the systematic error due to lack of knowledge of the exact beam size and and transducer calibration (up to about 10 %).

The power remaining within the interferometer was measured for a few of the larger values of misalignment. The results of this are shown (table 3.1). The power

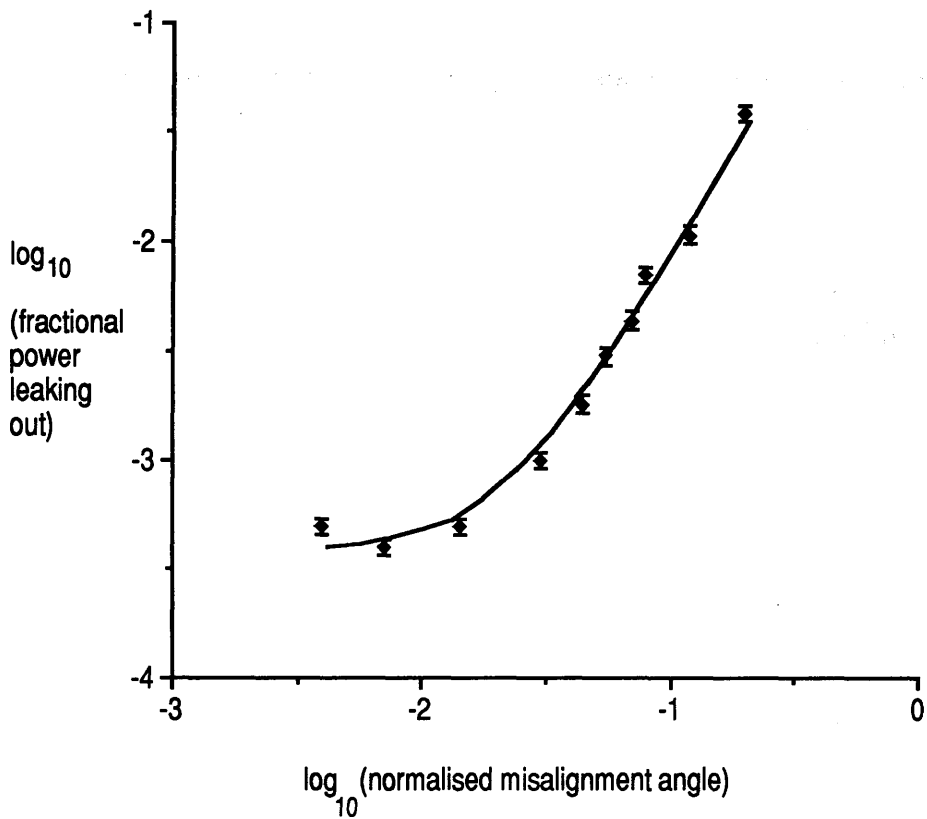


Figure 3.15: *The fractional power of the light emerging from the recycling interferometer as a function of the normalised angle of one of the interferometer mirrors. The points plotted are the experimental measurements. The line is the best fit of the theory to the experimental points.*

Misalignment angle θ_n	Predicted power	Measured power
0.05	0.96	0.95 ± 0.05
0.1	0.84	0.80 ± 0.05
0.2	0.53	0.60 ± 0.05

Table 3.1: *The power within the recycling interferometer as a function of the normalised misalignment angle. The power has been scaled so that the maximum observed power equals unity.*

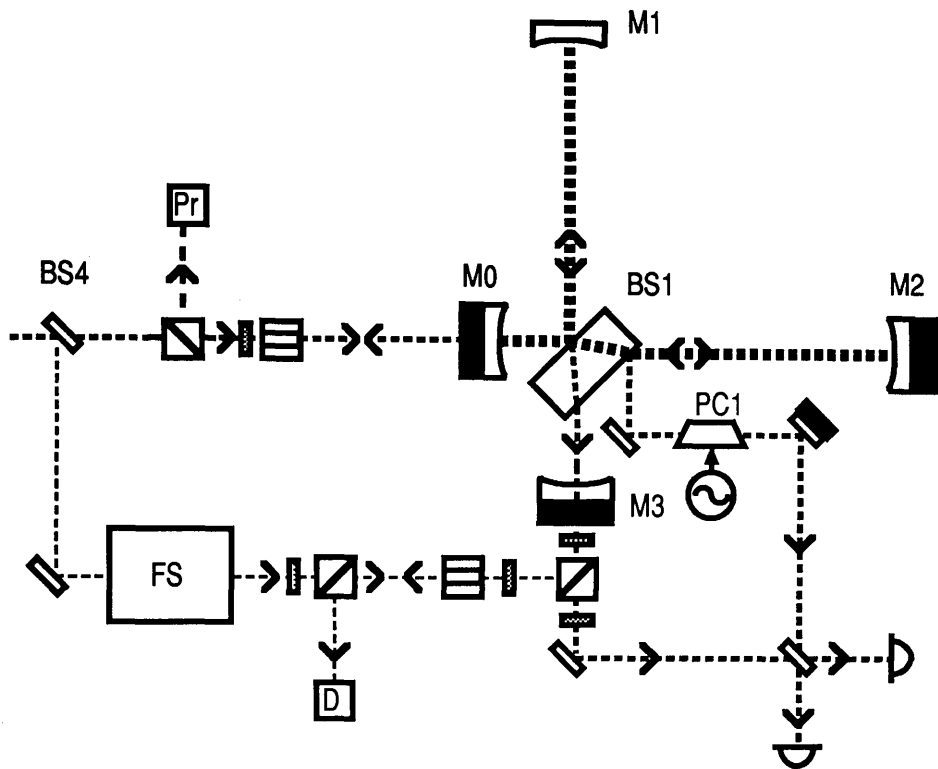
build-up expected from this system can be calculated using the equation(A.1) for the amplitude in a cavity if the losses from the output are represented by assigning the same loss to one of the cavity mirrors. The expected relationship between the loss from the power recycling cavity and the power build up was confirmed to reasonable accuracy.

3.4.5 Conclusion

The test of the recycling system was successful and the control system, with the automatic gain control, was found to work reliably. The amplitude and signal to noise increase predicted in section 2.4 was observed to within reasonable limits. The predicted power loss from the output due to the misalignment of one of the interferometer arms was also confirmed over a range of angles. The last measurement will provide a useful comparison with dual recycling.

3.5 Dual recycling

The optical system for dual recycling is shown in slightly simplified form (figure 3.16). The change from power recycling is the addition of the signal recycling mirror and its control system. The range of gains of the automatic gain control had to be increased to allow for the greater dynamic range of signal sizes now possible. A further stage was added to the automatic gain control amplifier to increase the



KEY

- M0 - power recycling mirror on piezo-electric transducer
- M3 - signal recycling mirror on piezo-electric transducer
- BS4 - 10 % beamsplitter

- FS - frequency shifter (see figure3.17)
- Pr - power recycling control signal
- D - signal recycling control signal

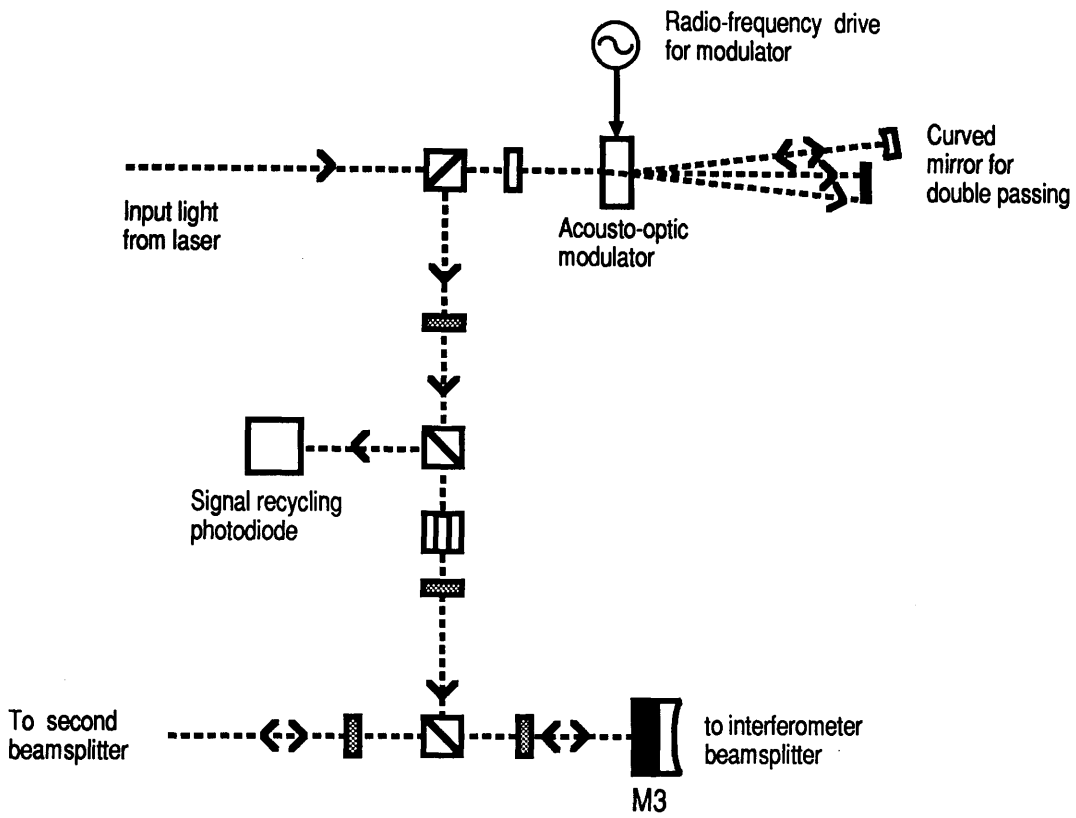
-  - 45 degree Faraday-effect rotator
-  - polarising beamsplitter
-  - half-wave plate

Figure 3.16: A simplified diagram of the optical system for dual recycling. The essential optical elements are shown. The input light was generated using the same system as for external modulation. The detail of the frequency shifter is shown in the subsequent figure.

range of gains by about 20 dB to over 60 dB.

The signal recycling cavity, formed by the interferometer arms and the signal recycling mirror, was about 0.592 m long. The free spectral range of this cavity was, therefore, approximately 253 MHz. The transmittance of the signal recycling mirror was 10 %. The control beam used to illuminate the signal recycling cavity, in order to provide a signal to control this cavity, needs to be tunable over a range of frequencies about the initial carrier frequency. It was decided to frequency shift a fraction of the input light by a multiple of one free spectral range of the signal recycling cavity. The amount of this frequency shift could then be varied to allow the frequency of this beam to be scanned through a resonance of the signal recycling cavity. The frequency shifting was achieved using an acousto-optic modulator. The first diffraction order was used and this gives a frequency shift equal to the drive frequency to the modulator. The modulator used had an operating frequency range of 200 ~ 250 MHz but was double-passed to cancel the angular deviation produced on each pass. The control beam produced could therefore have its frequency adjusted about two free spectral ranges of the signal recycling cavity from the original laser frequency. The control beam was adjusted to be of the orthogonal polarisation to the main light in the interferometer to allow it to be separated from the main light at the output. Since all of the output light from the laser was phase modulated, the control beam also carried this phase modulation. It could therefore be used to control the dual recycling cavity by the reflection fringe method. The optics used to generate the control beam are shown in detail (figure 3.17).

The power of the control beam, measured at the photodiode for the signal recycling mirror control system was $\sim 0.2\%$ of the power within the power recycling cavity. As discussed in section 2.5 this should be adequate to avoid imposing excess noise due to photon shot noise on the detected power via the signal recycling mirror provided that the internal contrast (the ratio of the amplitude approaching the beamsplitter from the power recycling mirror to that approaching the signal recycling mirror from the beamsplitter) is greater than 40. (There was additional protection against this since the signal to noise ratio measurements were made at



KEY

- M3 - signal recycling mirror
- half-wave plate
- quarter-wave plate
- polarising beamsplitter
- 45 degree Faraday-effect rotator

Figure 3.17: *The optics used to generate the control beam for dual recycling. The light from the first diffraction order in the acousto-optic modulator was reflected back through the modulator using a curved mirror spaced its own radius from the modulator. The resulting first order diffraction spot was then used to form the control beam. The effect of this ‘double-passing’ was to eliminate most of the change of angular deviation produced when the modulator drive frequency was altered.*

frequencies at which the signal recycling servo-system was inoperative.)

The frequency noise on the control beam, the same as the laser light as a whole was sufficiently low not to limit the sensitivity by adding spurious motion to the signal recycling mirror. The bandwidth of the signal recycling mirror servo-system was ~ 2 kHz and above this frequency the motions imposed by this servo-system for a given signal at the error point would be reduced as if filtered by a single-pole low pass filter at 2 kHz. The displacement imposed on the signal recycling mirror due to the measured frequency noise in the region of 10 kHz would be $\sim 4 \times 10^{-17} \text{ m}/\sqrt{\text{Hz}}$. The resulting noise sidebands produced would be equivalent to those due to motion of the beamsplitter or interferometer mirrors by the above displacement divided by the internal contrast.

The fraction ($< 0.3\%$) of the control beam which reached the main output photodiodes contributed little to the total power there. The frequency of the control beam has been shifted by ~ 500 MHz so any frequency noise contributions caused by beating of this with the output light at the output photodiodes have also been shifted by a similar frequency. The large low frequency contributions are therefore shifted out of the signal band.

The servo-system used to control the position of the signal recycling mirror was similar to the one used for the power recycling mirror with the exception that the overall gain was increased to compensate for the smaller signals produced by the low power of the control beam.

The operation of the dual recycling system as a whole was controlled by selecting the frequency shift applied by the acousto-optic modulator. This then controlled the resonant frequency of the signal recycling cavity. (As explained in section 2.5.)

3.5.1 The experimental test of the frequency response and signal to noise ratio of the dual recycling interferometer.

The frequency response of the dual recycling system was measured by again making use of the 6 kHz arm length modulation. The dynamic range of the output signal

was now excessive due to the signal enhancement properties of dual recycling. The output signal was high pass filtered to remove the large low frequency components and the amplitude of the 6 kHz arm length modulation was reduced by a factor of 5. This allowed the output signal to be handled more easily. (It was also necessary to make some reduction to avoid excessive loss of power at the output of the interferometer due to the arm length modulation.)

The arm length modulation represents a very low frequency differential phase signal with respect to the expected linewidth of the signal recycling cavity and so this behaves just like a low frequency phase signal in broadband dual recycling. Scanning of the control beam frequency past a free spectral range of the dual recycling cavity should then trace out the shape of the tuning curve of the signal recycling cavity. The signal produced at the output should be a maximum when these sidebands and the carrier light are resonant in the signal recycling cavity.

The automatic gain control would counteract any change in the signal size produced by dual recycling as measured at the error point of the Michelson interferometer control servo-system. It was therefore necessary to provide an additional, fixed gain, radio-frequency amplifier for the output signal. This was provided and the resulting signal separately demodulated and monitored.

The control system for dual recycling operated very satisfactorily: it was able to acquire the correct operation from almost any starting condition. The system did not always lock to the fundamental mode of the recycling cavity but sometimes to higher order modes. This was probably due to the unconditional nature of the signal recycling mirror and power recycling mirror servo-systems. These systems would allow the overall cavity to lock in a variety of modes. In a working detector there would need to be some system to prevent this locking in unwanted modes.

The frequency response of the dual recycling interferometer was measured as described above. This is shown with the expected result (figure 3.18). The tuning curve was predicted from equations 2.54 and 2.41. The known optical parameters of the system were used to calculate the coefficient of finesse. The resulting expression for the signal enhancement (G) over power recycling as a function of signal frequency (taking zero frequency as the resonant frequency of the fundamental

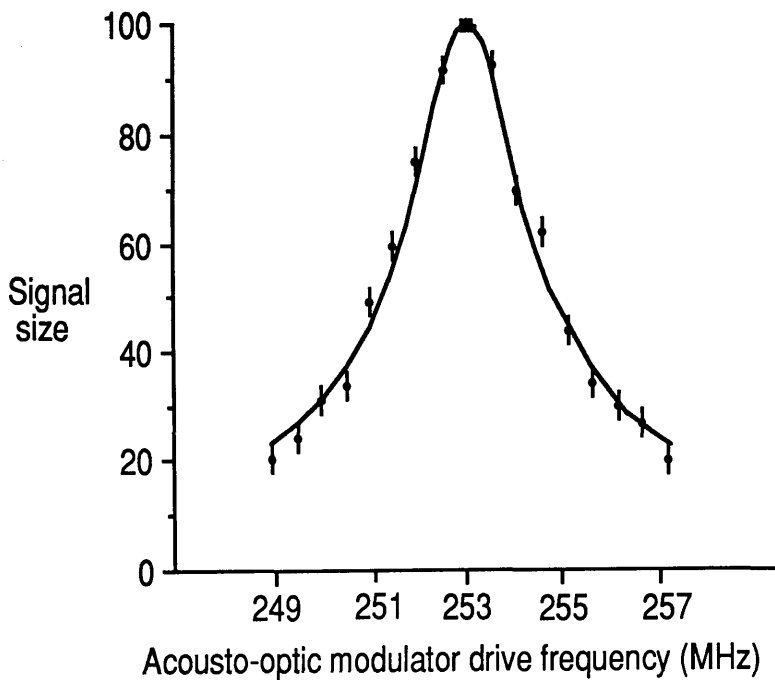


Figure 3.18: *The frequency response of the dual recycling interferometer. The curve shown is the expected line-shape as described in the text. The experimental measurements are shown with the estimated error. The systematic difference between the expected and observed centre frequencies (about 0.5 MHz) has been removed. It should be noted that the frequency by which the light is shifted by the double-pass of the acousto-optic modulator is twice the drive frequency.*

mode of the signal recycling cavity) is therefore

$$G = 6.16 \left[1 + 1440 \sin^2 \left(\frac{\pi f}{253 \text{ MHz}} \right) \right]^{-1/2}, \quad (3.5)$$

where f is the signal frequency (in megahertz). The result shows very good agreement between the expected and observed tuning curves. The experimental error was mostly due to low frequency laser intensity noise which limited the precision with which the signal sizes could be compared.

The signal to noise ratio corresponding to the peak of the tuning curve was measured. The output spectrum from the interferometer is shown (figure 3.19). The shot noise level corresponding to the appropriate amount of light on the output photodiode is superimposed. The signal to noise ratio is enhanced by a factor of ~ 7 . This is slightly more than the signal was enhanced. This is due to the slightly non-optimum level of the reference beam in the power recycling case. It will be seen below that dual recycling improved the effective contrast of the interferometer and so the light power on the photodiode has actually decreased slightly (by $\sim 40\%$) while the signal has increased by the factor expected from dual recycling with the optical parameters used.

3.5.2 The alignment properties of the dual recycling interferometer

The alignment properties of dual recycling were investigated to allow comparison with the power recycling case. The apparatus remained as described above. The experiment was divided into two separate sections which are discussed in turn.

Misalignment and broadband dual recycling

The first experiment was a measurement of the alignment effects with broadband dual recycling (that is with the carrier light fully resonant in the signal recycling cavity). The mirror was misaligned from its optimum angle and the light power leaving the output was measured by monitoring a fraction of the light emerging from the output and comparing this with a measurement of the power in the local

Displacement noise
spectral density
($\text{m}/\sqrt{\text{Hz}}$)

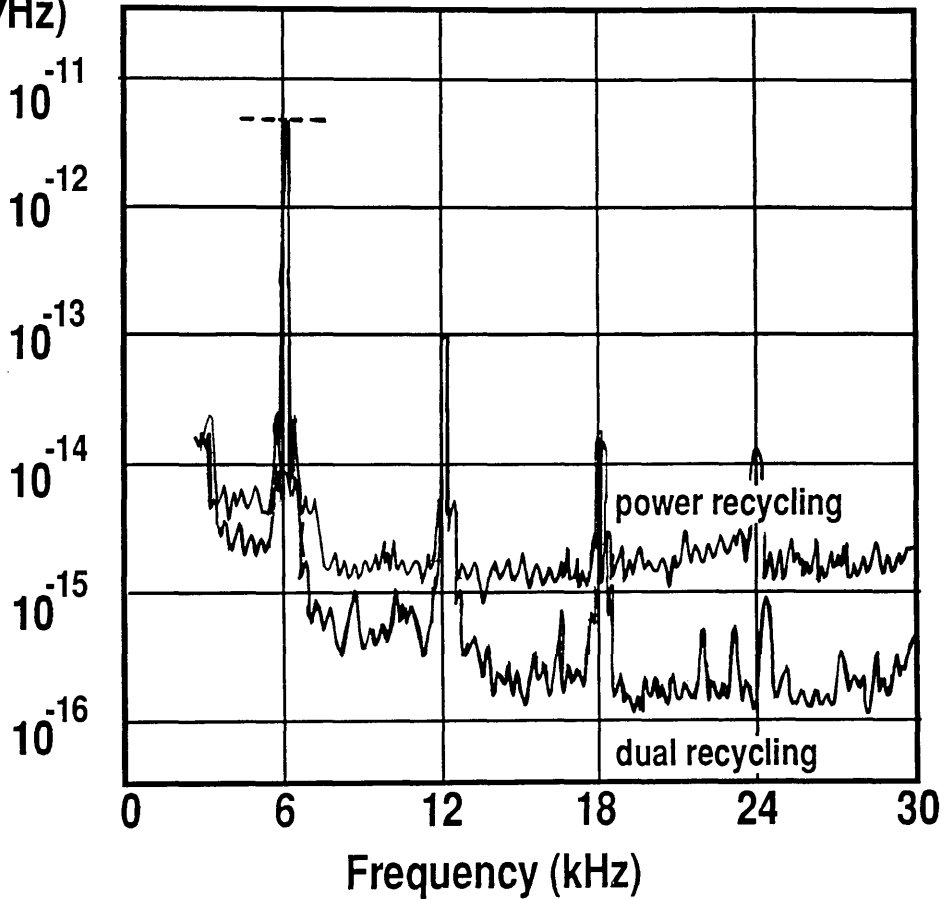


Figure 3.19: *The output spectrum for optimised broadband dual recycling. The peak at 6 kHz was used as calibration. The result for power recycling with the same internal power and effective contrast of ~ 50 is shown for comparison. The signal to noise ratio improvement by a factor of ~ 7 can be seen.*

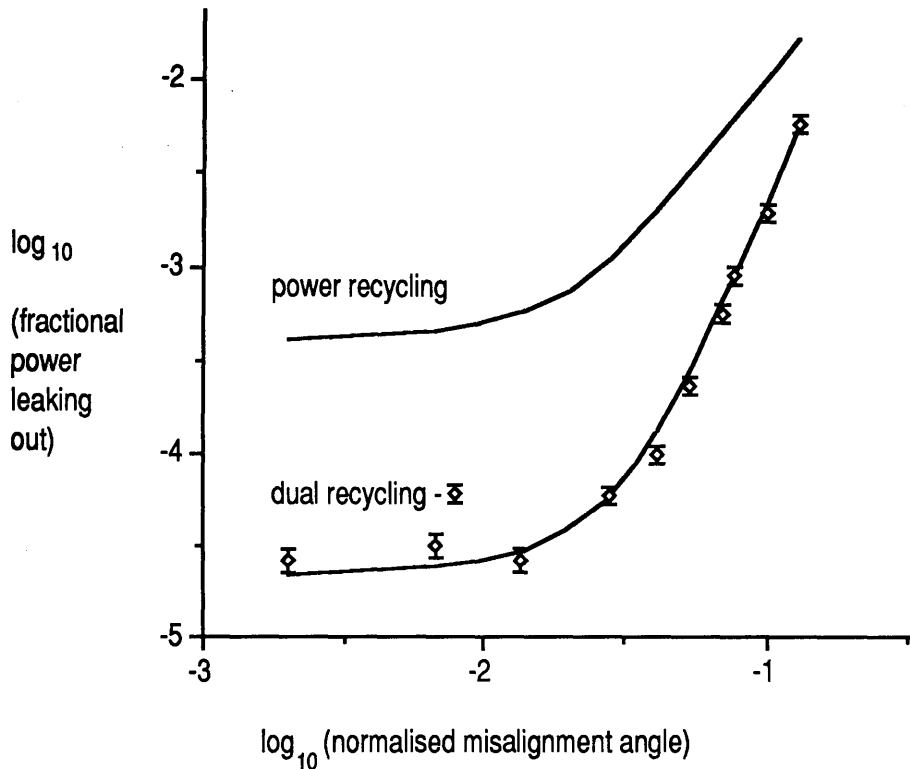


Figure 3.20: *The effects of misaligning one arm of the broadband dual recycling system. The best fit obtained in power recycling is restated for comparison (upper curve). The lower curve is the predicted result for dual recycling assuming that the upper curve is correct and that the contrast was limited at small misalignment angles by the production of, mainly, second order mode by the distortion process. The experimental measurements are shown.*

oscillator^{beam}. The results are shown (figure 3.20). The results expected from this were calculated using equation 2.58 and are shown on the graph. The expected values of the suppression coefficients (g_m) for the first and second order modes were calculated using the known cavity geometry and equation 2.41 to find the round trip phase shifts for each of the modes. The resulting values of the suppression were $g_1 = 0.175$ and $g_2 = 0.236$. The fit with the expectation is good. The losses at large misalignment angles are high due to the leakage of the resonant fundamental mode from the system.

At the smallest angles the effective contrast was increased by a factor of 4.3 ± 0.8 . This can be adequately explained by assuming most of the light lost at these angles is in the second order mode of the recycling cavity. The expected suppression of the second order mode in the signal recycling cavity can be calculated by inserting the known cavity properties into equation 2.58. (It could also be in some mixture of high order modes, this is not constrained by the experiment.) The effective contrast reported is extremely high for small angles at 210 ± 15 . The amplitude of the reference beam was then appropriate to give the optimum displacement sensitivity in this system.

The power within the interferometer was measured as a function of misalignment of one arm. This power could only be measured to about 5% accuracy due to the fluctuations of the laser intensity. Only measurements at the largest angles were thus possible, Here the power build up was in good agreement with effects expected from the the measurement of the power lost. The signal size was measured for two of the largest values of misalignment and was found to be proportional to the power within the interferometer. The extent to which the input laser light was coupled into the misaligned interferometer was not expected to change significantly even for the largest value of misalignment used. The results of these measurements are summarised in table 3.2.

Misalignment θ_n	Expected power or signal	Measured power	Measured signal
0.10	0.93	0.95 ± 0.05	0.90 ± 0.03
0.14	0.89	0.90 ± 0.05	0.85 ± 0.03

Table 3.2: *The effect of relatively large misalignments on the power build-up and signal size with broadband dual recycling. The last three columns have been scaled to a maximum value of unity.*

Detuning frequency (MHz)	Misalignment θ_n	Predicted contrast	Measured contrast	Power (normalised)
4	0.1	37.7	40 ± 3	1.00 ± 0.05
4	0.2	11.3	10 ± 1	0.80 ± 0.05
6	0.1	44.7	48 ± 3	1.00 ± 0.05
6	0.2	15.1	15 ± 2	0.90 ± 0.05
8	0.2	17.7	21 ± 2	0.95 ± 0.05

Table 3.3: *The contrast and power build up in the misaligned dual recycling interferometer. The power is scaled to a maximum value of unity as before.*

Misalignment of the dual recycling interferometer with the fundamental mode non-resonant.

In narrowband dual recycling the original carrier frequency is non-resonant in the signal recycling cavity. The effect of this type of recycling on the contrast of the interferometer can therefore be measured by detuning the resonance of the signal recycling cavity from the fundamental. This was done for several values of the detuning frequency. The results are summarised in table 3.3.

It can be seen that as the fundamental becomes non-resonant in the signal recycling cavity the loss of power due to non-overlap of the fundamental from the two arms is reduced (the resonance condition for the first order mode is changed only very slightly by the small detuning frequencies used). That the detuning allows high contrast to be achieved at relatively large values of misalignment, as predicted

Effective contrast	expected ratio	observed ratio
30 ± 2	9.5 ± 1	12 ± 2
85 ± 4	28 ± 2	24 ± 4

Table 3.4: *The size of the signal produced by motions of one of the interferometer mirrors compared to the signal produced by the same motion of the signal recycling mirror. The measured ratio has been normalised to allow for the different sizes of the motions which were imposed.*

in section 2.5, is therefore confirmed. The power within the interferometer can be compared with the power recycling case (table 3.1).

The effect of motions of the signal recycling mirror in the dual recycling system

The effect of motion of the signal recycling mirror was investigated by applying a sinusoidal position modulation to this mirror with the system fully operational in the broadband mode. The modulation frequency (3 kHz) was above the unity gain frequency of the dual recycling servo-system. The size of this signal at the output was compared to the size of the signal due to the 6 kHz motion.

It was expected that the size of the signal due to this modulation would be determined by the internal contrast of the interferometer (see section 2.5.2). The signals from the two modulations were compared at the output. This was repeated for two values of internal contrast (produced by misalignment). The relationship between the relative size of the signals produced by the two modulations and the contrast was confirmed to within 25%. These results are summarised in table 3.4.

3.5.3 Conclusion

The predicted properties of dual recycling were measured and confirmed within the limits given above. The frequency response of broadband dual recycling was

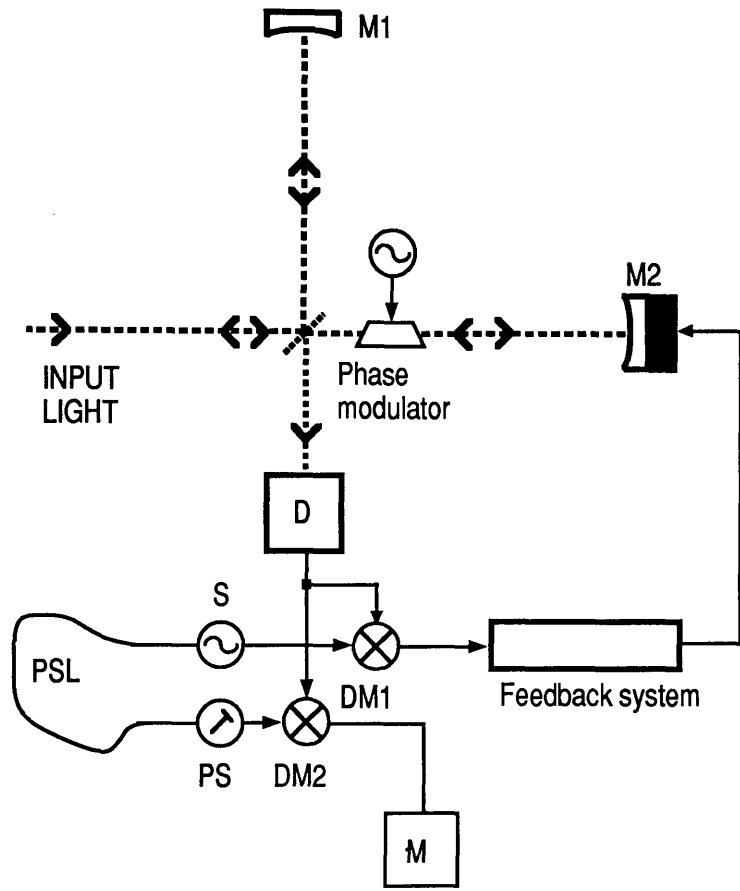
3.6 Internal modulation and measurement noise

Due to the perhaps surprising predictions which have been made about the effects of modulation on signal to noise ratio it was decided to carry out an experiment to confirm some of the predictions of section 2.2.3.

The optical system which had been used for recycling and external modulation experiments was adapted. A phase modulator (10 MHz modulation frequency) was inserted into one of the arms of the interferometer. The Michelson interferometer control system was adapted to keep the interferometer on an interference minimum. The layout of the system used is shown (figure 3.21). The phase modulator limited the effective contrast of the interferometer to a give a minimum output power of 0.040 ± 0.002 of the interferometer input power. (The typical input power was a few mW and the output power a few hundred μW .) The modulation index was chosen to produce an output power of three times this at an interference minimum (to 2% accuracy).

The signal from the photodiode was band pass filtered by the tuned photodiode amplifier. The tuned circuit here had a 'Q' of ~ 25 . so there could be no contribution from the demodulation of any frequencies apart from those close to the modulation frequency. This implies that the shape of the waveform (provided it has its fundamental component at the modulation frequency) used for the demodulation is not important as any shape will have the same effect as a sine wave.

It was necessary to compare the noise due to photon shot noise in the case where the demodulation was in phase with the modulation to the noise in the case with the demodulation in the quadrature phase. Great care was taken to ensure that the gain of the radio-frequency electronics did not change between these two measurements. The phase of the demodulation waveform could be varied by altering the length of one of the cables carrying this waveform or by using a radio-frequency phase shifter. It was thought that either of these methods of changing the phase could lead to a change in the level of the demodulation waveform. In order to ascertain that this effect was not causing a significant change in the gain in



KEY

- | | | | |
|-----|----------------------------------|-----------|--|
| D | - photodiode | PS | - phase shifter |
| S | - modulation source | PSL | - selectable length of cable used as phase shifter |
| DM1 | - demodulator for control signal | M | - low noise amplifier and signal monitor |
| DM2 | - demodulator for measurement | Feed back | - control system to maintain the output of the interferometer on an interference minimum |

Figure 3.21: The system used to measure the effects of modulation on measurement noise.

the signal channel various combinations of the two methods of changing the phase were employed. There was no observed change in noise levels produced by these methods (less than 0.1 dB). The phase of the demodulating waveform was measured by monitoring the size of the signal due to the 6 kHz arm length modulation at the output. The minimum of this signal corresponded to the quadrature phase and the maximum to the in phase case. The phase was known to $\sim 3^\circ$.

The signal from the photodiode was measured on a radio-frequency spectrum analyser (before the demodulation) and compared to noise due to torch light producing the same photocurrent. Apart from excess noise at low frequency the two results were the same to within the accuracy of the instrument used (~ 0.5 dB). This measurement confirmed that the laser power was shot noise limited at the measurement frequency.

The signal from the photodiode was demodulated to provide separate control and measurement signals (as for dual recycling). The (measurement) demodulation was set up for the in-phase case. The demodulated signal was amplified using a low noise amplifier. This signal was spectrum analysed in the region of 99 to 100 kHz. This region was chosen since there was no sign of any excess noise over photon shot noise (peaks of noise or non-white noise). The signal was averaged several hundred times to reduce the measurement uncertainty. The mean photocurrent was found by measuring the the average photocurrent in the photodiode. The laser power supply was adjusted to maintain the photocurrent to within 2% of the initial value throughout the measurement period (~ 10 minutes). (The internal power stabilisation in the laser was also used.) The measurement was repeated with torch light producing the appropriate photocurrent.

The phase of the demodulation was changed and the above measurements were repeated. There was no discernable difference between the two results produced by the torch light. Unmodulated light directly from the laser but attenuated by using a polarising beamsplitter to remove some light was also used to illuminate the photodiode. The results from this, at the light intensities used in the measurement noise experiment, were very close to the results produced by the torch light (within 0.15 dB). (It was observed that at considerably higher photocurrents than the 100

	Predicted noise (dB)	Measured noise (dB)	Corrected noise (dB)
In phase 1	1.25	1.1 ± 0.2	1.2 ± 0.2
Torchlight 1	0	0	0
Quadrature 1	-1.76	-1.4 ± 0.2	-1.6 ± 0.2
Electronic 1	—	-10 ± 1	—
In phase 2	1.25	0.9 ± 0.2	1.2 ± 0.2
Torchlight 2	0	0	0
Quadrature 2	-1.76	-1.2 ± 0.2	-1.8 ± 0.2
Electronic 2	—	-5.1 ± 0.5	—

Table 3.5: *A summary of the results of the experiment to investigate the effects of modulation on measurement noise. All of the results are normalised so that the noise produced by torch light is 0dB. The first column of figures shows the noise level predicted with one third of the light unmodulated. The second column shows the measured noise levels and in the final column the electronic noise power has been subtracted and the results renormalised to torch light. The two sets of results shown (1 and 2) were obtained for the two slightly different signal levels, as described in the text.*

to 200 microamperes used in this experiment there was some difference in the behaviour of the photodiode with laser light as opposed to torch light. This effect was briefly investigated but no obvious reason to explain the difference was found. The spatial distribution of the light had little effect on this difference.)

The results of these measurements are shown (figure 3.22). The results shown must be corrected to allow for the presence of electronic noise in the measurement system. This was done by subtracting the noise power appropriate to the observed noise with no light reaching the photodiode. The results of this are shown in table 3.5. In order to calculate the change in noise levels attributable to the modulation effects it was necessary to allow for the noise power due to the one third of the detected power which was unmodulated. The expected results for

this situation are shown in the table for comparison. The whole experiment was repeated with a different light power and with a 3 dB attenuator placed on the signal input to the mixer. This changed the signal level on the photodiode slightly. The results were very similar to those from the earlier experiment. These results are also shown.

It can be seen that the experimental results were fully compatible with the expected results. This gives some confidence that the methods used to make these predictions are reliable.

3.7 General conclusion

All of the optical configurations introduced in the previous chapter have been tested experimentally by the author. Control systems to operate these schemes have been successfully implemented. These control systems use techniques which *may* be applicable to a future full-scale gravitational wave detector. The dual recycling system was tested for the first time in any form and the basic optical properties of this were confirmed. The perhaps surprising predictions of the effects of modulation schemes on measurement noise were confirmed for the case of internal modulation.

Chapter 4

Mirrors for gravitational wave detectors

4.1 Low loss mirrors

The need to minimise the losses of the mirrors which form the arms of an interferometer which is to be used for gravitational wave detection can be seen by considering the effect of such losses on the interferometer with recycling (section 2.4). The amplitude within the arms of the interferometer, for a given input power, is limited by the losses of the mirrors (if the losses from the output can be sufficiently reduced).

The mirrors with the lowest losses are made using multi-layer thin-film techniques. Alternating layers of dielectric materials of high and low refractive index are deposited using ion-beam sputtering techniques to form a ‘stack’ [29]. The losses of these mirrors can be divided into two categories: (Here upper-case symbols are used to indicate intensity coefficients.)

a) the ‘absorption’ (A) is the fraction of the incident intensity which is absorbed by the materials of the mirror coating

b) the ‘scattering’ (S) which is the fraction of the light reflected but in a direction which would not occur if the mirror were perfect. This can arise through either surface or bulk scattering. Surface scattering is due to the roughness of the surface of the substrate used to hold the stack and of the boundaries of the layers of the stack [30]. The bulk scattering takes the form of Rayleigh scattering from ‘inclusions’ within the layers of the mirror.

In order to evaluate the losses of the mirrors supplied to the gravitational wave group at Glasgow a measurement technique based on the storage time of Fabry-Perot cavities made from the test mirrors was developed. A paper describing this work is included (Appendix C). The mirrors to be tested were formed into a Fabry-Perot cavity and the reflected fringes from this were monitored to reveal the storage time of the cavity. In combination with the measurements of the transmittances of the mirrors this allowed the losses to be calculated. The production of lower loss mirrors by improved manufacturing techniques was observed. The lowest losses measured were $\sim 8 \times 10^{-5}$ for mirrors which were made on ‘superpolished’ substrates using the ion-beam sputtering technique. (Superpolishing is intended to provide mirrors with a root mean square surface roughness of less than 0.1 nm.) It was not clear what the division of the loss between absorption and scattering was in these mirrors.

In order to try to determine which of the possible loss mechanisms was dominant the surface roughness of one of the ‘Set 3’ mirrors mentioned in Appendix C has been measured using a modified ‘Talystep’—the ‘NanoSurf 2’ [31] (at National Physical Laboratories, Teddington). The result, either on or off the coated area was a root mean square surface roughness of ~ 0.06 nm. (This was very close to the measurement noise of this system, thought to be ~ 0.05 nm.) The measurement was made over length scales ranging from $0.25 \mu\text{m}$ to $25 \mu\text{m}$. If the surface scattering of the type of dielectric stack used for this mirror is close to the value which would be obtained from a single reflecting surface with the same roughness then the scattering of green light should be very small ($\sim 10^{-6}$). (The relationship between mirror design and surface scattering could be more complicated than this [30].) This indicates the possibility that the loss is mainly absorption. It has been suggested by the manufacturers of the mirrors that the absorption of green light in one of the materials used to make the mirrors (titanium dioxide) could cause this.

New mirrors intended for the 10m prototype interferometer at Glasgow were obtained and tested. These mirrors had a coated diameter of 100 mm (mainly to ascertain whether ultra-low loss coatings could be made in sizes needed for the

full-scale detector) and it was interesting to test if the optical properties were constant over the coated area. These mirrors were designed to form cavities for the arms of this interferometer, one set having a transmittance of 5×10^{-4} and another set having the maximum reflectivity possible. The transmitting mirrors were plane and the reflecting mirrors had a radius of curvature of 15 m. They were manufactured in a similar way to the Set 3 mirrors.

The transmittance of the transmitting mirror was measured at several points on a cross shape formed by two diameters of the coated area. The results showed very little variation over this surface. One of the mirrors had a transmittance of $485 \pm 10 \times 10^{-6}$ with no variation seen at this level of measurement accuracy. Another mirror coated at the same time had a typical transmittance of $492 \pm 10 \times 10^{-6}$. There was therefore no evidence of variability exceeding 2%.

To enable measurement of the losses of these coatings to be made on a compact cavity on the bench a mirror with 1 m radius of curvature had been coated simultaneously with the transmitting mirrors above. This mirror could then be used to form a short (40 cm) stable cavity with any of the large mirrors.

The mean loss of two of the transmitting coatings (one on the small mirror) was found to be $(53 \pm 10) \times 10^{-6}$ per mirror. The loss of a cavity formed by one of the large 'non-transmitting' mirrors and the curved transmitting mirror was measured. The loss of the reflecting mirror was calculated to be $(70 \pm 20) \times 10^{-6}$ (with the assumption that the two transmitting mirrors had similar losses). These results are based on averaging 12 measurements for each cavity. A later evaluation of the storage time of one of the arms of the 10 m prototype gave the average mirror loss of $\sim 6 \times 10^{-5}$ for a pair of the large mirrors. This is compatible with the bench-top measurements.

Conclusion to mirror loss measurements

The measurement technique presented above has allowed the evaluation of the losses of the very high quality mirrors which are being developed for both laser gyroscopes and gravitational wave detectors. The losses and large mirror sizes

required for the gravitational wave detectors are currently being approached by the latest manufacturing techniques. It is possible that the losses may be reduced still further by the avoidance of titanium dioxide as a coating material in mirrors which are designed to operate with green light (515 nm). (Bulk titanium dioxide shows strong absorption as the wavelength is decreased towards 350 nm while an alternative material, hafnium dioxide remains reasonably transparent until < 200 nm [29].)

4.2 A test of the effect of mirror heating in a cavity

If the mirrors in a gravitational wave detector have significant absorption then there is the possibility that the performance of the detector could be limited by the effect of the heat produced by the absorbed laser light. (This was stimulated by earlier work by several colleagues, especially J. Y. Vinet, A. Marraud and F. Raab [33, 34]). There are two possible effects which can be identified. The heating of the substrate material will lead to some local expansion of the mirror surface and a change in the shape of the mirror. The heating may also produce a lensing effect on the light transmitted by the mirror if the refractive index of the substrate material is a function of temperature. If a cavity is formed by such mirrors then either of the above effects can lead to the reduction of the power matched into the fundamental mode of the cavity [11]. In the arms of a detector these effects could cause loss from the output and reduction of the amplitude within the recycling cavity.

In an interferometer with cavities in the arms the power is concentrated in one spot on each mirror while with delay-lines the power is distributed over several spots. In addition for a delay-line there need be no transmission through the substrate of a mirror (one beam must still pass through the beamsplitter, however.) This not only avoids the effect of heating on the transmission but also allows the choice of opaque materials, perhaps with better thermal properties, for the delay-line mirrors (e.g. silicon [3]).

In order to estimate the effects of mirror heating a simplified model of the

heating effect can be used (as suggested by Meers [32]). If the power from the laser beam is absorbed by the coating on the surface of the mirror and the spot which is heated is small compared to the size of the mirror then an estimate of the resulting temperature increase (ΔT) and expansion along the normal to the surface (Δz) can be made. If the system is in equilibrium then the power flow away from the heated spot is equal to the absorbed laser power (P). This flow occurs through an area given approximately by the (Gaussian) size of the laser beam at the mirror. In this case

$$\Delta T = \frac{Pw}{2\pi w^2 K}, \quad (4.1)$$

where w is the Gaussian radius of the laser beam and K is the thermal conductivity of the substrate. The resulting expansion is

$$\Delta z = \epsilon \Delta T w = \frac{\epsilon P}{2\pi K}, \quad (4.2)$$

where ϵ is the thermal expansion coefficient of the substrate material. For the case of the lensing properties due to heating the same expression applies if Δz is the change in the optical path at the centre of the spot due to the heating and ϵ is the rate of change of refractive index with temperature.

The case of a simple cavity was considered to allow a test of the effect of heating. The experiment was designed to test the properties of the input mirror which was on a fused silica substrate. For this material the lensing effect should dominate and the above equation becomes

$$\Delta z = 2.5 \times 10^{-7} \text{m} \left[\frac{P}{0.2 \text{W}} \right] \quad (4.3)$$

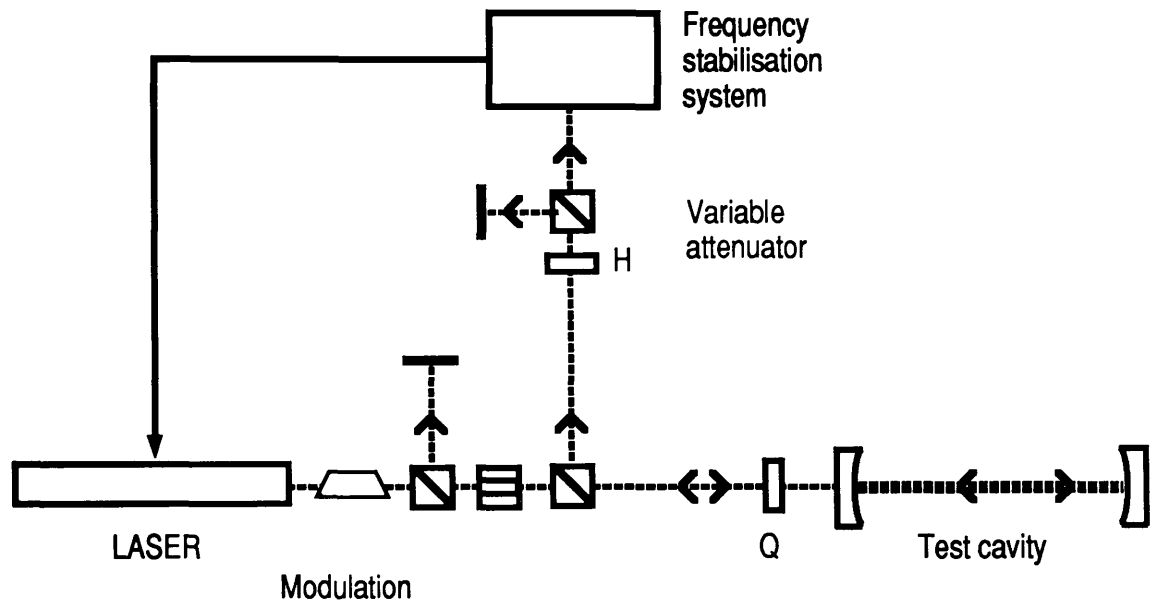
(for fused silica $K = 1.4 \text{Wm}^{-1}\text{K}^{-1}$ and $\epsilon = 10^{-5}\text{K}^{-1}$, the thermal expansion coefficient is small, $1.5 \times 10^{-6}\text{K}^{-1}$). This represents an effective change in the optical thickness of the substrate of about half of a wavelength (at 514 nm) over the beam size for an absorbed power of 0.2 W and will lead to a significant change in the curvature of the beam passing through the mirror and a reduction in the efficiency of light coupled into the fundamental mode of the cavity. There should therefore

be a 'self-limiting' effect on the power within the cavity when the absorbed power is increased above approximately this value.

The experimental test of this was done using the optical system shown (figure 4.1). A high power argon-ion laser (Spectra-Physics 170) was used to illuminate a cavity formed by the test mirror (input) and a mirror on a 'Zerodur' low expansion substrate. The laser was frequency stabilised to this cavity using the technique described in Appendix B.

At low input power ($\ll 0.5\text{ W}$) the cavity could be locked to the laser for periods of, at least, several seconds. As the power was increased the locking became progressively less reliable (the power incident on the photodiode was maintained constant by means of a variable attenuator placed in front of the photodiode in an effort to prevent any problems due to changes in the signal level). With the input power in excess of 0.7 W the laser could not be stabilised to the usual fundamental mode of the cavity for more than $\sim 1\text{ ms}$ and was seen to try to lock to higher order modes. (The servo-system was conditionally stable and could not stabilise the laser to these other modes which yield a considerably smaller loop-gain.) In order to ensure that the light reflected from the test cavity back to the laser was not causing problems with the stabilisation system, an extra stage of isolation, using a second faraday isolator, was introduced. This had no effect on the operation of the system.

The power which is actually absorbed in the input mirror was estimated using the measured mirror parameters. The visibility of the reflected fringes from the fundamental mode in the cavity was 0.80 ± 0.05 (at low illuminating power) and this allowed the power actually lost from the light in the cavity to be calculated. The total losses in the cavity were measured (from the storage time) to be $(5.5 \pm 0.5) \times 10^{-4}$ and this agreed with previous measurements of the properties of the two mirrors involved. The losses of the input mirror were thought to represent $\sim 2/3$ of this. With these figures $\frac{2}{3} \times 0.8 \approx 0.53$ of the input power should be associated with the loss of the input mirror. The fraction of the loss due to absorption was not known but if it is assumed that the losses are dominated by absorption then the power absorbed when the locking was clearly deteriorating was $\sim 0.3\text{ W}$ which is close to the expected limiting value.



-  Polarising beamsplitter
-  Phase modulator
-  45 degree Faraday effect isolator
-  Quarter wave retardation plate

Figure 4.1: *the optical system used to test the effects of heating on a fused-silica mirror.*

Conclusion to mirror heating

The above result suggests that the thermal properties of mirrors used in the gravitational wave detectors should be considered. The use of delay-lines may prove important if the absorption of light by the mirrors cannot be decreased since the power loss is then distributed over many spots and a transparent material is not required for the mirrors allowing the use of materials with higher thermal conductivity. The implications of mirror heating on the interferometer with (dual) recycling have been calculated [35] and the contrast enhancing properties of dual recycling may be required to reduce the effects of mirror heating.

Chapter 5

A variable reflectivity mirror for laser interferometers

5.1 Introduction to variable reflectivity mirrors

In the gravitational wave detector it may be useful to have mirrors whose reflectivity can be varied. In this chapter two possible uses of such a mirror are discussed briefly and an experimental test of the use of an optical cavity as a variable reflectivity mirror is described.

One application is in the frequency response of an interferometer with dual recycling. This is determined by the reflectivity and position of the signal recycling mirror (for a given arm design). If the reflectivity of the signal recycling mirror was variable it would be possible to achieve various responses (and so to search for different sources of gravitational radiation) without physically changing the detector components.

Another application is in an interferometer with cavities in the arms where the rejection of frequency noise is determined by the symmetry of the two cavities [22]. At present it seems that mirrors from one batch may have transmittances which vary by of order 1% between samples and this would limit the frequency noise rejection to ~ 100 . This is at least 10 times less than the rejection which could be expected in a delay-line system. One possible way of improving the rejection of frequency noise would be to replace one of the cavity mirrors with a variable reflectivity mirror to allow the cavities to be balanced.

5.2 A variable reflectivity mirror

A Fabry-Perot cavity has a reflectivity which is a function of the mirror spacing and so could be used as a variable reflectivity mirror if a suitable control system can be made to maintain the desired mirror spacing. The reflectivity of such a cavity is a complex quantity representing an amplitude reflectivity and a phase shift both of which are functions of frequency. The reflectivity (\mathfrak{R}) is given by the expression for the amplitude reflected from a cavity

$$\mathfrak{R} = r - \frac{t^2 \rho e^{i\delta}}{1 - r \rho e^{i\delta}}, \quad (5.1)$$

where t and r are the transmittance and reflectance of the first mirror which the light reflects from after approaching the cavity, ρ is the reflectance of the other mirror and δ is the round trip phase shift in the cavity. This has a maximum value, approximately r when $\delta \approx \pi$ (modulo 2π) and is a minimum when $\delta = 0$ (modulo 2π). The application of this type of mirror to a system where the light has several important frequencies (for example carrier and sidebands) must be considered in each individual case since there are several parameters which must be fixed.

The example applications above use the variable reflectivity mirror as part of an optical cavity. It was therefore decided to investigate the properties of a cavity with a variable reflectivity mirror. The optical system used is shown (figure 5.1). The ‘three mirror linear cavity’ was designed so that mode-matching would be consistent throughout. This was achieved by adjusting the lengths of the two cavities so that the shared waist, at the plane central mirror, had the same calculated size for both cavities. (The availability of only certain curved mirrors limited the choice of physical configurations which could be used.)

The frequency of the illuminating laser was stabilised to maintain the laser light resonant in the coupled cavity. The size of a frequency noise peak (of otherwise constant amplitude) on the laser light should then be inversely proportional to the loop-gain of the frequency stabilising servo-system (for high loop gain) and this is dependent on the cavity properties (equation A.17). In order to measure this gain a second cavity was made to resonate with the laser light by adjusting its

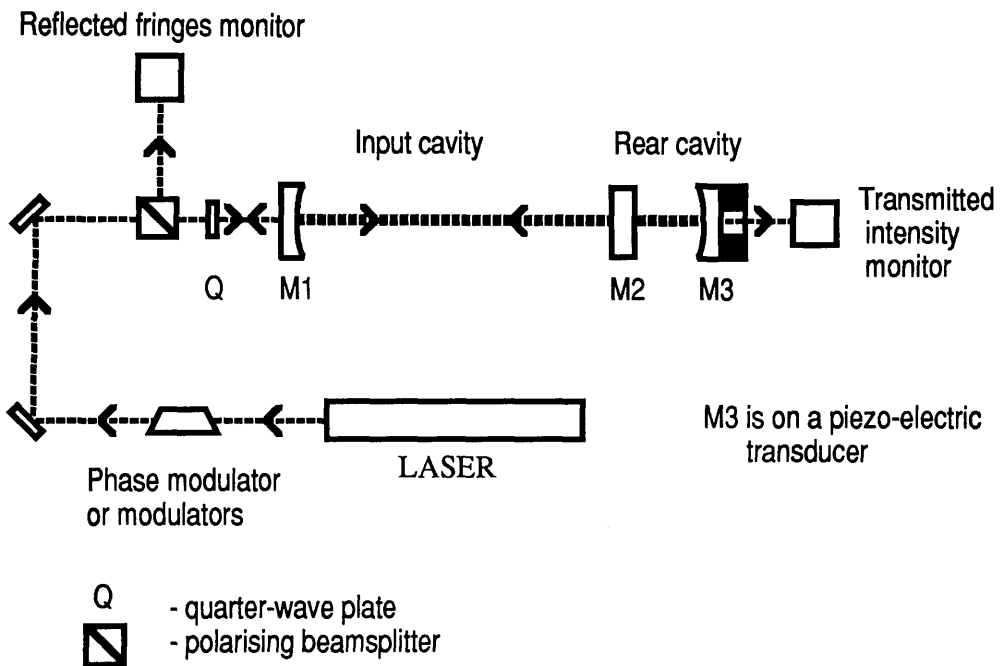


Figure 5.1: *The optical system used to test the idea of a cavity as a variable reflectivity mirror. A radio-frequency reflection-fringe laser stabilisation system (with 12 MHz phase modulation) was used to stabilise the laser frequency with respect to a resonance of the coupled cavity.*

length to follow the laser frequency. The signal used to change the length of this cavity was a measure of the laser frequency noise (or the frequency noise peak) at frequencies where the loop gain of this second control system was high. This then gave a measure of the effect of the variable reflectivity mirror on the properties of the three mirror cavity.

5.2.1 A low-frequency control system for the variable reflectivity mirror

As a first test of this apparatus a simple control system was used to set the spacing of the rear pair of mirrors. The intensity transmitted through the whole three mirror cavity was detected, compared to a reference and used to control the position of the rear mirror. This required a photodiode which could measure quite a low light power (as little as 10^{-7} W) with low enough noise to work in a control system. A low noise, low bias current, operational amplifier (Analogue Devices 50J) was used with a low dark current photodiode. A schematic diagram of the complete control system is shown (figure 5.2). The bandwidth of the rear mirror control system was about 3 kHz and the gain at frequencies less than 30 Hz was ~ 40 dB.

Initially the rear part of the three mirror cavity was blocked and the storage time of the resulting 'normal' cavity was measured. The finesse of this cavity was found to be 2500 ± 200 and this was reasonably close to the value expected from the known mirror properties (~ 2400). The term 'effective finesse' is used here to indicate the apparent value of the finesse of the three mirror cavity as measured by its effect on the laser stabilisation system and, consequently, the residual frequency noise. When the rear cavity was far from resonance its effect on the longer cavity was negligible and the effective finesse was then taken as 2500. The variable reflectivity mirror control system was used to increase the transmission through the rear cavity by bringing this cavity toward resonance with the carrier light. The frequency noise on the laser light was seen to increase indicating that the effective finesse was reduced. (The visibility of the reflected fringes was also measured and the signal reduction due to the changed visibility was taken into account.) The effective finesse could be reduced to ~ 1000 indicating that the reflectivity of the

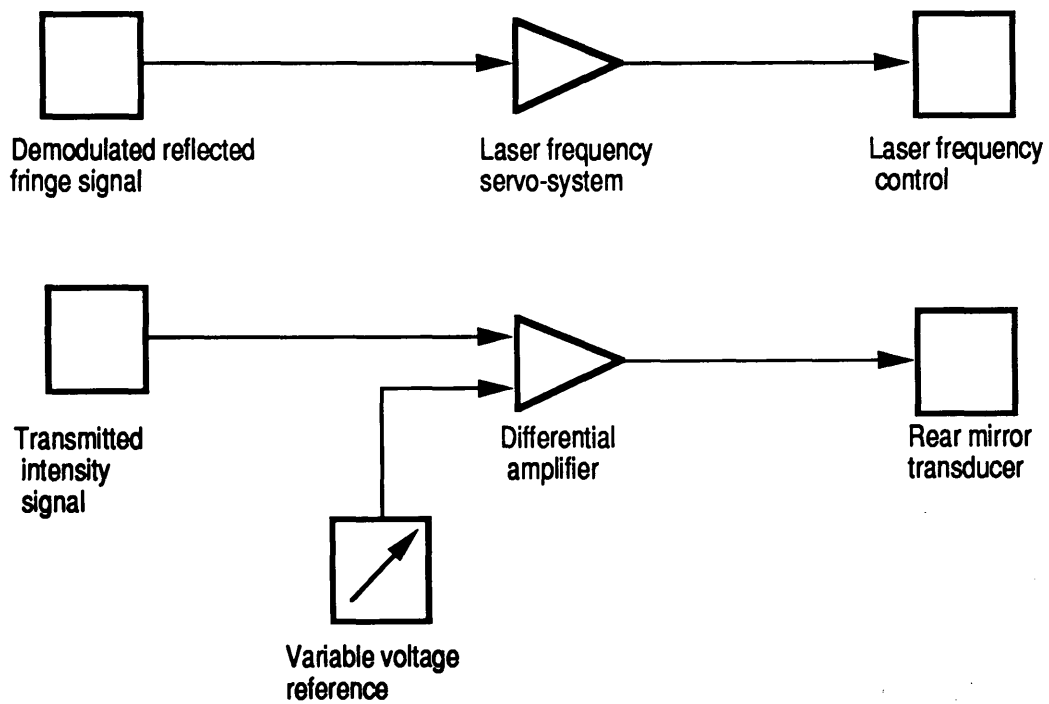


Figure 5.2: *The first control system for the variable reflectivity mirror.*

rear mirror combination was indeed variable. Beyond this point the light intensity on the low frequency photodiode caused the amplifier to saturate.

One disadvantage of this type of control system is a susceptibility to both stray light and laser intensity noise which are not discriminated from a true signal. It was therefore thought to be worthwhile to investigate a system which did not rely on measuring the transmitted intensity.

5.2.2 A 'reflection-fringe' control system for the variable reflectivity mirror

In order to obtain two independent pieces of information from the light reflected from the overall cavity it was necessary to find a modulation scheme which would give signals associated with the two different path lengths in the three mirror cavity. The information required to control the overall cavity was obtained by using the standard reflection fringe method described in Appendix B. The information concerning the rear cavity was obtained by using sidebands spaced from the carrier by one free spectral range of the input cavity to interrogate the rear cavity.

The approach used was based on the presence of a series of longitudinal resonances of the input cavity spaced from each other by the free spectral range of this cavity. The input cavity was much longer than the rear cavity so the free spectral range of the rear cavity was very large compared to that of the input cavity. In isolation each of the cavities would have a linewidth considerably narrower than the free spectral range of the long cavity (the finesse were over 1000). If the laser light was close to being on resonance in each of the cavities then only one longitudinal resonance of the input cavity would be altered by the presence of the rear cavity (at least in the frequency region of interest). A sketch of the resonant frequencies of such a pair of cavities illustrates this (figure 5.3).

When the laser light begins to resonate in the rear cavity the round trip phase shift and, therefore, the resonant frequency of the input cavity are changed slightly. In the proposed scheme the frequency stabilisation servo-system was designed to keep the laser light on resonance with the coupled cavity system and it must

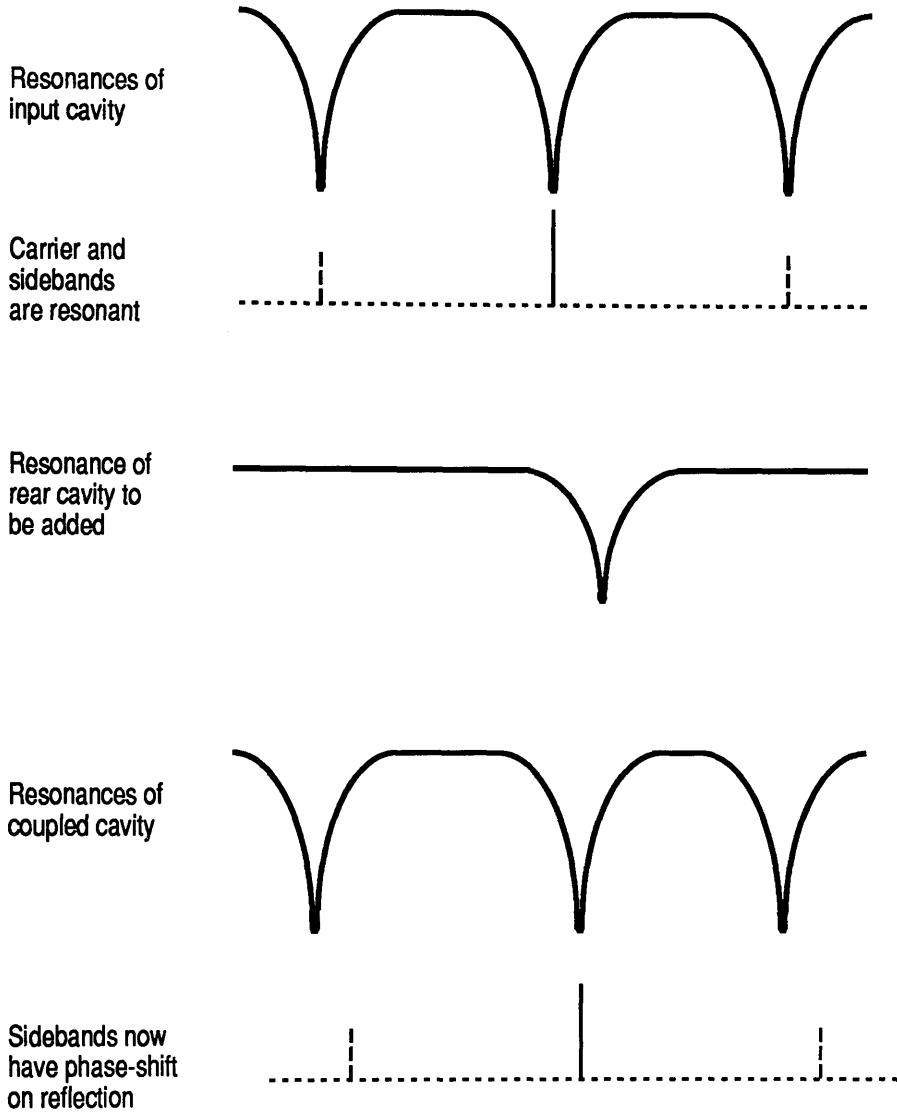


Figure 5.3: *The resonances of two cavities as an illustration of the reflection-fringe control system for the variable reflectivity mirror. The upper curves show the resonant frequencies of the isolated cavities. The lower curve shows the effect of the coupling on the resonances of the cavity (very low finesse cavities have been used for clarity). The carrier and the two new modulation sidebands are also shown in each case.*

change the carrier frequency to do this. In order to measure the degree of this frequency shift (and so the effect of the rear cavity) modulation sidebands were added at the frequency corresponding to the free spectral range of the input cavity (as shown in the figure). These will be shifted by the same frequency as the carrier light and will then suffer a phase change on reflection from the coupled cavity. The normal reflection-fringe detection and demodulation scheme, at this new modulation frequency, now gives a measure of the phase shift of the sidebands with respect to the carrier which is in turn a measure of the resonance condition of the rear cavity (compare with the usual application of this scheme as described in Appendix B).

This method was tried to see if it allowed at least the same degree of control as the low frequency scheme described above. The control system used is shown (figure 5.4). The required new modulation frequency was ~ 95 MHz. This was accurately set by finding the frequency which produced a null in the response of this signal to phase shifts of the input cavity. Some care was required to match the radio-frequency power into the modulator at such a high frequency but sufficient modulation index was achieved (~ 0.4). About 20% of the reflected light was detected and demodulated at the new modulation frequency. The resulting signal was compared to a variable reference voltage and used to control the position of the rear mirror.

The apparatus operated with the new control system. It was noted that sometimes an unstable state was reached where the signals became very complicated and no improvement could be made without reducing the gain of the rear cavity control considerably. This was not fully understood but seemed to represent an interaction of the two control systems. When this situation was avoided a stable state was achieved with the particular behaviour set predictably by the operation of the two control systems.

With the 12 MHz control system keeping the overall cavity on resonance with the laser but with the rear cavity significantly off resonance the behaviour was very similar to that with the low frequency control system. The effective finesse was measured in the same way and the results were similar. Since the laser stabilisation

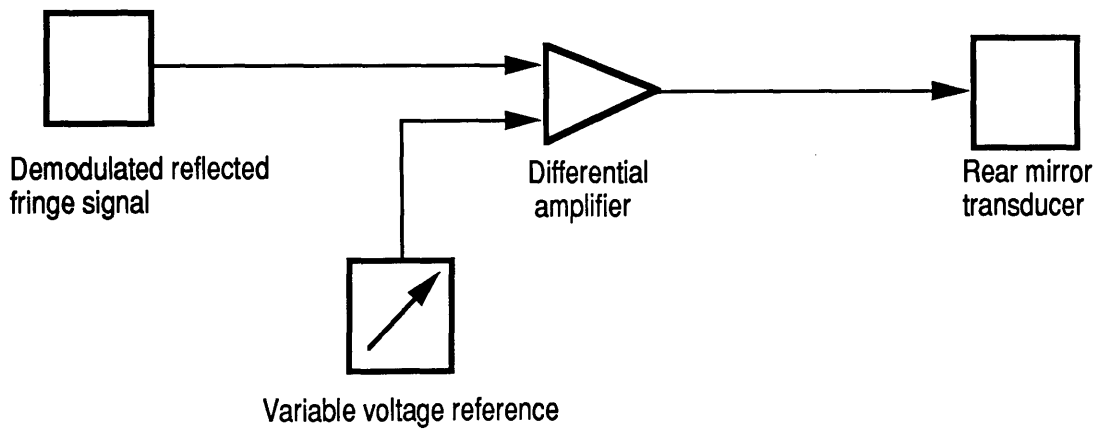
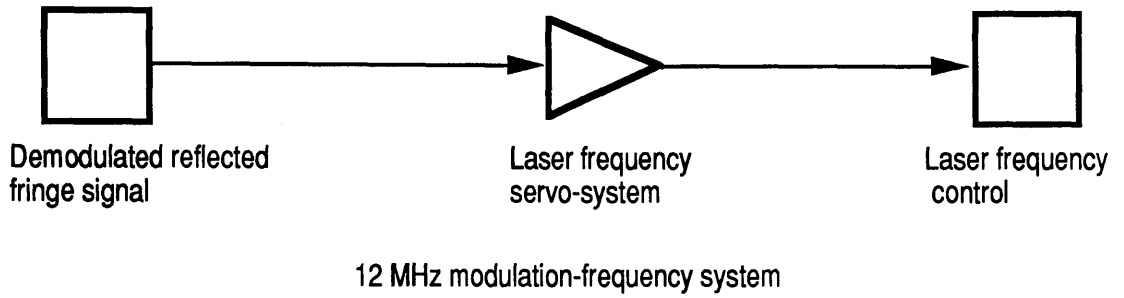


Figure 5.4: A reflection-fringe control system for the three mirror cavity. The gains and bandwidths of the control systems were intended to be similar to those of the first system.

visibility	optical gain (dB)	effective finesse	reflectivity
0.83 ± 0.03	0	2500	$1 - [(30 \pm 3) \times 10^{-5}]$
0.96 ± 0.02	-11 ± 3	1200 ± 200	$1 - [(14 \pm 2) \times 10^{-4}]$
0.30 ± 0.03	-39 ± 3	240 ± 50	$1 - [(12 \pm 2) \times 10^{-3}]$
0.08 ± 0.02	-62 ± 3	70 ± 20	$1 - [(44 \pm 7) \times 10^{-3}]$

Table 5.1: *A summary of the measurements of the properties of the variable reflectivity mirror with the reflection-fringe control system. The first row of data corresponds to the measurement with no rear cavity. The second column has been scaled to give a maximum gain of unity. The visibility has been corrected for the effects of imperfect mode-matching and the phase modulation.*

was conditionally stable the reduction in gain as the effective finesse was reduced had to be compensated by increasing the electronic gain. An additional wide-bandwidth amplifier was used for this and gain of this amplifier then had to be taken into account when calculating the effective finesse.

The effective finesse could now be reduced to 70 ± 20 after adjustment of the gains of the two control systems to avoid oscillations. It was thought that this limit was due to the small size of the signals (in both control systems) associated with lower values of effective finesse and visibility. The results of these measurements are summarised (table 5.1).

Another state of operation was investigated briefly. Now the intention was to have the rear cavity on resonance and use the input cavity as a variable reflectivity mirror (or indeed a variable transmittance mirror). The above control system can operate in this way but the requirement to start with the laser stabilised to the input cavity made this quite difficult to achieve. The rear cavity was gradually brought on resonance by reducing the offset in the rear mirror control system while simultaneously adding an offset to the laser stabilisation control to allow the whole system to be locked slightly off resonance. The rear cavity was set on resonance by then adjusting the offset on the rear mirror control to maximise the light intensity transmitted through the whole cavity. The effective finesse was

measured for one particular operating case and was found to be 200 ± 30 : this corresponds to a transmittance of the input cavity of 0.17 ± 0.04 . This indicated that the transmission properties of the variable mirror could also be controlled by this control scheme.

5.2.3 Conclusion

It was possible to control the three mirror cavity using either the reflected and transmitted light or only the reflected light to obtain the two signals required. The use of a cavity as a variable reflectivity mirror has thus been demonstrated to be possible on a simple system. The application of such a mirror to any of the more complicated systems suggested in the introduction will require control systems specifically designed for each case.

The use of a cavity as the signal recycling mirror of dual recycling should have further implications for the contrast of the interferometer [36]. The cavity could be designed to be highly reflective to the high order modes of the recycling cavity so preventing them from escaping from the system.

Chapter 6

Conclusions and future prospects

This chapter is a summary of what has been achieved in the work described in this thesis. The conclusions are linked to the problem of the design of a particular interferometric gravitational wave detector [3] which is intended to reach astrophysically interesting levels of sensitivity (e.g. the broadband response indicated in figure 1.2). The basic design is to be a Michelson interferometer with 3 km long arms illuminated with several tens of watts of laser light (wavelength either $\sim 1 \mu\text{m}$ or $\sim 500 \text{ nm}$).

The first chapter introduced the idea of gravitational radiation and the use of laser interferometry as a candidate method for its detection. The signal which could be expected from the simplest interferometer configuration was considered and compared to the likely important noise sources. It was seen that if the storage time of the light in the arms could be optimised to gravitational wave frequencies in the range $< 100 \text{ Hz}$ to $> 1000 \text{ Hz}$ then useful displacement sensitivities could be obtained. The main obstacle to this lies in the difficulty of obtaining the required storage time (up to 5 ms) to optimise the detector for the lower frequencies. This could be achieved by using Fabry-Perot cavities with a finesse of ~ 1000 in each of the arms. There are two reasons why this may not be the best method. Firstly, an interferometer with cavities in the arms is probably more difficult to control than one with delay-lines since the light must be made resonant in the arms before the interferometer can operate. Secondly, the effects of mirror heating, discussed in Chapter 4, are likely to seriously limit the performance of an interferometer with cavities in the arms. As an example of this last point consider the effect of

the absorbed power limit of around 0.25 W per mirror (with fused-silica mirrors) observed in Chapter 4, on the 5 ms storage time cavities described above. With the presently available mirror losses several tens of watts of input laser power would be required to achieve a light amplitude in the arms of the detector sufficient to reach the desired sensitivity. Since the performance is then limited by the mirror losses this implies that the laser power is absorbed or scattered mainly by the four cavity mirrors. If, as it seems from the results of Chapter 4, absorption is an important contribution to the loss then several watts of light may be expected to be absorbed by each mirror. While it may be possible to make mirrors with either very low thermal expansion and refractive index coefficients or extremely low absorptions it seems reasonable to consider other methods of obtaining the long storage times required.

If a delay-line system is to be used then there may be as few as thirty bounces of the light in each arm, limited by the available mirror size (~ 0.50 m). With very low loss mirrors power recycling can be used to enhance the light amplitude in the arms for a given input laser power. This system is also susceptible to mirror distortions, perhaps due to heating, and the resulting loss of power from the output due to a predictable and controllable distortion (angular misalignment of one of the interferometer mirrors) was considered in Chapter 2.

It turns out that both of the problems with delay-line systems with power recycling (short storage time and power leaking from the output due to small distortions) can be overcome by using dual recycling. As discussed in Chapter 2 dual recycling should both increase the storage time of the signal sidebands within the interferometer, allowing better low frequency response, and increase the interferometer contrast. It will reduce the power loss from the output resulting from a wide range of distortions. It should also allow narrowband responses peaked at a chosen frequency and this may be useful to search for sources of gravitational radiation where the frequency can be predicted (e.g. perhaps pulsars).

The proposed interferometer design including dual recycling and external modulation is quite complicated and rather different from the present prototype interferometers. This was the motivation for the experimental investigation of dual

recycling presented in Chapter 3. The basic frequency response and signal to noise ratio enhancing properties of broadband dual recycling were confirmed experimentally: the results were in very good agreement with the predictions. The predicted contrast improving features were also demonstrated using the example of misalignment of the interferometer arms and again the experiment confirmed the expectations. Importantly, a control system quite similar to the one proposed to operate the full-scale detector was implemented and found to work very reliably. These tests provide confidence that the basic ideas involved are well understood and that they should be applicable to the proposed detector. There is still, however, a great deal of work required to enable dual recycling to be implemented on a system with suspended test masses in an evacuated enclosure.

The other work presented has significance for the design of the full-scale detector, in some cases relating to more detailed aspects of the design. An example of this was the demonstration of the optical properties and control systems for a cavity used as a variable reflectivity mirror (Chapter 5). This technique is likely to find some application either in a detector with cavities in its arms or in one with dual recycling. The experimental test of this system was successful: the control systems operated sufficiently well to allow the optical properties of the variable reflectivity mirror to be measured. There remains, however, the design of the control systems which are required in the particular applications.

Mirrors of very low loss were discussed in Chapter 4 and it was found experimentally that it is now possible to obtain mirrors with intensity losses of $\sim 6 \times 10^{-5}$ with coated areas beginning to approach those that would be required for the delay-line mirrors and almost adequate in size for a Fabry-Perot based interferometer (that is a coated diameter of 0.1 m). This is one advantage of the Fabry-Perot based system.

The experimental verification of the effects of internal modulation on the fundamental measurement noise supported the model used to calculate these effects. The application of the results to interferometers indicates that to achieve the last dB or two of the potential signal to noise ratio some care in the choice of modulation and demodulation waveforms may be required.

If it is possible to use Fabry-Perot cavities (perhaps with improved mirrors) in the detector then it is useful to understand some of the control problems likely with this type of system. The signals which can be expected from this configuration were evaluated and their impact on control systems considered. It was found that, for the configuration investigated, there could be a change in the sign of one of the control systems at high frequency but that this should not present a control problem in practice. This was confirmed by the experimental test of such an interferometer where the control systems operated correctly.

Several aspects of the design of laser interferometers for gravitational wave detection have been considered and tested by the author in the work presented in this thesis, especially the advanced optical techniques required to reduce the fundamental photon shot noise to an acceptable level. There are, however, many other challenging sides to the design of such an interferometer including the reduction of all other noise sources, the provision of the high input laser powers required and the design of systems to control the positions of the suspended test masses. All of these are currently under investigation.

Appendix A

Some properties of Fabry-Perot cavities

In this appendix the properties of optical cavities relevant to the work presented in this thesis are summarised.

Consider a cavity illuminated with monochromatic light of angular frequency ω_c . The light is partially transmitted by the input mirror and reflects back and forth along the cavity according to the reflectivities of the two mirrors. The resulting amplitudes are illustrated (figure A.1).

If the amplitude coefficients of transmission of the mirrors are t and s respectively and their amplitude coefficients of reflection are r and ρ then the amplitude (A_i) within the cavity (returning to the input mirror) can be obtained by summing

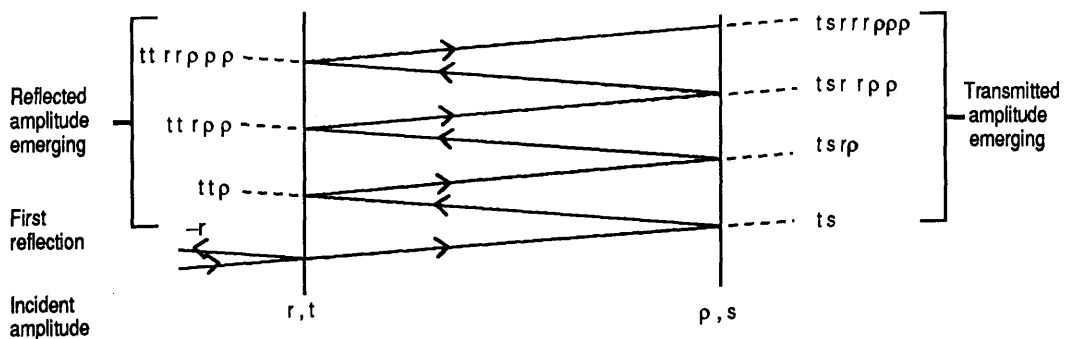


Figure A.1: The amplitudes which arise after several traverses of an optical cavity.

the amplitudes obtained after each traverse

$$\frac{A_i}{A_0 e^{i\omega t}} = t\rho \sum_{N=1}^{\infty} (r\rho)^{N-1} e^{iN\delta} = \frac{t\rho e^{i\delta}}{1 - r\rho e^{i\delta}} \quad , \quad (\text{A.1})$$

where δ is the round trip phase shift within the cavity and A_0 is the magnitude of the incident amplitude. The amplitude transmitted by the cavity (A_t) is obtained by multiplying the above by $(s/\rho)e^{i\frac{\delta}{2}}$ and the amplitude emerging from the cavity (A_c) at the input is obtained by multiplying by t . The expression for the internal amplitude can be used to evaluate the amplitude build-up in the recycling cavity (section 2.4). The losses from the output of the interferometer can be represented by losses in one of the mirrors.

The total amplitude reflected by the cavity can be found by adding the amplitude leaking out of the cavity to the amplitude reflected by the input mirror alone (these must be out of phase due to the difference in the number of reflections which occur at the low and high refractive index sides of the mirrors). The total reflected amplitude is

$$\frac{A_r}{A_0 e^{i\omega t}} = r - \frac{t^2 \rho e^{i\delta}}{1 - r\rho e^{i\delta}} \quad . \quad (\text{A.2})$$

This can be written as

$$r - \frac{t^2 \rho}{(1 - r\rho)^2} \left[\frac{e^{i\delta} - r\rho}{1 + F' \sin^2 \frac{\delta}{2}} \right] \quad , \quad (\text{A.3})$$

where the coefficient of finesse F' which is related to the finesse (F) is given by

$$F' = \frac{4F^2}{\pi^2} = \frac{4r\rho}{(1 - r\rho)^2} \quad . \quad (\text{A.4})$$

The effective number of traverses (N_c) of the cavity (i.e. the number of traverses that a delay-line of the same length would need to have to give the same phase change on the emerging light for a given movement of one of the mirrors) is related to the finesse

$$N_c = \frac{F}{\pi} \quad . \quad (\text{A.5})$$

This also allows a storage time (τ) to be introduced:

$$\tau = \frac{2N_c l}{c} = \frac{2Fl}{\pi c} \quad . \quad (\text{A.6})$$

Another useful quantity is the visibility (V) defined by

$$V = \frac{I_{max} - I_{min}}{I_{max}} \quad , \quad (\text{A.7})$$

where the intensities I_{max}, I_{min} are the maximum and minimum values observed when the light reflected from the cavity is monitored as the cavity phase is changed by 2π . This can be expressed in terms of the mirror properties

$$V = 1 - \left[r - \frac{t^2 \rho}{1 - r\rho} \right]^2 \quad (\text{A.8})$$

(this applies only if the mode-matching is perfect).

An important property of cavities is the suppression (or enhancement) of non-resonant modes either when the cavity is used to transmit a beam or when the modes are generated within the cavity (e.g. in the split cavity of dual recycling). Consider a mode which has unit amplitude added to it on each round trip of the cavity. The magnitude of the suppression of this mode can be obtained by calculating the square root of the power which emerges from the cavity as a function of round trip phase shift of the mode within the cavity. The emerging power is

$$I_t = \frac{t^2}{1 + (r\rho)^2 - 2r\rho \cos \delta} = \frac{t^2}{[1 - r\rho]^2 \left[1 + F' \sin^2 \frac{\delta}{2} \right]} \quad , \quad (\text{A.9})$$

where t is the amplitude transmission coefficient of the mirror through which the light emerges. The magnitude of the suppression of the amplitude of the mode at the output is therefore given by

$$\frac{t}{[1 - r\rho]} \frac{1}{\sqrt{\left[1 + F' \sin^2 \frac{\delta}{2} \right]}} \quad . \quad (\text{A.10})$$

The response of the cavity to phase-modulated light is now considered. The case of light with frequency noise is taken as an example. With one Fourier component of frequency noise the laser light has an angular frequency of the form

$$\omega = \omega_c + \Delta\omega \sin \omega_n t \quad , \quad (\text{A.11})$$

where ω_c is the mean laser angular frequency and ω_n is the frequency noise component with amplitude $\Delta\omega$. The corresponding phase is given by the integral of this with respect to time. In addition the laser light is phase modulated, that is the amplitude is multiplied by

$$e^{\beta \sin \omega_m t} \approx J_0(\beta) + i2J_1(\beta) \sin \omega_m t + \dots, \quad (\text{A.12})$$

where β is the modulation index of the phase modulation at an angular frequency ω_m . Higher order terms are not important as the signal will be obtained by demodulating in phase with the modulation at the fundamental modulation frequency.

The amplitude reflected from the input mirror of the cavity is now

$$A_r = A_0 r \exp i \left(\omega_c t - \frac{\Delta\omega}{\omega_n} \cos \omega_n t + \beta \sin \omega_m t \right), \quad (\text{A.13})$$

which for small $\Delta\omega$ becomes

$$A_r = A_0 r \exp i (\omega_c t + \beta \sin \omega_m t) \left[1 - i \frac{\Delta\omega}{\omega_n} \cos \omega_n t \right]. \quad (\text{A.14})$$

The amplitude emerging from the cavity is (for small $\Delta\omega$)

$$A_c = -A_0 t^2 \rho J_0(\beta) e^{i\omega_c t} \sum_{N=1}^{\infty} (r\rho)^{N-1} e^{iN\delta} \left[1 - i \frac{\Delta\omega}{\omega_n} \cos \omega_n \left(t + \frac{2Nl}{c} \right) \right], \quad (\text{A.15})$$

where the frequency of the phase modulation has been chosen to be much higher than the cavity linewidth but not equal to an integer multiple of the free spectral range of the cavity. This ensures that the modulation sidebands do not resonate in the cavity.

The power on a photodetector illuminated by the light reflected from the cavity can be calculated by multiplying the total amplitude by its complex conjugate. The resulting signal is demodulated in phase with the modulation $\Delta\omega$ to pick out the terms in $\sin \omega_m t$. The signal produced is quite complicated and here only special cases are considered.

The basic signal which is obtained due to a phase shift can be seen by considering the case of zero frequency noise. The power can be shown to be

$$\frac{4r\rho t^2}{(1-r\rho)^2} J_0(\beta) J_1(\beta) \frac{\sin \delta}{1 + F' \sin^2 \frac{\delta}{2}}. \quad (\text{A.16})$$

This provides a bipolar control signal with a high slope region corresponding to zero phase shift (light on resonance).

If the laser frequency is to be stabilised to the cavity then the particular case of $\delta = 0$ is of interest. The result can be split into two cases depending on the frequency of the noise compared to the linewidth (ω_f) of the cavity. If ω_f is defined to be ω_{fsr}/F where $\omega_{fsr} = \pi c/l$ then the cases are:-

1) $\omega_n < \omega_f$ when the power becomes

$$\frac{4r\rho t^2}{(1-r\rho)^2} J_0(\beta)J_1(\beta) \frac{2\pi}{\omega_f} \times \Delta\omega \sin \omega_n t, \quad (\text{A.17})$$

2) for $\omega_{fsr} > \omega_n > \omega_f$ it becomes

$$\frac{4r\rho t^2}{(1-r\rho)^2} J_0(\beta)J_1(\beta) \frac{2\pi}{\omega_f} \times \frac{\Delta\omega}{\omega_n} \cos \omega_n t. \quad (\text{A.18})$$

Comparison of these two expressions shows the integrating effect of the cavity on the frequency noise as the frequency is increased above the critical value, ω_f . This integrating effect applies to other causes of round trip phase change, for example, gravitational waves.

A fundamental limit to the degree to which the frequency noise can be reduced is set by the shot noise on the detected light. This limit has been evaluated [13] and is stated here for reference. The shot noise limited frequency noise is

$$\delta\omega = \omega_f \cdot \sqrt{\frac{\hbar\omega(1-J_0(\beta)V)}{16\eta P}} \cdot \frac{1}{J_0(\beta)J_1(\beta)} \cdot \frac{1}{1 \pm \sqrt{1-V}} \sqrt{1 + 2 \left(\frac{\omega_n}{\omega_f}\right)^2} / \sqrt{\text{Hz}}, \quad (\text{A.19})$$

where P is the illuminating laser power, η is the photocurrent produced by the photodiode per unit incident power and it has been assumed that the mode-matching is perfect. The above expression was used to calculate the minimum light power which had to be devoted to laser stabilisation in the various experiments. The effects of the use of sinusoidal modulation on the shot noise limited frequency noise have not been taken into account in equation A.19. These effects are too small to be of any significance in the calculations where this equation was used.

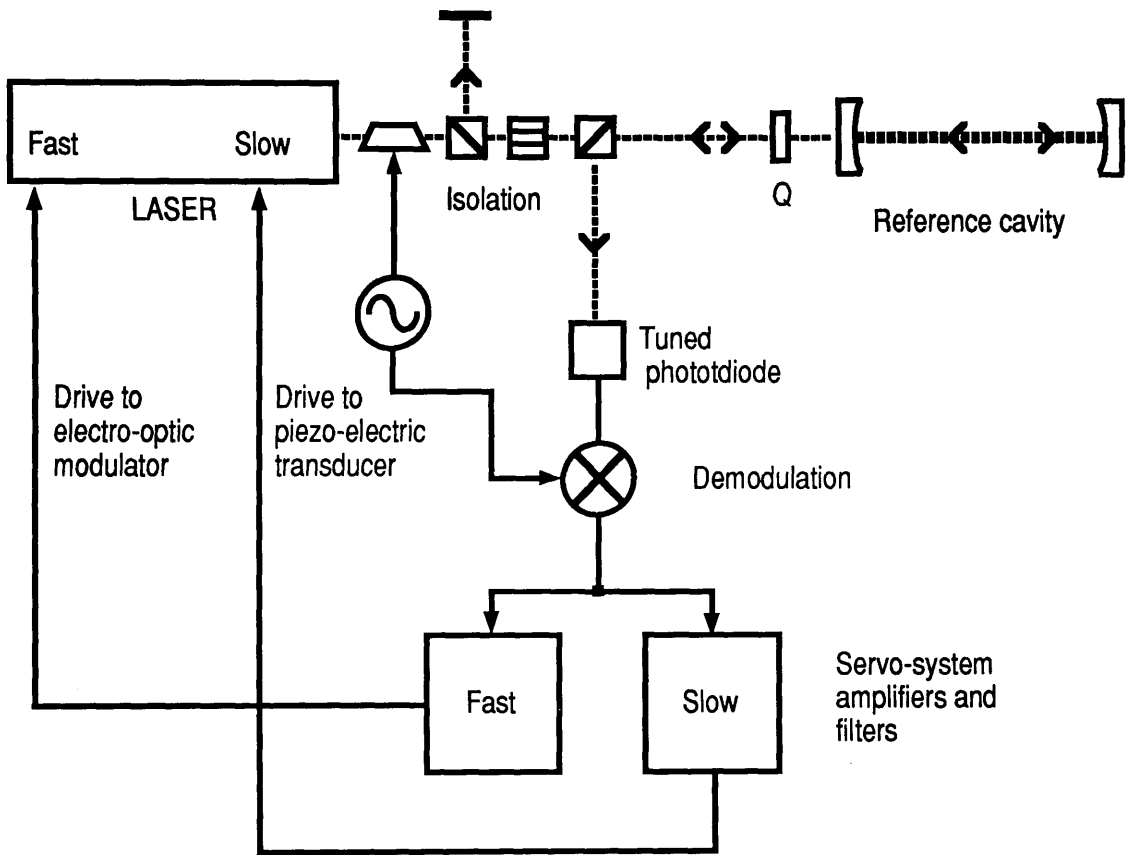
Appendix B

Laser stabilisation

The gravitational wave groups which use laser interferometry have developed frequency stabilisation techniques based on the reflection-fringe scheme [12]. There are several reviews of this topic (e.g. [13]) and the objective here is to summarise some features of the system used in the work presented in this thesis.

The aim was to stabilise the frequency of the laser to the frequency defined by a resonance of a Fabry-Perot cavity. This is done using the signal obtained from the light reflected from the cavity. The laser light was phase modulated using an electro-optic modulator and used to illuminate the cavity to which the laser frequency was to be stabilised. A polarization scheme was used to allow the reflected light to be detected and the resulting signal was demodulated in phase with the modulation. This produces a bipolar error signal with a high slope region at the zero-crossing which corresponds to the light being on resonance with the cavity (the form of the signal obtained was shown in Appendix A). This signal was amplified and filtered to provide the laser frequency correction. The arrangement which was used is shown (figure B.1).

The performance of the servo-system can be represented by a Bode magnitude plot of the loop gain. Such a plot is shown for a typical configuration (figure B.2). This represents the factor by which the frequency fluctuations of the laser are reduced with respect to the cavity resonance (where the gain is greater than unity). It was necessary to achieve a high loop-gain in this servo-system to reduce sufficiently the laser frequency noise at the measurement frequencies used in the experiments (several to many kilohertz). The transducer used here to provide the



-  -polarising beamsplitter
-  -modulation source (12 MHz)
-  -phase modulator
-  -45 degree Faraday effect isolator
-  -quarter wave retardation plate (or Faraday rotator)

Figure B.1: *The apparatus used to stabilise the laser frequency to the Fabry-Perot cavity*

high frequency feedback (up to at least 1 MHz) was an electro-optic modulator within the laser resonator. The dynamic range of this type of transducer was not sufficient to compensate for the observed large frequency deviations at low-frequency. A piezo-electric transducer fitted to one of the mirrors in the laser cavity was used to provide feedback at these low frequencies. This resulted in a control system with a cross-over at a moderate frequency (a few kilohertz) below which the large frequency fluctuations lay. In most of the experiments it was important to have a laser stabilisation system which was tolerant of small changes in the overall gain. The transfer function of the servo-system was chosen to allow this.

The residual relative frequency noise could be measured at the error point of the control system since the optical and electronic parameters were known. A spectrum of the resulting residual noise is shown as an example (figure B.3). .

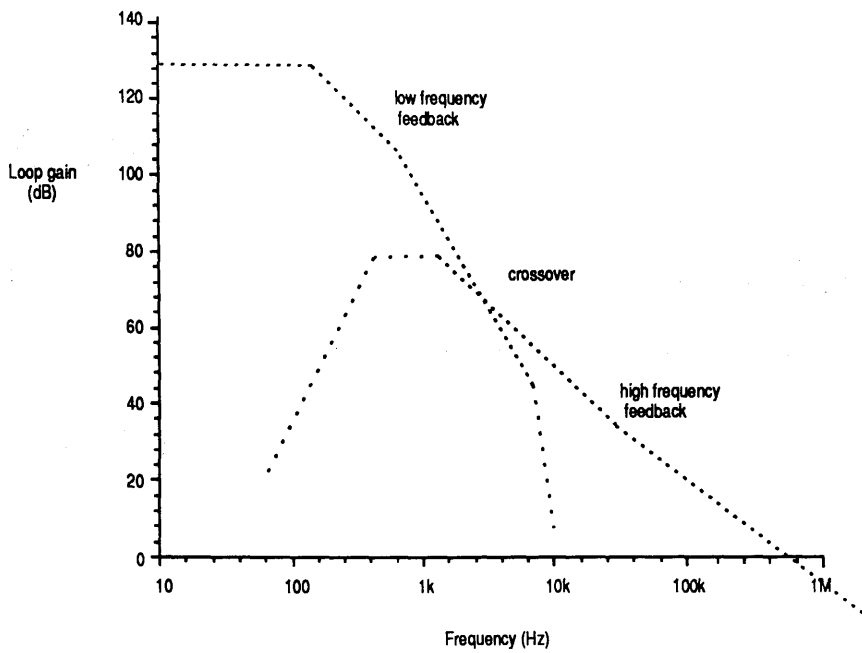


Figure B.2: A Bode plot of the loop gain of the frequency stabilisation system

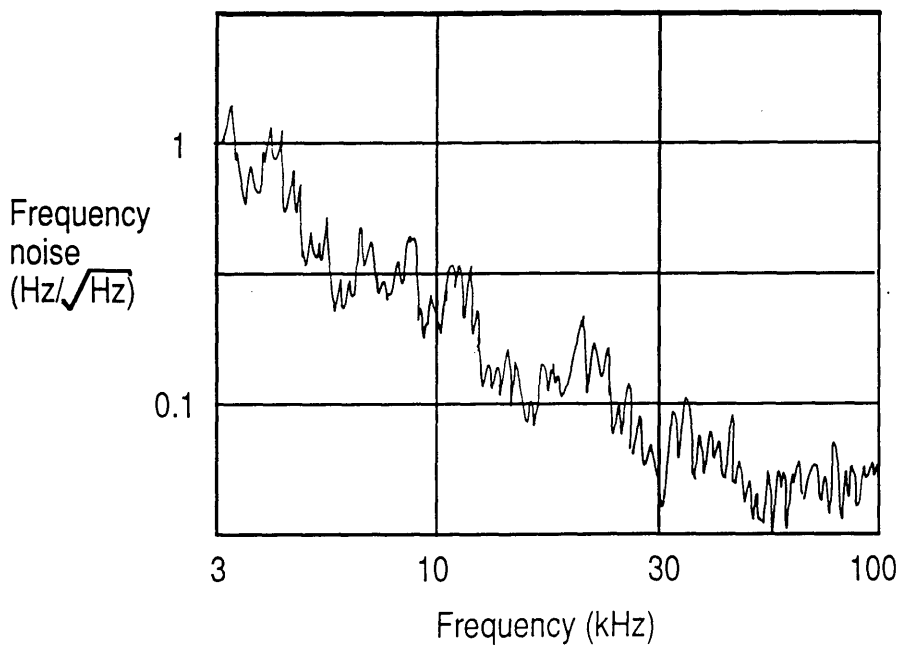


Figure B.3: The residual frequency noise of the stabilised laser.

Appendix C

Measurements of losses in high reflectance mirrors coated for $\lambda = 514.5 \text{ nm}$

There is a growing interest in the development of ultra-low loss mirrors for applications in laser interferometric gravitational wave detectors, especially a pair of two orthogonal mirrors that are part of a Michelson interferometer. Such a pair of mirrors is used by North et al. [1] in the LIGO detector and by Bruma et al. [2] in the VIRGO detector. The mirrors are made of fused silica and are coated with a dielectric multilayer coating.

The interest in ultra-low loss mirrors arises from the development of a laser interferometric gravitational wave detector, especially a pair of two orthogonal mirrors that are part of a Michelson interferometer. Such a pair of mirrors is used by North et al. [1] in the LIGO detector and by Bruma et al. [2] in the VIRGO detector. The mirrors are made of fused silica and are coated with a dielectric multilayer coating. The mirrors are used in a Michelson interferometer to measure the strain of the mirrors. The mirrors are coated with a dielectric multilayer coating that is designed to have a reflectance of 99.9999% at the operating wavelength of 514.5 nm. The mirrors are used in a Michelson interferometer to measure the strain of the mirrors. The mirrors are coated with a dielectric multilayer coating that is designed to have a reflectance of 99.9999% at the operating wavelength of 514.5 nm.

The mirrors are used in a Michelson interferometer to measure the strain of the mirrors. The mirrors are coated with a dielectric multilayer coating that is designed to have a reflectance of 99.9999% at the operating wavelength of 514.5 nm. The mirrors are used in a Michelson interferometer to measure the strain of the mirrors. The mirrors are coated with a dielectric multilayer coating that is designed to have a reflectance of 99.9999% at the operating wavelength of 514.5 nm.

The mirrors are used in a Michelson interferometer to measure the strain of the mirrors. The mirrors are coated with a dielectric multilayer coating that is designed to have a reflectance of 99.9999% at the operating wavelength of 514.5 nm. The mirrors are used in a Michelson interferometer to measure the strain of the mirrors. The mirrors are coated with a dielectric multilayer coating that is designed to have a reflectance of 99.9999% at the operating wavelength of 514.5 nm. The mirrors are used in a Michelson interferometer to measure the strain of the mirrors. The mirrors are coated with a dielectric multilayer coating that is designed to have a reflectance of 99.9999% at the operating wavelength of 514.5 nm.

MEASUREMENTS OF LOSSES IN HIGH REFLECTANCE MIRRORS COATED FOR $\lambda=514.5$ nm

N.A. ROBERTSON, K.A. STRAIN and J. HOUGH

Department of Physics and Astronomy, University of Glasgow, Glasgow G12 8QQ, Scotland

Received 18 July 1988

We have measured the losses of high reflectance mirrors coated for $\lambda=514.5$ nm using the decay time of light in a Fabry Perot cavity. Currently the lowest losses we have measured in air, for substrates polished by General Optics and coated by British Aerospace using the ion beam sputtering technique, are 80 ± 20 ppm. As expected, both the quality of the substrate and the method of deposition of the coating are important for achieving the best results.

1. Introduction

There is at present considerable effort being devoted to the development of ultra-low loss mirrors for use in laser gyros. The introduction of an ion-beam sputtering technique for the deposition of dielectric coatings [1], coupled with substrates polished to a residual roughness of ~ 1 Å rms, has led to the availability of mirrors coated for the HeNe laser wavelength ($\lambda=632.8$ nm) with total loss, A , less than one hundred parts per million. Figures of 30 ppm have been achieved [2], and a figure as low as 15 ppm has been reported [3]. These losses are considerably lower than those achieved using standard evaporation techniques.

Our interest in ultra-low loss mirrors arises from our development of a laser interferometric gravitational wave detector which essentially consists of two resonant optical cavities arranged at right angles to each other [4]. The sensitivity of such a detector is expected to be limited by photon counting statistics on the light detected at the output. At present these detectors use argon ion lasers operated at $\lambda=514.5$ nm, for maximum continuous wave output power in the visible, and thus the availability of cavity mirrors of low loss at this wavelength is a very important factor for the optimum performance of such a detector.

2. Method of measurement

To measure the losses for a mirror one requires to find both its reflectance and transmittance. For a particular mirror, we have the following relationship between the power coefficients,

$$A + R + T = 1,$$

where A =total loss (due to absorption and scattering), R =reflectance, and T =transmittance.

T may be measured using a photodiode, but considerable care must be taken. One requires to use a photodiode with good linearity, and attention must be paid to filtering out any wideband light from the discharge in the laser. The error associated with the final result for A will depend very strongly on how accurately the transmittance can be determined.

R may be determined by measuring the finesse, F , of a Fabry Perot cavity, where F is given by

$$F = \pi\sqrt{\bar{R}}/(1 - \bar{R}) \approx \pi/(1 - \bar{R}), \quad \text{for large } \bar{R}.$$

Here \bar{R} is the geometric mean of the reflectance of the two mirrors forming the cavity. It should be noted that to get measurements of individual mirrors will require a minimum of three mirrors of suitable transmission and curvature characteristics. The finesse can be found by measuring the decay time of light leaking from a cavity when it comes off resonance, either due to the input light being switched off or to the frequency of the laser shifting with re-

spect to the cavity resonance [5]. It can be shown that, provided the change of light level or frequency is fast with respect to the decay time of the cavity, the intensity of transmitted light falls off exponentially as $\exp(-t/\tau)$ with a decay time τ given by

$$\tau = dF / c\pi,$$

where d = length of cavity, and c = speed of light.

Thus by measuring τ and d , F and hence \bar{R} may be found.

Commercial systems based on this idea are now available [6]. Here a measurement of decay time is made with two mirrors of known characteristics, and then the unknown mirror is introduced to form a three mirror cavity and the measurement is repeated. R and hence $(A+T)$ may be found for the unknown mirror by comparing the two decay times.

For our measurements, we have preferred to look at the light reflected from the cavity. This facilitates the measurement when a cavity is composed of one partially transmitting mirror (typically a few hundred ppm) and one mirror of essentially zero transmission (less than a few ppm). This is the configuration used in our interferometric gravitational wave detector [4]. One could in principle still look at the transmitted light, using a low noise photodiode or a photomultiplier. However it is much easier to look at the higher light level coming from the input mirror with its much higher transmission. The disadvantage in looking at the reflected light is that this is composed of the interference of light directly reflected from the input mirror and light leaking from the cavity. If it is assumed that the decay is produced by the frequency of the laser light going off resonance with the cavity, one sees a decaying beat signal whose envelope is not a simple exponential. In fact it can be shown that the upper envelope is of the form

$$a_0^2 + a_1^2 \exp(-t/\tau) + 2a_0 a_1 \exp(-t/2\tau),$$

and the lower envelope is of the form

$$a_0^2 + a_1^2 \exp(-t/\tau) - 2a_0 a_1 \exp(-t/2\tau),$$

where a_0 is the amplitude of the light directly reflected from the input mirror, and a_1 is the amplitude of light leaking out of the cavity in reflection on resonance. One can see that the required decay time τ may be recovered either by taking the sum or by taking the difference in height of the two envelopes.

In practice it is better to take the difference, since this gives a slower decay curve which is more easy to analyse. In fact it is interesting to note that the mixture of two exponentials in the envelopes of the beat signal only becomes noticeable when one is working in a regime where the reflected light and the light leaking out of the cavity are of a similar magnitude. If one were working with mirrors of substantial loss compared to the input transmission of the cavity, in which case $a_1 \ll a_0$, one would only see the exponential term due to the cross product.

An example of a typical decay curve for light reflected from a Fabry Perot cavity is shown in fig. 1. An alternative method of obtaining a suitable decay signal to analyse is to modulate the input light to the cavity at a radio frequency (typically around 10 MHz) and to observe the reflected fringes from the cavity after demodulation. The frequency is chosen to be higher than the cavity linewidth such that the carrier and sidebands do not simultaneously resonate. This technique of r.f. modulation and subsequent detection of reflected fringes from a Fabry Perot cavity forms the basis of the r.f. reflection locking technique developed for the wideband frequency stabilisation of laser to a cavity [7]. The important point for the purpose of measuring the finesse of a cavity is that the demodulated signal is proportional to the amplitude of the light leaking out of the cavity

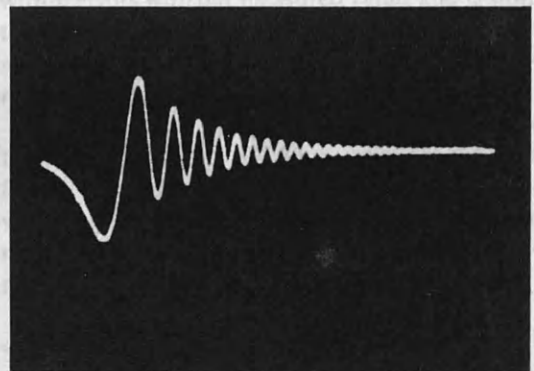


Fig. 1. Example of a typical decay curve for light reflected from a Fabry Perot cavity. Scale in x direction: one division = 10 μ s. Cavity length = 1 m.

in reflection and thus is a simple exponential of the form $A \exp(-t/2\tau)$.

3. Results

We have used the above techniques to make measurements of several sets of mirrors produced both by conventional evaporation and by ion beam sputtering. The mirrors investigated were typically 20 to 25 mm in diameter with coated area slightly smaller than the diameter. All mirrors tested had substrates of fused silica, except set 2b, which were made of Zerodur. Cavity lengths were typically 0.4 to 1 m, and measurements were made in air.

Set 1. Substrates of high quality surface (roughness of a few Å rms), but not so-called "superpolished", were coated by evaporation. The sum of the losses of two mirrors, one with $T \approx 0.2\%$, and the other with T of less than 0.01% was found to be approximately 1%. This implies that the losses for each mirror, if assumed to be equal, are approximately 0.5% (5000 ppm).

Set 2a. Similar substrates to set 1 were coated for us by British Aerospace by ion beam sputtering, and the sum of the losses for two mirrors, one with $T \approx 0.12\%$ and the other with T less than 0.01% was found to be almost an order of magnitude better, at approximately 0.14%. This implies that the losses for each mirror, if assumed to be equal, are approximately 0.07% or 700 ppm.

Set 2b. During the same batch of coating runs as for set 2a substrates of superpolished quality, that is with surface roughness of approximately 1 Å rms were coated. The losses were found to be in the region of 200 to 250 ppm, both for mirrors with $T \approx 250$ ppm and $T < 10$ ppm. These measurements were made with more than two mirrors in such a way that the losses could be established for individual mirrors. It was found that the losses for the two different transmittances were approximately the same.

The coating runs which produced sets 2a and 2b were the first runs which British Aerospace had carried out for the wavelength of 514.5 nm.

Set 3. The most recent set of mirrors which we have obtained consist of substrates with superpolished finish supplied by General Optics (USA) and coatings by British Aerospace using ion beam sputtering.

We found that the sum of losses of two mirrors, one with $T = 360 \pm 20$ ppm, and the other with $T < 10$ ppm, to be 160 ± 40 ppm. Assuming each mirror has the same loss, this gives a figure of $A = 80 \pm 20$ ppm.

4. Discussion

From the results above we can draw several conclusions.

(a) From comparing sets 1 and 2a we can see the large improvement that was gained using the ion beam sputtering technique.

(b) From comparing sets 2a and 2b we see the importance of the quality of the substrate for obtaining optimum results.

(c) It is instructive to compare the most recent results from set 3 with those of the best laser gyro mirrors coated for $\lambda = 632.8$ nm, where a conservative figure of 30 ppm may be taken. It is not known whether these losses are dominated by absorption or scattering, or are a fairly equal combination of both mechanisms. If we assume that scattering is important, then we can extrapolate from the figure of 30 ppm at $\lambda = 632.8$ nm to the expected losses dominated by scattering at $\lambda = 514.5$ nm by using the inverse λ^4 scattering law. This would give a figure of approximately 70 ppm. This figure is consistent within errors with our measured value, and is similar to a figure of 60 ppm measured by Anderson for a set of laser gyro quality mirrors coated for $\lambda = 514.5$ nm obtained from Litton Industries, USA [5].

Since losses of 15 ppm have already been achieved for mirrors coated for 632.8 nm, we might expect that further improvements can be made at the shorter wavelength, unless absorption is already the dominant loss mechanism for the coatings at $\lambda = 514.5$ nm^{#1}.

^{#1} We note that depending on the source of the scattering, the inverse λ^4 law is not always applicable. For example for a simple reflecting surface, scattering may be closer to being inversely proportional to λ^2 , not λ^4 [8]. If this applies here, we might expect lower losses from scattering than the total loss actually measured at $\lambda = 514.5$ nm, and thus would conclude that absorption may be playing a significant role. Further investigation of losses in these multilayer coatings is required for a fuller understanding of the situation.

Appendix D

A measurement of ground displacement noise at one site

As was mentioned briefly in Chapter 1, one of the limits to the low frequency performance of gravitational wave detectors is due to motion of the ground coupling into motion of the test masses. This motion can either be due to natural movements of the ground or to man-made vibration especially that due to mechanical apparatus which forms part of the installation.

The natural background spectral displacement, in either horizontal or vertical directions, has been measured in several locations (e.g. [37]). A moderately quiet site (away from a town etc.) can be expected to have a root mean square displacement (δx) at frequency (f) of

$$\delta x \sim \frac{10^{-7}}{f^2} \text{ m}/\sqrt{\text{Hz}} \quad (\text{D.1})$$

Several methods of isolating the test masses against the effects of this motion have been employed [38] including the use of vibration isolation stacks, air-springs and active systems as well as the suspension of the test masses as pendulums (or multiple stage pendulums). The isolation provided by all of the passive systems increases rapidly with increasing frequency and in combination with the falling background noise this allows sufficient isolation to be obtained if the frequency is sufficiently high.

The vertical seismic displacement noise at one possible site of a gravitational wave detector (Tentsmuir forest, Scotland [3]) was measured to find out if it was a ‘reasonably quiet site’. This was done using a calibrated Willmore MkIV seis-

momenter and the electronics required to measure the average displacement in four frequency bands (1 – 3, 3 – 10, 10 – 30 and 30 – 100 Hz). (The instrument was of a coil and magnet design and it measured velocity in this frequency range.) The results are shown (figure D.1). This is close to the result expected for a moderately quite site.

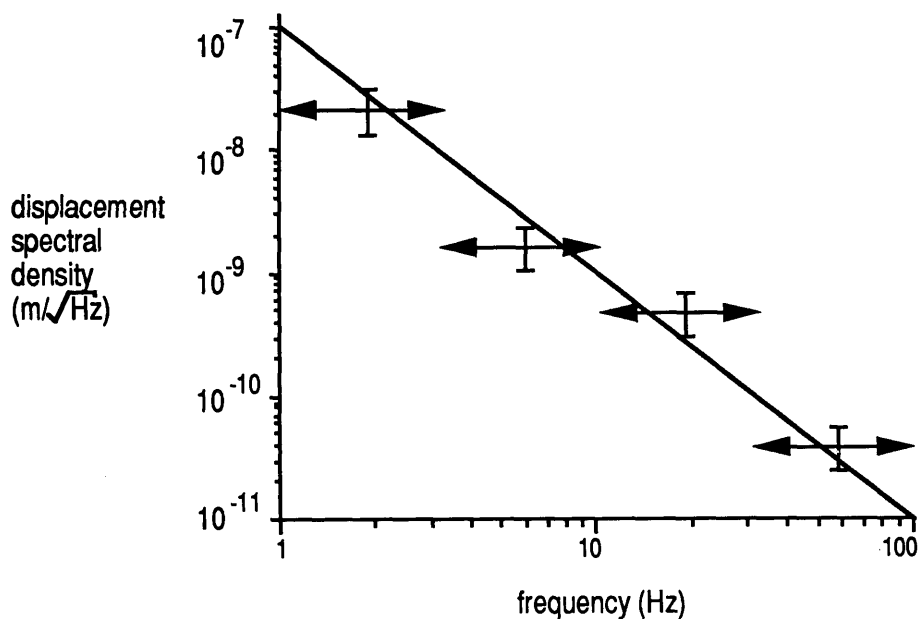


Figure D.1: *The measured vertical displacement noise in Tentsmuir forest as a function of frequency. The horizontal arrows indicate the width of each of the measurement bands while the vertical error bars indicate the range of the observed measurements and their likely uncertainty.*

Bibliography

- [1] A. Einstein, *Sitzungsber Preuss. Akad. Wiss* **688** (1916)
- [2] C. W. Misner, K. S. Thorne and J. A. Wheeler, *Gravitation*, (Freeman, San Fransico, 1973)
- [3] J. Hough et al., *Proposal for a Joint German-British Interferometric Gravitational-Wave Detector*, Report **MPQ 147** (1989)
- [4] K. S. Thorne, in *300 Years of Gravitation* edited by S. W. Hawking and W. Israel (Cambridge University Press, Cambridge, 1987)
- [5] B. F. Schutz, *Gravitational-wave Sources and their Detectability*, *Clas. Quant. Grav.* (1989)
- [6] M. Zimmerman, *Phys. Rev. D* **20** 351 (1979)
- [7] J. Weber, *Phys. Rev* **117** 306 (1960)
- [8] C. M. Caves, *Phys. Rev. D* **26** 1817 (1982)
- [9] C. M. Caves, *Phys. Rev. D* **23** 1693 (1981)
- [10] C. M. Caves in *Quantum measurement and Chaos* edited by E. R. Pike (Plenum, New York, 1987)
- [11] B. J. Meers, Ph.D thesis, Glasgow University (1983)
- [12] R. W. P. Drever et al., *Appl. Phys. B* **31**, 97 (1983)
- [13] J. Hough et al. in *The Detection of Gravitational Radiation* edited by D. Blair (Cambridge University Press, Cambridge, in press).

- [14] W. Winkler in *The Detection of Gravitational Radiation* edited by D. Blair (Cambridge University Press, Cambridge, in press).
- [15] J. B. Mangan, Ph.D thesis, Glasgow University (1987)
- [16] R. Weiss, *Electromagnetically coupled broadband gravitational antenna*, Quarterly Progress report, Research Laboratory of electronics, MIT **105 54** (1972)
- [17] R. E. Vogt, R. W. P. Drever, K. S. Thorne, F. J. Raab and R. Weiss, *LIGO proposal*, (Caltech, 1989)
- [18] R. W. P. Drever, *personal communication* (1983)
- [19] L. Schnupp, *personal communication* (1990)
- [20] T. M. Niebauer et al, *Non-stationary shot noise and its effect on the sensitivity of interferometers* submitted to Phys Rev A (1990)
- [21] B. J. Meers, *personal communication* (1990)
- [22] G. A. Kerr, Ph.D thesis, Glasgow University (1986)
- [23] R. W. P. Drever, in *Gravitational Radiation*, edited by N. Deruelle and T. Piran (North-Holland, Amsterdam, 1983)
- [24] H. Kogelnik and T. Li, Proc. IEEE **54** 1312 (1966)
- [25] B. J. Meers, Phys. Rev. D **38**, 2317 (1988)
- [26] B. J. Meers, Phys. Lett. A **142**, 465 (1989)
- [27] D. Shoemaker et al, *unpublished paper*, Dept. of Physics and Center for Space Research, MIT
- [28] C. N. Man, D. Shoemaker, M. Pham Tu and D. Dewey, Phys. Lett. A **148**, 8 (1990)
- [29] H. A. Macleod, *Thin-film Optical Filters (second edition)* (Adam Hilger, Bristol, 1985)

- [30] P. Bousquet, F. Flory and P. Roche, *J. Opt. Soc. Am.* **71** 1115 (1981)
- [31] M. Stedman and K. Lindsey, *Proc. SPIE* **1009** (1988)
- [32] B. J. Meers, *personal communication* (1990)
- [33] J. Y. Vinet and A. Marraud *personal communication* (1988)
- [34] F. Raab, Abstracts, 12th International Conference on Gravitational Radiation and Gravitation, Boulder (1989)
- [35] B. J. Meers, *unpublished paper* (1989)
- [36] B. J. Meers and K. A. Strain, submitted to *Phys. Rev.* (1990)
- [37] N. A. Robertson, Ph.D thesis, Glasgow University (1981)
- [38] N. A. Robertson in *The Detection of Gravitational Radiation* edited by D. Blair (Cambridge University Press, Cambridge, in press).
- [39] A. Rüdiger et al., *Optica Acta* **28** 641 (1981)

(In addition there is a separate bibliography included in Appendix C.)

